Development and Evaluation of a Novel Robotic Gait Simulator

A Thesis

Presented to

the faculty of the School of Engineering and Applied Science

University of Virginia

in partial fulfillment
of the requirements for the degree

Master of Science

by

Watson A. Spivey

May 2020

APPROVAL SHEET

This Thesis
is submitted in partial fulfillment of the requirements
for the degree of
Master of Science

Author Signature: ______________________

This Thesis has been read and approved by the examining committee:

Advisor: Jason R. Kerrigan

Committee Member: Shawn D. Russell

Committee Member: Joseph S. Park

Committee Member: Tomonari Furukawa

Committee Member: ______________________

Committee Member: ______________________

Accepted for the School of Engineering and Applied Science:

Craig H. Benson, School of Engineering and Applied Science

May 2020

Abstract

Biomechanical research on living subjects is limited to what can be measured without causing pain or permanent damage to volunteers. Utilizing cadaveric, or post-mortem human surrogate (PMHS), models can allow for invasive measurements that could augment our understanding of the biomechanics of the foot and ankle complex. Dynamic gait simulators, which replicate tibia kinematics and the dynamic muscle forces that occur during gait on PMHS, have the potential to produce repeatable and biofidelic foot and ankle mechanics to permit such investigations. Therefore, the goals of this thesis were to 1) develop a novel robotic gait simulator, 2) to use the simulator to capture repeatable foot bone kinematics, 3) to assess how well the captured foot bone kinematics can predict realistic foot bone kinematics, and 4) to assess how much variation in response can occur when using the same inputs across different anthropometries. A simulator that utilizes a 6-degree of freedom serial robotic arm to prescribe tibia kinematics and an array of nine linear tendon actuators to control muscle forces, was developed to recreate biomechanically accurate gait in a PMHS model and address these goals. Then, through experiments on five PMHS, bony kinematics for nine different foot/ankle joints were recorded, The correlation and analysis (CORA) method was used to make quantitative comparisons of bony kinematics across multiple tests on the same subject (repeatability), between PMHS and volunteers (biofidelity) and across subjects (subject-specific effects). Output bone kinematics from repeated trials were found to be repeatable within a subject, to vary between subjects despite having similar generalized inputs, and to generally represent volunteer bone kinematics data. Utilizing this system as a foundation, future studies could investigate biomechanical changes resulting from orthopaedic implants, the effects of muscular deficiencies or diseases, and determine how active musculature affects the risks of traumatic injury.

Table of Contents

Table of Figures

Table of Tables

1. Introduction

1.1 Motivation

Biomechanical research on living subjects is limited to what can be measured without causing pain or permanent damage to volunteers. Critical parameters like joint pressure distribution, bone and ligament strain, and bone kinematics cannot be measured directly *in vivo* and must be inferred through model simulations. Further, the *in vivo* effects of surgical interventions can only be studied by prospectively enrolling volunteers who will have the surgery, which is not feasible in fracture fixation and does not yield useful results in fusion/replacement patients. These model simulations could be either computational or cadaveric.

As a result, cadaveric gait simulators have been developed as an attempt to understand the complex structure/function relationship of anatomical structures of the foot and ankle. Specifically, they have been developed to investigate surgical interventions, disease/deficient pathologies, and injury mechanisms involving active musculature. State of the art gait simulators are currently capable of simulations at less than full body weight, fixing the leg and moving the ground relative to the foot, and creating an unrealistic interaction with gravity by moving the control load cell (Aubin et al., 2012; Baxter et al., 2016; Whittaker et al., 2011). Because of these limitations, only an estimation of the *in vivo* conditions can be achieved.

1.2 Goal

The goals of this thesis are:

1. to develop a robotic gait simulator capable of moving the foot relative to the ground in a realistic orientation under varying body weight conditions, with dynamic control of active muscle forces
2. to use the simulator to capture repeatable foot bone kinematics
3. how well the captured foot bone kinematics can predict realistic foot bone kinematics
4. to assess how using the same input across different anthropometries varies the bone kinematic response

Chapter 2 provides a review of dynamic gait simulators, biological parameters that define gait, and methods to capture bone kinematics. Chapter 3 outlines the first goal of the thesis, a description of the currently developed system in terms of hardware, software, and testing methodology. Chapter 4 outlines the second goal of the thesis, capturing bony kinematics, through a larger experimental study. Chapter 5 outlines the third goal of assessing how realistic the output bony kinematics are, through comparing the bony kinematic results from the previous chapter with a volunteer study, and looking at the how differences in anthropometry with a generalized input changes the output bone kinematics. Finally, Chapter 6 ends the thesis with the conclusions that can be drawn, a review of what has been accomplished, a review of the limitation of the current system, and what could be done in the future.

2. Background

This chapter outlines the important background details necessary for each of the goals in the thesis. First, a short review of other dynamic gait simulators and their capabilities. Next, a review of the biological parameters namely muscle forces of the achilles and the other smaller tendons, as well as how fast there are pulled to inform the decisions for acquiring actuators to control the tendons. Lastly, a short review of recording bony motion is included to inform the decisions on how to record bone motion and what specific bones should be targeted for comparison.

2.1 History of Dynamic Gait Simulation

Dynamic gait simulators have existed for at least two decades, with the first system being documented through publication in 1998. Over this time, six different research groups have developed and utilized these systems to investigate applying gait to cadaveric specimens. Each of these simulators are generally composed of two systems. The first system is used to control to the tibia and impose tibia kinematics either directly, attached to the tibia, or indirectly by controlling the ground. The second is used control dynamically the individual tendons. The following section will outline all of the different dynamic gait simulators that have been used in the past, information that was used to guide development of the system in this thesis.

2.1.1 Pennsylvania State University

Neil Sharkey's group at Pennsylvania State University developed what can be called the first dynamic gait simulator, aptly named the dynamic gait simulator (DGS) (Sharkey & Hamel, 1998). The DGS consisted of a carriage system with a set path that dictated the forward and lateral motions of the tibia. The carriage translates the specimen through the stance phase of gait based on the tibia kinematics of a volunteer. The system is able to complete stance phase in 1/20th of normal gait speed. Additionally, a set of five actuators were mounted onto the carriage and coupled to the following tendons: Achilles, tibialis posterior, combined peroneus brevis and peroneus longus, flexor hallucis longus, and the flexor digitorum longus. The system was redesigned and was renamed the Robotic Dynamic Activity Simulator (RDAS). Two additional motors were added to change the height of the specimen relative to the plate. Control of the vertical ground reaction force (GRF) was done iteratively via trial and error. Between each of the simulations, the tibia position could change along with muscles forces to alter the GRF. No bony motion was collected during testing, only the plantar pressure distribution during the gait cycle.

2.1.2 University of Salford

Nester *et al.* (2007) at the University of Salford, in collaboration with Iowa State University created another carriage-style dynamic gait simulator. Similar to the one developed at Pennsylvania State, the system consisted of a metal frame that is pulled along a track, via a motor and pulley system (Nester et al., 2007). A pneumatic cylinder provided vertical load to the specimen through a passive knee joint. Although the system allowed for tibia motion in the frontal and transverse planes, it was not controlled. Additionally, the system was mechanically locked to have only one degree of freedom in the sagittal plane and the knee joint. Motion tracking arrays were installed on the tibia, talus, calcaneus, navicular, cuboid, three cuneiforms, five metatarsals, and the proximal phalanx of the hallux. Nine tendons were controlled by eight muscle actuators (extensors were tied together), through an open loop trial and error control method. This method primarily involved adjustments to cable pre-tensioning based on a visual inspection during repeated walking trials. Due to mechanical constraints of the system, toe off was not simulated in the specimens, and test trials end at maximal dorsiflexion of the first metatarsal. Each simulation took approximately two seconds to complete at half body weight, simulations with the system were possible at higher speeds, but compromised matching the vertical GRF and adjusting the tendon motors.

2.1.3 Medical School of Hannover

A third dynamic gait simulator was developed by Hurschler *et al.* at the Medical School of Hannover, Germany. Unlike the other carriage-style systems the tibia is rigidly mounted, and the force plate translates underneath (Hurschler et al., 2003). The tibia was fixed in the sagittal and coronal planes, but allowed to rotate in the transverse plane. The force plate utilized a hydraulic cylinder to adjust its superior position, which is used during force control, while another motor controls the angle at which the plate interacts with the foot. Nine hydraulic cylinders were attached to nine tendons via a clamp and pulley system. To achieve the desired kinetics and kinematics, the maximum value for each of the simulated muscles was determined iteratively. Motion tracking marker arrays were attached to the tibia, talus, calcaneus, navicular, and cuboid. Tendon and GRF forces were scaled to one-half body weight over a sixty-second gait cycle.

2.1.4 Cleveland Clinic

Noble *et al.* (2010) and the Cleveland Clinic developed one of the first dynamic gait simulators that utilized a robotic test system as opposed to individual motors (Noble et al., 2010). The system, named the musculoskeletal simulator was designed to apply muscle forces to more than just the foot and ankle. Similarly to the last system, the specimen was rigidly fixed and the force plate was attached to a six degree of freedom parallel robot (R2000, Parallel Robotics Systems Corp.) known as a rotopod. The specimen was mounted horizontally creating an unrealistic condition that gravity was not acting on the system in the correct direction. A set of five tendon actuators were used to control the Achilles, and four muscle groups. Vertical GRF was controlled with an iterative optimization routine. Any of the simulators input parameters can be adjusted based on results from the previous trial, using an error between what happened during the trial and the desired signal. Using this system, the system optimized superior and anterior offsets during the first half of the simulation, and optimized Achilles force during the second half. Gait simulations were performed in three seconds at sixty-six percent body weight.

2.1.5 University of Washington

Aubin *et al.* (2008, 2012), building on what was learned by Noble and the Cleveland Clinic, developed another robotic-based gait simulator (Aubin et al., 2012; Aubin et al., 2008). Utilizing the same parallel robot that was developed before, Aubin created a more complicated fuzzy logic control scheme, and returned to using nine actuators for nine different tendons. Like the previous systems, the specimen was rigidly mounted and the force plate moves relative to the specimen, and the specimen was mounted horizontally. The smaller tendons were attached to a cable system using a screw driven through the tendon tied using climbing rope with a clove hitch; for the larger Achilles tendon a liquid nitrogen freeze clamp was used. Using a fuzzy logic control scheme, the simulator was able to change inputs automatically based on recorded data from previous trials. To achieve the primary target of vertical GRF, the response is split into three sections over the stance phase. In the first section, the force in the tibialis anterior was modulated to achieve the desired force, the second section tibia vertical positon was modulated to achieve the desired force, and in the last section, force in the Achilles tendon was modulated to achieve the desired force. Trials for this simulator were conducted at a three-second cycle time at twenty-five percent body weight.

2.1.6 Hospital for Special Surgery

The group at the Hospital for Special Surgery use a system similar to what was used at the University of Washington, with some minor improvements (Baxter et al., 2016). Most notably, the robotic test platform was updated to a more state of the art model that allowed for control that is more precise and more powerful. Additionally, the orientation of the system was flipped so that the foot was vertical, creating a realistic condition for gravity to act on the system. Gait simulation trials were conducted at a three-second cycle time at twenty-five percent body weight.

Table 2-1: Other Gait Simulator Parameters

System	Simulated GRF (%)	Simulated Stance Phase Speed (s)	Tibia Orientation
Pennsylvania State University	100	12	Vertical
University of Salford	50	2	Vertical
Medical School of Hannover	60	60	Vertical
Cleveland Clinic	66.7	3.2	Horizontal
University of Washington	25	3.2	Horizontal
Hospital for Special Surgery	25	3.2	Vertical

2.2 Biological Considerations

In order to build a system that is able to replicate normal gait, the hardware of the system must be able handle physiologic loading and gait conditions. Komi *et al.* (1990) developed a force transducer that was attached to the Achilles tendon *in vivo*. Subjects were then tasked with walking and running along a long force platform (Komi, 1990). Achilles force was found to be highest during the second half of stance phase. During walking, peak Achilles force was measured at approximately 1500 ± 500 N, and during running was found to be approximately 3000 N. Follow-up studies determined the speed at which the Achilles pulls during loading, approximately two hundred millimeters per second. Fukunaga *et al.* determined an estimated pulling force of the smaller muscles in the foot with the tibialis anterior generating the most force, around 450 N (Fukunaga et al., 1996).

2.3 Bony Motion Review

Past gait research has utilized motion-tracking markers attached to the skin near anatomic landmarks to record approximate motion of the foot (Wright et al., 2011). Current standards, like the Oxford Foot Model, had been developed to maximize the capture of motion data with the least amount of information sources (markers). The model simplified the foot into three separate regions, with the tibia, hindfoot, and forefoot discretized as different segments. It is primarily used to look at the motion of the segments relative to each other as combined systems. The method of using skin markers has the advantages of being noninvasive and easy to setup. A major limitation of skin markers are that they are not directly measuring the motions of the bones, and motion of the foot segments do not represent individual foot bone motion.

More invasive measurement techniques have been attempted to record bony kinematics, notably two studies that were published by Ardnt *et al.* (2004) and Lundgren *et al.* (2008) utilized pins drilled in and attached to individual bones, known as bone pins. Local anesthesia was applied to drill the pins into target bones. The Ardnt study targeted the tibia, fibula, talus and calcaneus as a proof of concept for the method. The follow-up studies, by Lundgren, collected kinematics on the majority of the bones in the foot including the tibia, fibula, talus, calcaneus, navicular, cuboid, cuneiforms, first metatarsal, and fifth metatarsal (Lundgren et al., 2008). The pins were inserted for a total of two hours, allowing the subjects to perform ten walking trials. While this data represents some of the most accurate bone kinematics in the literature, the comfort of the volunteers is called into question based on being anesthetized and having pins inserted into their feet. The data sets are also extremely limited with small sample sizes, and these methods have not been extensively repeated by other research groups.

Dynamic gait simulators allow direct measurement of bony foot motion that are otherwise too invasive and impractical for use in volunteers. Whittaker *et al.* (2019) and Baxter *et al.* (2016) demonstrate the use of a gait simulator to investigate the motion of bones, specifically the tibia, talus, calcaneus, and navicular for Baxter, and the tibia, talus, calcaneus, navicular, medial cuneiform, cuboid, metatarsal 1, metatarsal 3, and metatarsal 5 for Whittaker during gait (Baxter et al., 2016; Whittaker et al., 2011). Follow-up studies investigated the effects of different pathologies and surgical interventions on bone motion.

3. Development and Initial Evaluation

The goal of this chapter is to present the material needed to address the first goal of this thesis: to develop a robotic gait simulator capable of moving the foot relative to the ground in a realistic orientation under varying body weight conditions, with dynamic control of active muscle forces. The following sections will describe the development of the system, hardware and software used, and the initial testing performed to assess the system performance. The initial testing showed that the system was capable of optimizing the input parameters to achieve output objects to recreate the desired specimen response. Additionally, limits of body weight application and gait speed were investigated to determine the capabilities of the system.

3.1 Muscle Activated Robotic System (MARS)

3.1.1 System Hardware

The Muscle Activated Robotic System (MARS) consists of a 6 degree of freedom serial robot, nine linear tendon actuators, custom force plate, and a custom user interface (Figure 3-1). To simulate gait, the tibia is fixed to the end effector of the robot, and kinematics from a tibia taken during gait are inputted. Details on each of the components are discussed in the following sections.

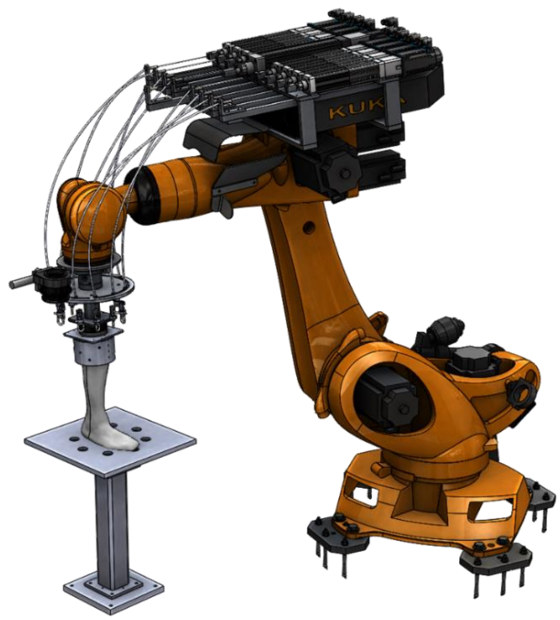

Figure 3-1: CAD rendering of MARS system

3.1.2 Serial Robot

The robot (KUKA, Augsburg, Germany) is a multipurpose serial robot, designed for flexibility of applications, and intended for integration with large number of tooling applications. The robot has six joints, creating the six degrees of freedom that the system is able to move in. The robot is a KR300 R2500 Ultra and is capable of carrying a 300 kg payload 2496 mm away from the base of the robot with an accuracy of 0.06 millimeter. It has an 830 by 830 mm foot print a weighs approximately 1120 kg. Six DC motors control the pose of the robot; the motors are powered by three-phase 240 V power supply. Axis 1, the base, is able to rotate 185 degrees in either direction. Axis 2, the arm, is able to rotate 140 degrees. Axis 3, the elbow, is able to rotate 120 degrees in one direction and 155 degrees in the other. Axis 4, the wrist is able to rotate 350 degrees. Axis 5 is able to rotate 122.5 degrees. Axis 6 is able to rotate 350 degrees. All of the axes are able to rotate approximately 110 degrees per second. Control of the robot is handled through the Kuka control PC and attached pendant, commands are sent through the SimVitro PC via Ethernet (described below).

3.1.3 Tendon Actuator System

The tendon actuation system can be broken into two separate pieces, the upper and lower assembly. The upper assembly consists of the tendon actuators themselves mounted on top of the robot and the lower assembly consists of the tendon guide ring, load cell, and tendon attachment hardware.

3.1.4 Upper Assembly

There were two main requirements that guided the design for the tendon actuators. First, the actuators need to be able to recreate the force and speed that is representative of the biological tissue (Chapter 2.2). Second, the actuators need to be controlled and able to communicate with LabVIEW software. After reviewing multiple options of motors and drive controllers the Electric Cylinder (EC) series by Kollmorgen Corporation (Kollmorgen, Radford, VA), accompanying AKM motors, and AKD motor drives was chosen for this application. The EC linear actuators rely solely on a ball screw resulting in a high accuracy, low backlash system. Two sizes of cylinders were purchased due to the vastly different requirements of the Achilles tendon versus the other smaller tendons. The smaller actuators (AKM42G EC3) are capable of generating 1500 N at a maximum speed of 533.4 mm/s, while the larger actuator (AKM52L EC4) is capable of 4000 N at a maximum speed of 533.4 mm/s. In order remove the complication of the actuators mounted stationary while the robot is moving, the actuators were mounted directly to the robot along Axis 3 via a custom designed and manufactured support structure (Figure 3-2).

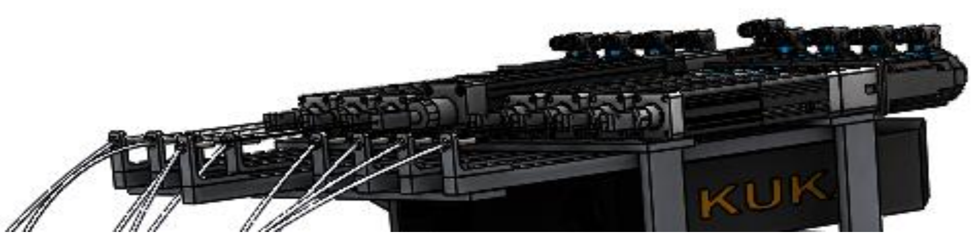

Figure 3-2: CAD rendering of Upper Assembly, notably the Tendon Actuators

3.1.5 Lower Assembly

Each actuator was connected to a tendon via a steel cabling system. This system was comprised of the steel cable surrounded in a low friction cable housing connected to a Honeywell Model 31 load cell (Honeywell, Charlotte, NC) and then the tendon via surgical suture for the smaller tendons, and a freeze clamp for the Achilles tendon. For the smaller actuators, a 1.6 mm braided steel cable was used with a 5 mm housing, and the larger actuator a 3.25 mm braided steel cable was used with an 8.5 mm housing. The nine actuators were connected to the following tendons: Achilles, tibialis anterior, tibialis posterior, flexor hallucis longus, flexor digitorum longus, extensor hallucis longus, extensor digitorum longus, peroneus longus, and peroneus brevis. The cable housing allowed for the routing of the steel cable while the robot is moving without the need for a pulley system. Each cable was routed into an aluminum guide ring mounted at the end effector of the robot (Figure 3-3 Left). The ring has four radially spaced slots close to its outside radius to allow the cable attachments to be moved to create a better line of action for pulling the tendon. Due to the symmetry and unbalanced tendon groups between a right and left specimen, the positions of the cables needed to be adjustable. The ring also provided a rigid attachment point to limit the amount the load cells are able to swing during gait. For all of the tendons a CamJam XT aluminum cord tightener is attached to the end of the load cell via an eye nut. A braided Kevlar rope (DuPont Kevlar Fiber), with a 3.5mm diameter and tensile strength of 2000 lbs, was attached to the cord tightener, and then was tied using a knot into the surgical suture for the smaller tendons, and the freeze clamp for the Achilles (Figure 3-3 Right).

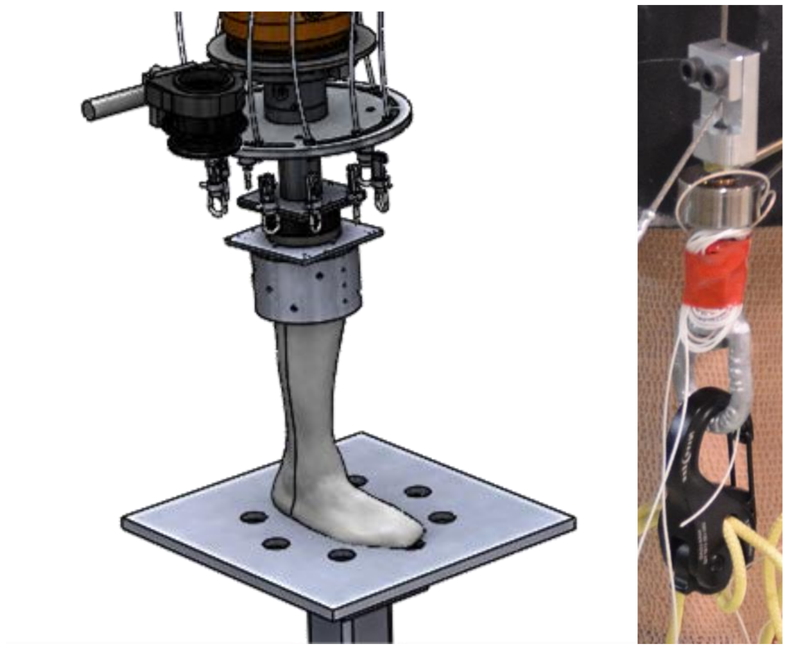

Figure 3-3: LEFT: 3-D rendering of lower assembly components, notably guide ring and load cells. RIGHT: Tendon load cell assembly, from top to bottom: steel cabling from tendon actuators, pancake load cell, aluminum cord tightener, braided Kevlar rope, and suturing from tendons

3.1.6 Force Plate

To create a walking platform for the specimen, a 24 by 24 in, 0.5 in thick Delrin plate is attached to an ATI Omega160 IP65/68 load cell, and then fixed to the ground via a steel tube. Mounted into each of the four corners of the plate are four motion tracking targets used for definition of the global coordinate system. The Omega160 load cell is used in the control loop in the simVitro software. Briefly, it is used in the optimization of the system. The vertical ground reaction force to measure and record the ground reaction forces as the specimen walks across the platform, and make decisions based on the measured response versus the target response.

3.1.7 System Software

Both the robot and actuators are controlled using a software package simVitro (Cleveland Clinic BioRobotics, Cleveland, OH) capable hardware integration and communication, rapid data collection and processing. The software package has a library of transformations based major joint areas (ex. spine, knee, foot) for replicating biofidelic motions. All of the MARS hardware components include: the robot's actuators and load cell, tendon linear actuators and load cells, and a coordinate digitization arm are interconnected and can actively communicate through simVitro. The software allows for the simultaneous control of tibia kinematics, ground reaction forces, and muscle forces. Each simVitro module contains information for different joints in the body, defined by coordinates that are digitized, for instance the foot and ankle module was used with the MARS, requiring digitization of the International Society of Biomechanics (ISB) definition of the foot coordinate system (Wu et al., 2002). The robot is capable of both position and force control, from encoders on the robot's motors, and a control load cell mounted at either the end effector of the robot or in a platform with dynamic gravity transformation included when necessary. The actuators are only capable of force control, with the control load cells mounted in between the actuator and tendon along a guide ring.

SimVitro uses a system of states to quantify unique measurements in a system. States are transformed based on a desired joint coordinate system (JCS). The system needs two states to operate, one based on JCS kinematics, from the robot position, and the other based on JCS kinetics, based on a six degree of freedom load cell. For all states, digitization of spatial relationships is required. For the MARS system specifically, a Romer Absolute Arm 7340 (Hexagon Metrology) was used for point digitization. The motion of the robot and axes of the load cell are recorded via the digitization arm this allows for the software to create transformations between the kinematics of the robot and kinetics from the load cell to the desired JCS (Equation 1).

$$\boldsymbol{T}_{RB1,RB2}(\vec{x}) = \boldsymbol{T}_{SENS1,RBI}^{-1} * \boldsymbol{T}_{WORLD1,SENS1}^{-1}(\overrightarrow{p_1}) * \boldsymbol{T}_{WORLD1,WORLD2} * \boldsymbol{T}_{WORLD2,SENS2}(\overrightarrow{p_2}) * \boldsymbol{T}_{SENS2,RB2}$$

$$Where\text{: } \vec{x} = Kinematic\ State$$

$$\overrightarrow{p_1} = Sensor\ 1\ Position$$

$$\overrightarrow{p_2} = Sensor\ 2\ Position$$

The $\boldsymbol{T}_{WORLD1,WORLD2}$ matrix can be an identity matrix, which indicates that World 1 and World 2 are the same location and orientation. However, having this matrix in the kinematic chain provides the necessary flexibility to allow two distinct position measurement systems to work together to calculate a kinematic state (Figure 3-4). In the generic instance of this class, the kinematic state is reported using X, Y, Z, roll, pitch, yaw conventions for translations and rotations. However, these methods can be modified to suit the conventions for the specific rigid bodies, for example, the Z direction being defined as superior motion of the foot.

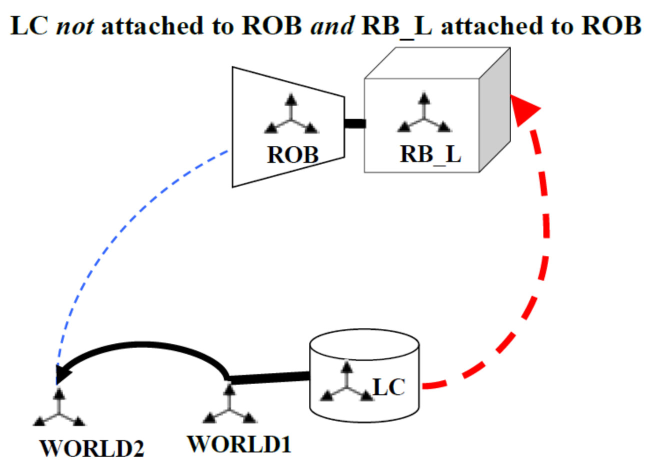

Figure 3-4: Diagram representing kinematic chain used by robot defining all coordinate systems and their relationships, where ROB is the robot, RB_L is the attached load (leg), LC is the load cell, and World 1 is the point digitization arm and World 2 is the robot's own coordinate system

Tests conducted through the software are called trajectories. Trajectories set all of the parameters necessary for the robot and actuators to perform a test. Information on desired kinematics or kinetics are supplied for the system to attempt to recreate. Parameters such as which control mode the test is performed in, gains for the control loops, and desired values for other actuators can also be supplied. Additionally, inputs can be changed based on previous test data and optimization routines.

3.1.8 Robot Control

The robot is capable of both a position and a force control mode. Each control loop is handled by a proportional, integral, derivative (PID) control scheme, commonly used for application requiring constantly modulating control. Current robot position or force from the control load cell is compared to the desired value, and an error between the curves is assigned. Using the values of the different gains, P gain, I gain, and D gain respectively, a correction of increased or decreased current is sent to the robot motors to move it close to its desired setpoint. The control loop is handled by the host SimVitro computer, and its changes are sent to the Kuka control PC to modify robot position.

3.1.9 Actuator Control

The actuators are controlled through a similar, but separate process as the robot. Again, a PID control loop is utilized, but the system is only able to control actuators through force control. Each actuator has its own individual control loop, associated parameters, control load cell, and desired values. Control of the motors is handled through the SoftMotion software (LabVIEW, National Instruments). A requirement for the muscle actuator system was being able to work off a LabVIEW system, as all of the SimVitro software is written in LabVIEW. The AKD motor drivers work natively with SoftMotion. As opposed to the robot control, the host SimVitro computer only passes along the time history to another controller. An off-board control system (cRIO-9035, National Instruments) was used to handle the PID control loop and SoftMotion motor control. Whereas decisions on how to change the system for the robot are made on the SimVitro computer, decisions on how the change the actuators are done on the off-board control system.

3.1.10 Optimization

The SimVitro software allows for the application of what is called "adaptive compensation". These mathematical schemes allow the user to create optimization routines using any number of input and output channels. These mathematical models can be made as complicated or simple as the user desires. For this application, a reduction of model error was chosen. A difference in the desired value versus the current setpoint was calculated and then multiplied by a weighing factor to create a change that has a physical meaning, for example changing position of the robot or changing the amount of force pulled in a tendon, a more in depth is given in Section 3.2.4. This model was similar to the PID control loop that was controlling the robot dynamically; however, this model changes the trajectory after each simulated gait trial, and utilizes only one weighting parameter.

3.2 Methods

An initial investigation on a small testing cohort, one matched pair, was conducted before the first study was conducted to investigate the capabilities of the assembled system and check if the specimen preparation was sufficient.

3.2.1 Specimen preparation

Post-mortem human surrogates (PMHS) were used in experiments performed to evaluate the system. The tissue donations were obtained and treated in accordance with the ethical guidelines established by the United States National Highway Traffic Safety Administration (NHTSA), and all testing and handling procedures were reviewed and approved by an institutional review board for human surrogate use at the University of Virginia. Specimen were dislocated at the knee joint, separating the femur from the tibia and rest of foot. 65 mm of tissue was removed from proximal end of tibia to allow for attachment of potting cup and potting material (Figure 3-5).

Figure 3-5: Specimen dislocated at the knee joint, with window of tissue removed at proximal tibia for attaching potting cup.

To preserve the natural motion of the fibula relative to the tibia, five ounces of plumber's putty (Oatey, Cleveland, OH) was molded around the fibula, enough to cover the fibula from all of the potting material. A six-inch diameter, four-inch deep, cylindrical potting cup was attached to the proximal tibia with wood screws and Fast Cast. Four steel No. 8 one-inch long wood screws were driven into the tibia to provide rigidity to the connection between the potting cup and the bone. Two screws were driven down into the tibial plateau, one in the center of the plateau and the other in the medial aspect of the plateau. The third screw was then driven into the tibial tuberosity from the front, and the fourth was driven into the medial plateau from the medial side. Six inches of R1 Fast Cast #891 (Goldenwest Manufacturing) potting material was then poured into the potting cup until the cup was full. Approximately 150 mm of tissue was removed circumferentially around the ankle 20 mm above the malleoli to expose the tendons of the muscles of the leg, and to ensure that the retinaculum below the malleoli was not disturbed (Figure 3-6).

Figure 3-6: Specimen with open window for attachment to the tendons

Eight of the nine actuators were then affixed to tendons using polyester surgical thread (BA028, Mopec) with a Krakow stitch, used typically for tendon reconstruction surgeries. Due to the greater magnitude of force required, the Achilles was clamped using a custom cryoclamp (Figure 3-7). Connects to the tendon actuators was further explained in Section 3.1.5.

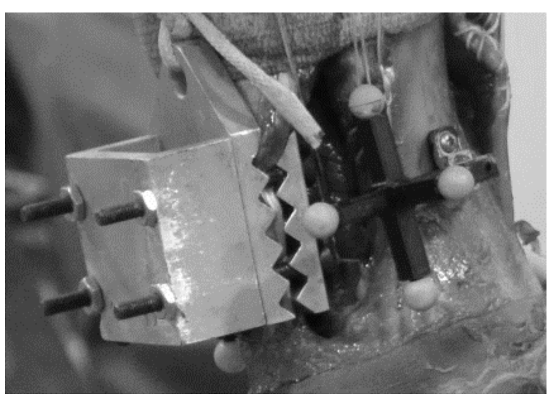

Figure 3-7: Specimen with attached Achilles cryoclamp, before being frozen.

3.2.2 Achilles Freeze Clamp

The freeze clamp consists of three parts. Two interlocking gripping plates that when tightened allow for gripping of the Achilles tendon, and a removable back piece that allowed for the containment of dry ice (Figure 3-8). The plates and back plate could then all be bolted together around the tendon. Aluminum was used due to its very high conductivity, transmitting the cold fast than that of steel. The clamp was filled with dry ice until frost visibly collected on the clamp.

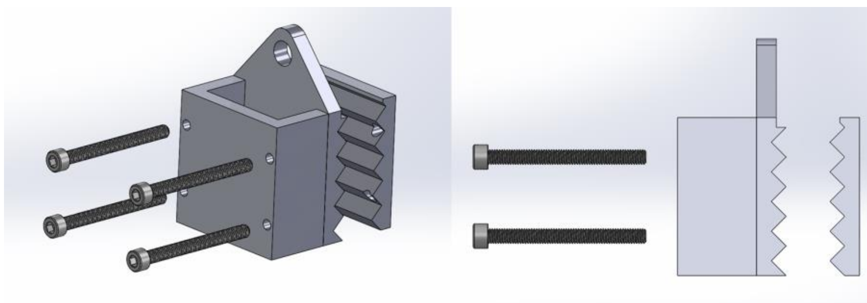

Figure 3-8: 3-D rendering of Achilles Freeze Clamp

3.2.3 System Input

Inputs to the system are a six degree of freedom time history of tibia kinematics, three translations and three rotations, and nine time histories of muscle forces. Both of these inputs are derived from data available in the literature.

3.2.3.1 Tibia Kinematics and Reaction Forces

Lee & Davis (2009) investigated the effects of diabetes on midfoot joint pressures using the Cleveland Clinic's Universal Muscle Simulator. For the study, kinematics were collected from a single volunteer at the Cleveland Clinic's gait laboratory, via a motion capture and force plate system. Eleven markers were attached to the subject's right leg to determine joint coordinate system and the three dimensional translation and rotations between the moving tibia and the stationary ground. The subject walked along a straight line at an average speed of 1.5 m/s. The desired tibia kinematics (Figure 3-9) and GRF curves (Figure 3-10) were generated by averaging the 10 walking trials. For reference, the global coordinate systems follow the body planes, x being anterior/posterior direction with rotations in the coronal plane, y being medial/lateral direction with rotations in the sagittal plane, and z being the superior/inferior direction with rotations in the transverse plane.

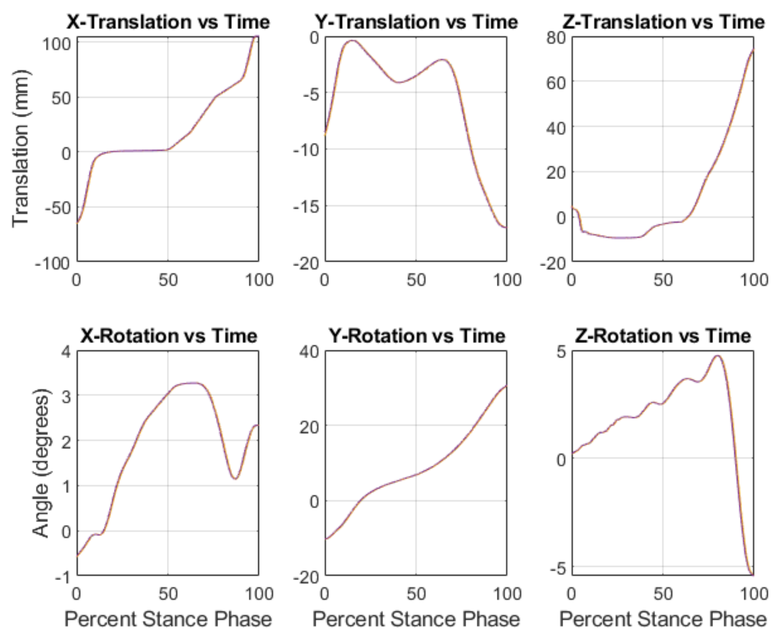

Figure 3-9: Average location (top) and orientation (bottom) of the tibia with respect to a fixed global reference frame from a volunteer experiment (Lee & Davis, 2009). This data was used as the input kinematics in the experiment described in this chapter.

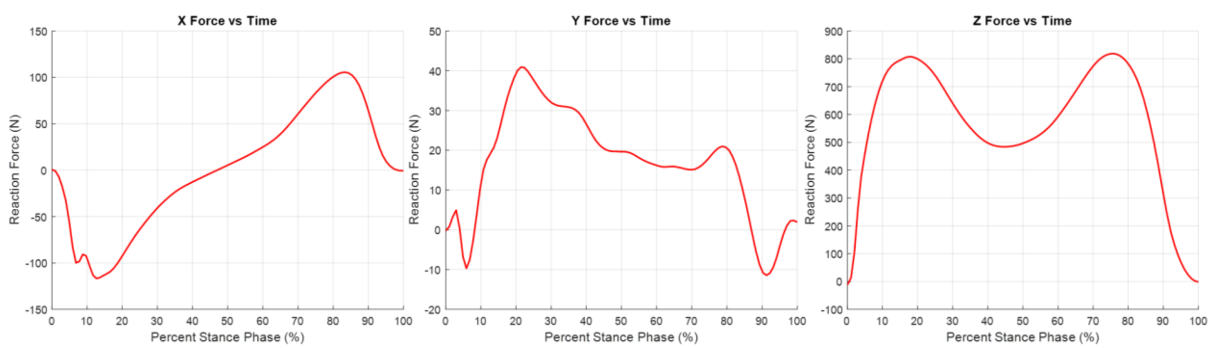

Figure 3-10: Average ground reaction forces with respect to a fixed global reference frame from a volunteer experiment (Lee & Davis, 2009). This data was used as the desired kinetics in the experiment described in this chapter.

3.2.3.2 Muscle Force Time Histories

Perry (1992) presents surface EMG measurements on the muscles in the leg during gait. Estimation of the muscles forces were made based on individual muscles cross sectional area, and specific tension (Fukunaga et al., 1996; Wickiewicz et al., 1983). Timing of the muscle pull was based on when the muscle was activated from the EMG measurements (Figure 3-11). Details on the Perry (1992) data are sparse, with no mention is made of how many volunteers were used to collect this data.

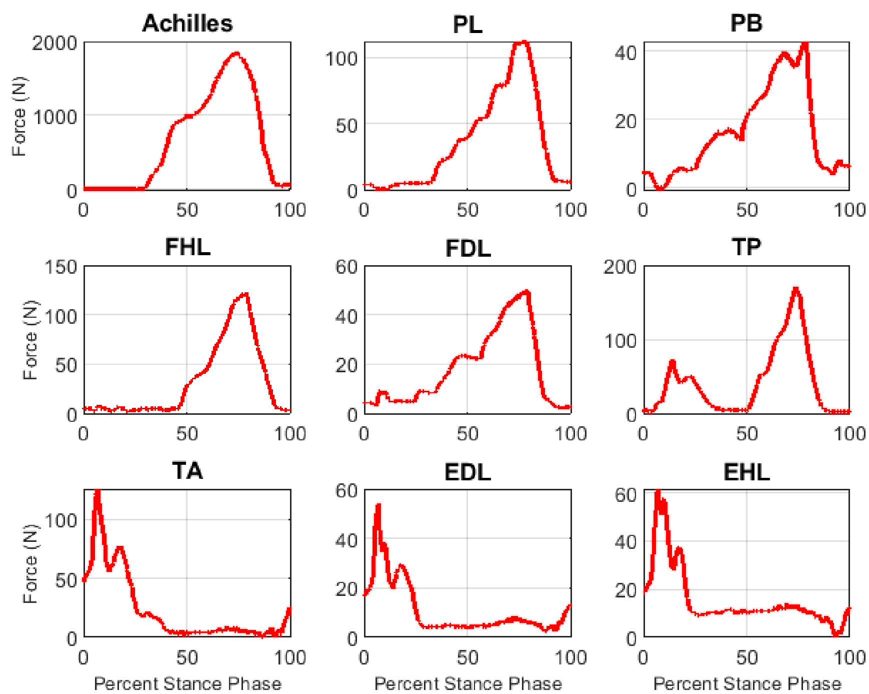

Figure 3-11: Muscle force time histories; TOP: Achilles, peroneus longus, peroneus brevis. MIDDLE: flexor hallucis longus, flexor digitorum longus, tibialis posterior. BOTTOM: tibialis anterior, extensor digitorum longus, extensor hallucis longus. Based on EMG data from volunteer experiments from (Perry, 1992) and cadaveric data on individual muscle specific tension and cross sectional area (Fukunaga et al., 1996; Wickiewicz et al., 1983).

3.2.4 Optimization Methods

Ten to fifteen training runs were used to create the final trajectory used for data collection runs. The averaged input tibia kinematics, and muscle force time histories are used as the first training run. The desired objective of the optimization is the match the experimental vertical GRF with the recorded vertical GRF from the volunteer experiments. In total fifteen parameters could be changed to match the desired force, six kinematics positions of the tibia, and nine different muscle forces. To reduce the complexity of the optimization problem, only three parameters were changed during three distinct time windows during training runs. Specifically, the three parameters are force in the tibialis anterior, superior position of the tibia, and force in the Achilles tendon were changed during the first 30% of stance phase, for the next 30%, for the last 40% respectively (Figure 3-12). Each training runs updates these three parameters until vertical ground reaction force is within 20% error of the desired vertical GRF.

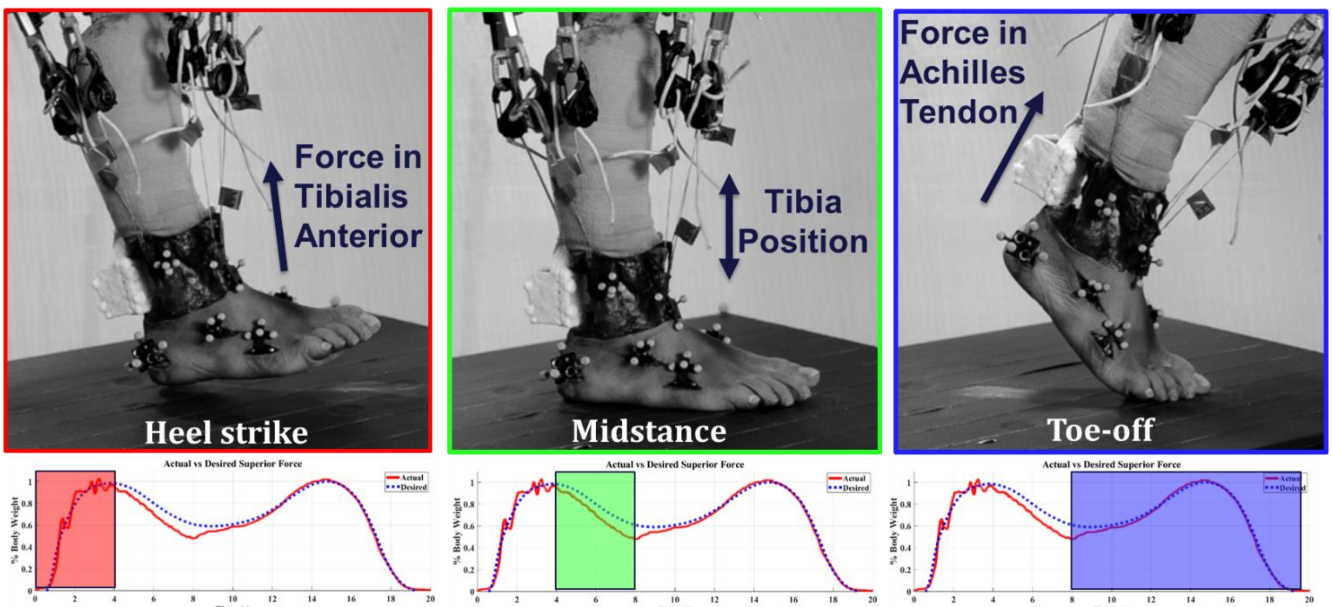

Figure 3-12: Depiction of different phases of gait and the optimization occurs at each point.

These parameters and regions were chosen based what is available in the literature, determined by previous by previous robotics gait simulators (Aubin et al., 2012). The regions of interest are heel strike, midstance, and toe off. During toe off, the Achilles was dominant, counteracting the standing weight and pulling the foot up off the ground. The tibialis anterior, as the main dorsiflexor, fulfills a similar role to the Achilles, only at the beginning during heel strike. During midstance, no single muscle force drives the response. Due to the large motions of the tibia during this phase of stance, the vertical position of the tibia was used as the optimization parameter.

3.2.5 Motion Tracking

In order to capture bony kinematics, an optical 3D motion tracking system was used (VICON MX 3D). Ten motion tracking IR-emitting cameras were positioned around the robotic test system base such that the camera capture volume included the entire range of motion of the specimen in all testing states. Custom 3D motion tracking arrays, capable of each holding four 4 mm diameter spherical retroreflective motion tracking markers, were designed for each bone-specific mount and manufactured by a monofilament printer (Figure 3-13). The retro-reflective markers were then affixed to each marker array via M4 plastic all-threaded rods that has been glued into the arrays. Once assembled, each marker array was rigidly affixed to its respective bone, with the base screwed in using a number 4 wood screw, and the array glued into the base.

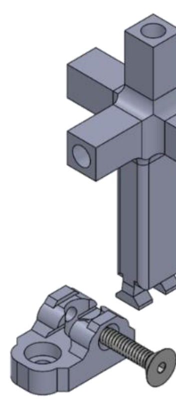

Figure 3-13: 3-D rendering of motion tracking array with base and detachable standoff component

A small 20 mm incision was made on the following target bones (and attachment location): tibia (mediodistally), fibula (laterodistally), calcaneus (lateral body), talus (anterior aspect of talar neck), navicular (dorsal tuberosity), cuboid, first metatarsal (dorsal mid-diaphysis), and fifth metatarsal (dorsal mid-diaphysis), for attachment of the motion tracking marker arrays (Figure 3-14).

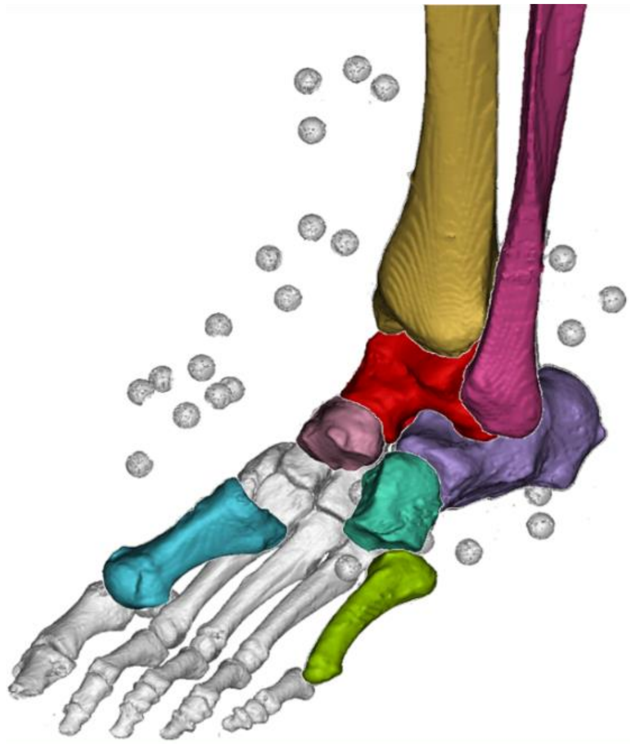

Figure 3-14: Visualization of bones in foot that were tracked via motion capture system.

3.2.6 Data Collection and Processing

The coordinate system of the tibia was initially created and used for all tracked bones. Using anatomic landmarks, shown as Points 1-4 (Figure 3-15), midpoints were calculated between the medial and lateral malleolus, and of the medial and lateral points on the tibial plateau, shown as points 5 and 6. A mid-tibia origin (point 7) was then set by finding the midpoint between points 5 and 6. A temporary anatomic positive Y-axis was created by averaging the slopes of the lines that connect the medial and lateral malleolus and the most medial and most lateral points on the tibial plateau. The axis started at the origin, and pointed medially for a right leg and laterally for a left leg. Anatomic positive Z-axis, always pointed distally. The Z-axis was calculated by subtracting the midpoint of the medial and lateral malleolus (point 5) from the midpoint of the medial and lateral points on the tibial plateau (point 6). Anatomic positive X-axis, points out of the page (anteriorly) and is calculated by taking the cross product of the positive Y- and Z-axes. Finally, to ensure an orthogonal coordinate system, the Y-axis was redefined as the cross product of the Z- and X-axes (Z x X).

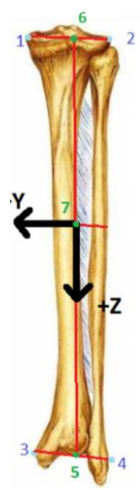

Figure 3-15: Tibia fixed coordinate system definition [Note +X points out the page].

Prior to the first test, the specimen and its rigidly affixed marker arrays, were digitized in a pretest CT scan. This CT scan was critical as it allowed for the calculation of:

1) the centroid of each target bone,
2) the projected tibial coordinate system onto each target bone, and
3) the rigid-body transformation relating each respective marker array coordinate system to the anatomic ISB coordinate system (Wu et al., 2002).

Finally, prior to testing each day, a laboratory reference frame was established using motion-tracking targets attached to the plane of the platform. This allowed the creation of a rigid-transform between all anatomic coordinate systems this lab reference frame, with the anterior direction being +X, medial direction being +Y for right specimens and lateral direction being +Y for left specimens, and superior direction being +Z. Finally, all of the bone motions were reported in the lab reference frame. It is important to note that, the coordinate systems of the foot used by the robot (ISB) and the global laboratory space are askew (Figure 3-16). VICON data was captured at 250 frames per second for all specimen.

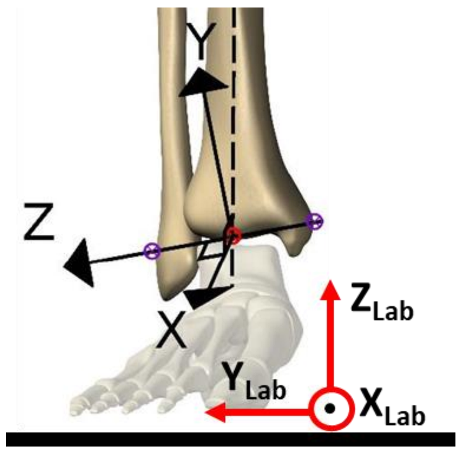

Figure 3-16: ISB coordinate system definition (Black) used in SimVitro shown with respect to Laboratory plate coordinate system [Note misalignment between YZ in the Lab coordinate frame and ZY in the ISB coordinate frame].

3.2.7 Testing Conditions

The left and right lower extremities from a single male PMHS were used (46 years, 99.3 kg, 175.3 cm) to evaluate different body weight conditions and gait cycle times conditions, and their potential effect on bony kinematics response. For the right lower extremity, target vertical GRF was scaled to 25%, 50%, 75% and 100% body weight (BW) over a ten-second stance phase (Figure 3-17). 100% BW is defined based on a 50th percentile male, 75kg, approximately 750 N.

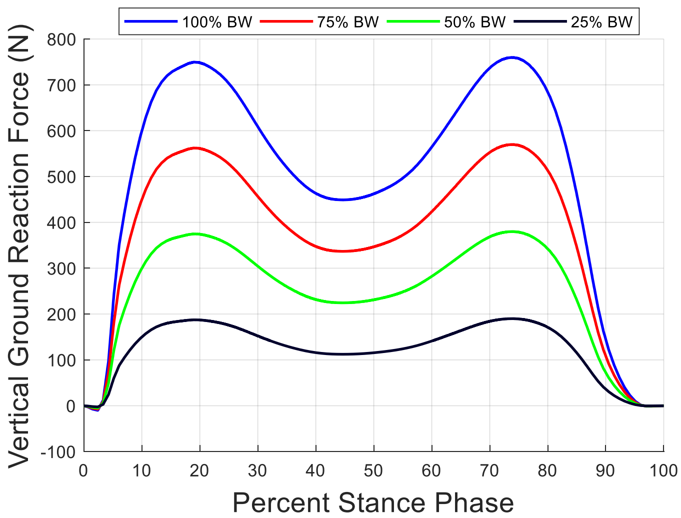

Figure 3-17: Target vertical ground reaction forces from 100% BW (Blue) to 25% BW (Black) in 25% BW increments.

For the left lower extremity, all inputs and targets were scaled temporally to create 20 second, 10 second, 6 second, and 4 second stance phase at 25% body weight (Figure 3-18).

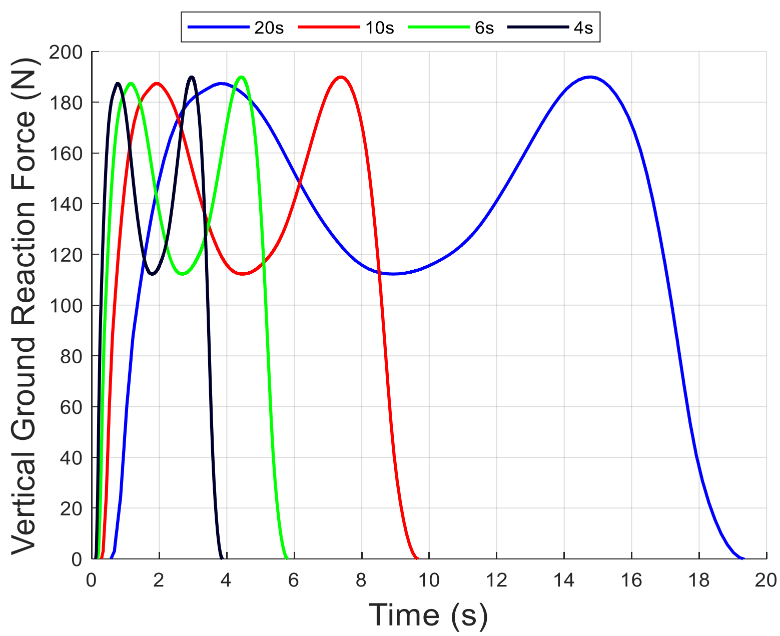

Figure 3-18: Target vertical ground reaction forces from 20s (Blue) to 4s (Black).

3.3 Results

First the response of the system was looked at, to determine if the hardware was capable of achieving the desired gait characteristics, body weight or stance phase. An average was created from three repeated walking trials, and it plotted against the desired vertical ground reaction force for both the change in body weight test conditions (Figure 3-19) and the change in stance phase test conditions (Figure 3-20)

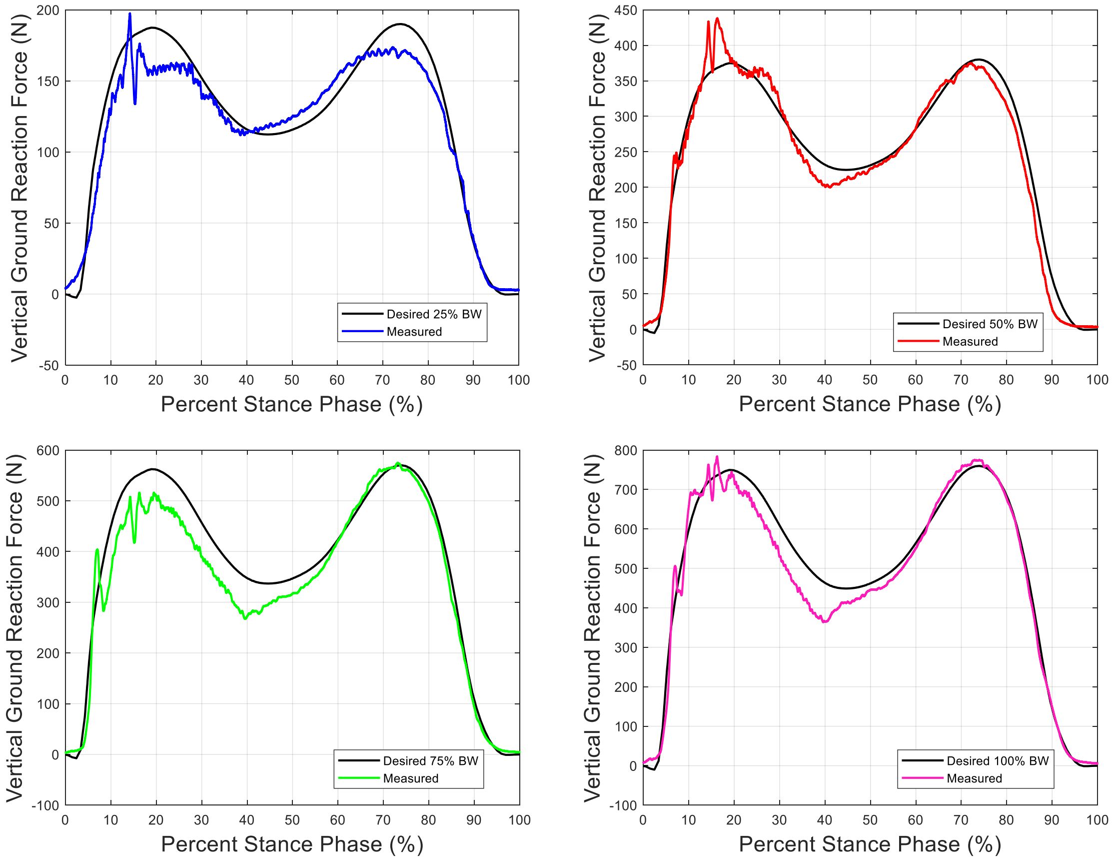

Figure 3-19: Desired vs measured vertical GRF for the change in test BW conditions TOP RIGHT: 25% BW condition, TOP LEFT: 50% BW condition, BOTTOM LEFT: 75% BW condition, BOTTOM RIGHT: 100% BW condition

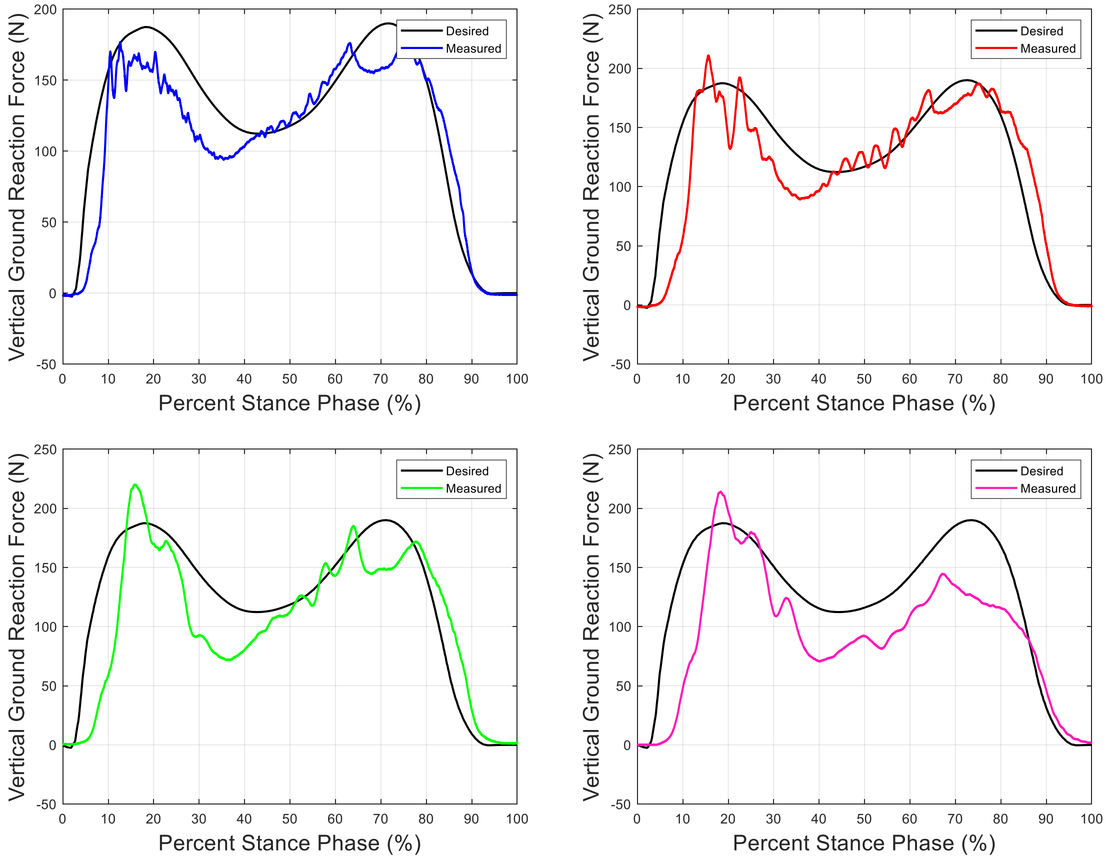

Figure 3-20: Desired vs measured vertical GRF for the change in test stance phase time conditions TOP RIGHT: 20 second condition, TOP LEFT: 10 second condition, BOTTOM LEFT: 6 second condition, BOTTOM RIGHT: 4 second condition

To determine the effect of the testing conditions on bony kinematics, three joints and their primary motion was investigated: eversion in the subtalar, plantarflexion in the talocrural, and rotation in the talonavicular joint (Figure 3-21). These joints were chosen based on a validation study done by the Hospital of Special Surgery (Baxter et al., 2016).

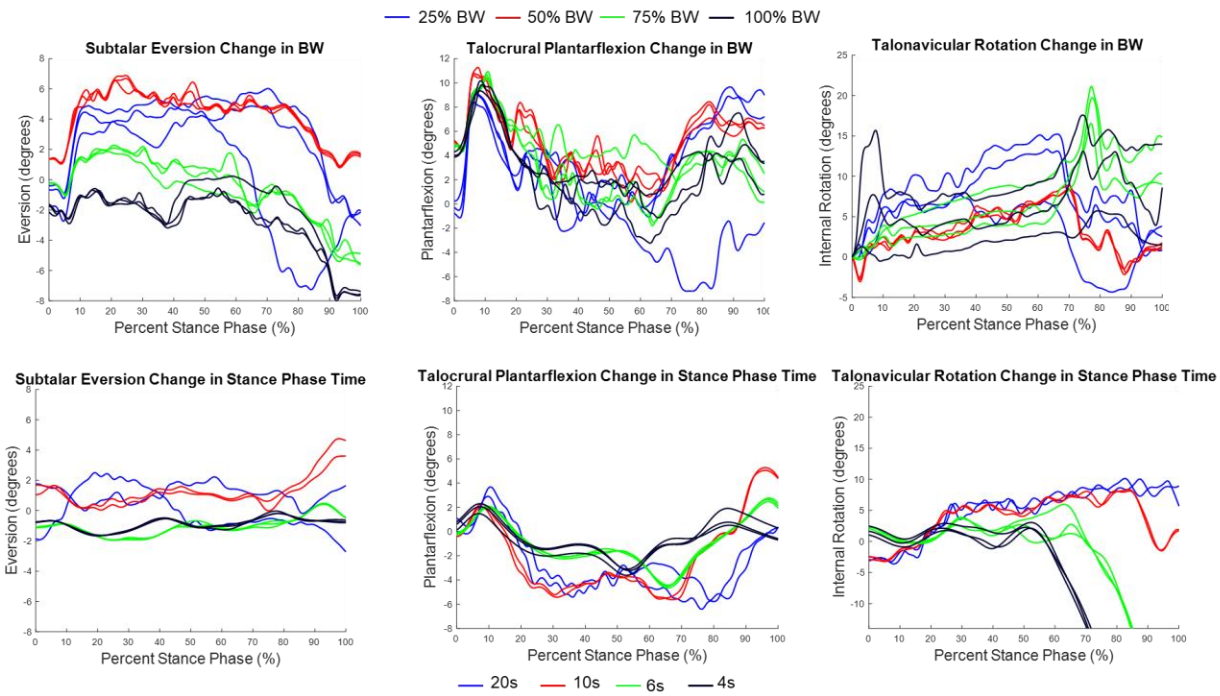

Figure 3-21: TOP: Differences in bone kinematics for the BW conditions. TOP LEFT: Subtalar eversion, TOP MIDDLE: Talocrural plantarflexion, TOP RIGHT: Talonavicular rotation. BOTTOM: Differences in the bone kinematics for the stance phase time conditions. BOTTOM LEFT: Subtalar eversion, BOTTOM MIDDLE: Talocrural plantarflexion, BOTTOM RIGHT: Talonavicular rotation.

Through optimization during the 100% body weight condition, the system was able to reliably reproduce the target input, within 5% error, and nominally bring the vertical GRF during heel strike close to the target, within 15% of the desired vertical GRF (Figure 3-22). The system performed similarly in tests using the other BW conditions, with the greatest amount of error occurring during heel strike, and the least amount of error during toe off. Tibia kinematics were likewise very repeatable with position and angles within 1 mm and 0.1 degree respectively.

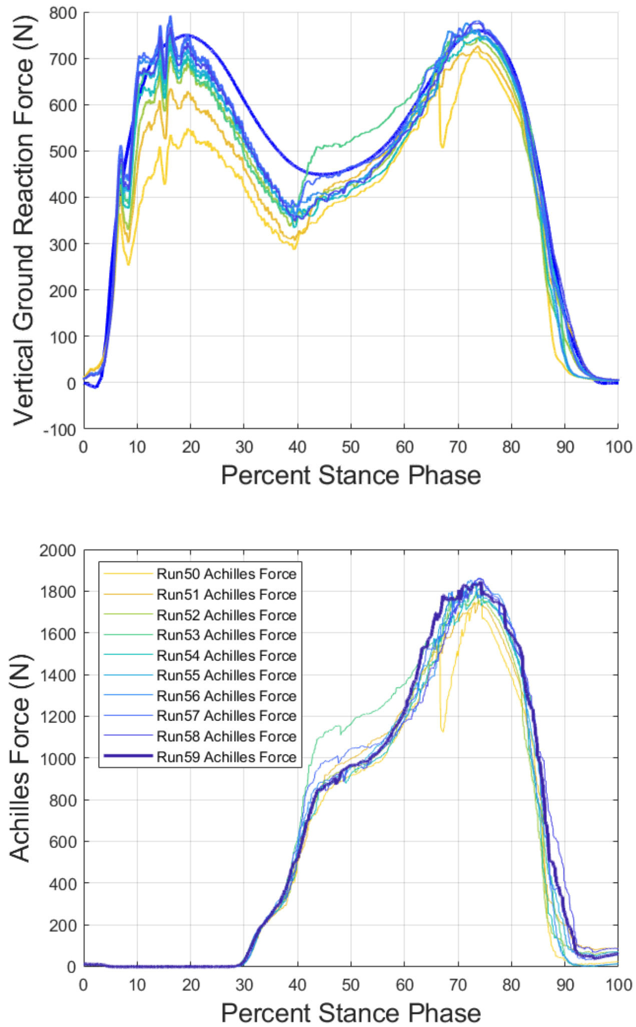

Figure 3-22: TOP - Desired GRF vs measured GRF for multiple optimization runs vs time in 100% BW condition. BOTTOM - Demonstration of optimization routine showing desired Achilles force vs. measured Achilles force.

The specimen were not damaged over the course of testing, even after approximately one hundred gait trajectories were completed for each specimen. Over the course of testing, there were no issues with tendon disintegration, although by the final day of testing it was noted the tendons were visibly pulling further away from core of the specimen.

3.4 Discussion

To determine the usefulness of the system, a set of standardized testing parameters needed to be determined to investigate further if the system is capable of outputting realistic bony kinematics. Previous gait simulators have been unable to test at true gait conditions, 100% body weight and around 0.7-second stance phase, with many running at 25% BW and around a 3-second stance phase. The system developed in this thesis is unlike previous gait simulators, using a new style of robotic system to prescribe tibia kinematics. This initial testing looked at different BW and stance phase test conditions to determine what is possible with this new system.

First looking at the change of BW data, the system was able to reasonably replicate all of the desired vertical GRF conditions, including 100% BW. This is important to note as other simulators run at 25% BW. In the higher BW conditions, 75% and 100%, a small distinct single peak in vertical GRF occurs around 10% of stance phase. This is potentially due to the heel sliding with respect to the force plate. The 25% and 75% BW conditions showed the system slightly underperformed just after heel strike, while the 50% and 100% BW conditions show that the system closely matched the desired BW condition. With more optimizations, the system could have been tuned better in the 25% and 75% BW conditions. The decision to do a limited number of optimization runs means that the system response may not perfectly match the desired vertical GRF, but the specimen can only be out for a limited amount of time before tissue degradation becomes an issue. As testing continued, it was noted that the tendons began pulling out further from the core of the specimen as if stretching under the repeated loading. No visible damage was noted on any of the tendons, and none of the tendons was disrupted.

Looking at the change of stance phase data, the system had a much harder time matching the desired vertical GRF across all testing conditions, with the fastest condition (4 seconds) performing the worst. This is primarily due to control system limitations of the assembled system. In the 4-second case the Achilles force was lagging, this can be seen in to the measured vertical GRF missing the second peak. The Achilles was only active during the last 40-50% of stance phase, giving the system around 2 seconds to reach the desired load, including accelerating and decelerating. This condition was also only at 25% BW, which was the lowest BW condition the system could achieve. Further exploration of the control system should be taken to improve system performance to match the in vivo stance phase time.

Looking at the joint rotations recorded, changing the BW condition seems to have the greatest effect. Between the 25% BW and 100% BW: eversion in the subtalar joint was decreased by 3 degrees just after heel strike, the flexion in the subtalar was decreased by 4 degrees during toe-off, and the rotation in the talonavicular joint was increased around 10 degrees. While the change in stance phase shows a large decrease in rotation during toe off in the talonavicular joint, this can be attributed more to noise in the motion tracking data. The marker arrays are more clustered in the middle foot and with the increasingly rapid motions of the change in stance phase, test conditions made the data for this joint unreliable. The change in stance phase had little effect on the other joints, with a group deviation around 2 degrees for both the eversion in the subtalar joint and the flexion in the talocrural joint. Additionally, the stance phase test conditions were more variable with how well they matched the desired vertical GRF when compared to the change in BW test conditions.

3.5 Conclusions

The goal of this chapter was to develop a robotic gait simulator capable of moving the foot relative to the ground in a realistic orientation under varying body weight conditions. A 6-DOF serial robot gait simulator, nine force controlled tendon actuators, real-time controllers, and PMHS lower extremity were integrated to create a robotic gait simulator. Through a study looking at the changes of bony kinematics based on different body weight and stance phase test conditions, the simulator was able to reliably recreate desired body weight conditions at slower stance phase times (greater than 10 seconds). Additionally, the resulting joint kinematics show a greater difference due to changes in body weight than changes in stance phase time. The next chapter will outline the next goal of the thesis, by conducting a test with a larger cohort of specimen to determine if the foot bone kinematics are repeatable.

4. Capturing Bone Kinematics

The goal of this chapter is to present the material needed to address the second goal of this thesis: to use the simulator to capture repeatable foot bone kinematics. To determine the repeatability of the bone kinematics, an investigation of repeated trials across five different specimen was conducted.

4.1 Methods

4.1.1 Testing Conditions

Five PMHS lower extremities were prepped using the same method described in Section 3.2.1 (Table 4-1).

Table 4-1: Subject anthropometry

Subject Anthropometry						
	Subject #	930R	901R	662R	662L	815L
	Weight (kg)	74.4	73.9	75.0	75.0	74.4
	Height (mm)	1778	1778	1730	1730	1778
	Measurements from CT (mm)					
1	Tibial Height	392	421	392	390	402
2	Ankle Height	98	98	101	102	97
3	Foot Breadth	90	97	93	92	111
4	Foot Length	227	268	249	245	276
5	Heel Pad thickness	9	8	15	15	11

Weight and height were taken from when the PMHS was initially acquired. The rest of the measurements were taken from the pre-test CT. Tibial height was defined as the length from the midpoint of the tibial plafond to the midpoint of the tibial plateau. Ankle height was measured as the distance between the most distal point of skin under the heel to the most proximal point on the talus. Foot breadth was measured as the distance between the most medial point of the first metatarsal to the most lateral point of the fifth metatarsal. Foot length was measured from the most posterior point on the heel to the most anterior point on the first phalange. Heel pad thickness was measured as the distance between the most distal point on the heel and the skin underneath it.

From the initial investigation, three changes were made to the testing methodology. First, two sutures were braided into the tibialis anterior. The optimization routine for 100% BW increased the force in the tibialis anterior higher than just a single suture could handle. Second, to prevent the foot from sliding during toe off the optimization was updated to account for anterior shear. The anterior ground reaction force optimization is similar to how the tibia position is changed based on the error to the desired vertical GRF. Anterior translation was changed based on the error in the anterior GRF, and was allowed to change during the entire stance phase. Third, the origin for the bony coordinate systems was modified to reflect the origin of the bony coordinate systems in the Lundgren data. The original method of creating the origin was determined to be not consistent between specimens. This is primarily due to the coordinate system for the CT being defined arbitrarily. Lundgren, prior to data recording, took a static capture of the volunteer in a neutral posture. The neutral posture was used as the origin for all of the bony coordinate systems. No static capture was taken on the tested specimen to replicate this procedure; however, an assumption was made that the specimen must pass through this neutral posture during the gait cycle. This was determined by finding when the long axis of the tibia was normal to a plane created by the markers on the walking platform, and this was found to be approximately at 33% stance phase (Figure 4-1).

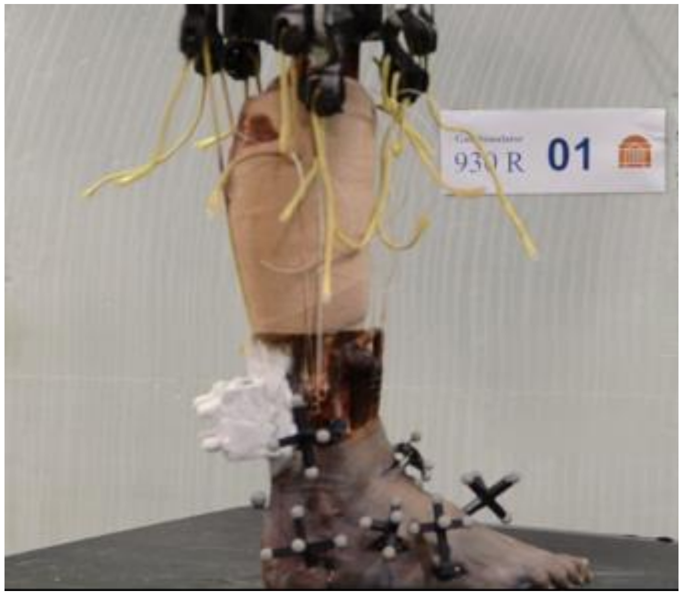

Figure 4-1: Specimen 662L mounted on the MARS during midstance.

Each specimen was tested in the 100% BW, 10-second gait cycle test conditions as these are the closest condition to normal human gait the robot can reliably achieve. 8-12 optimization runs were used before data collection was started. Each optimized trajectory was repeated three times to check the repeatability of the system.

4.2 Results

With every trial, a 6 degree of freedom time history of the recorded tibia position was created (Figure 4-2). Additionally, the GRFs were recorded (Figure 4-3).

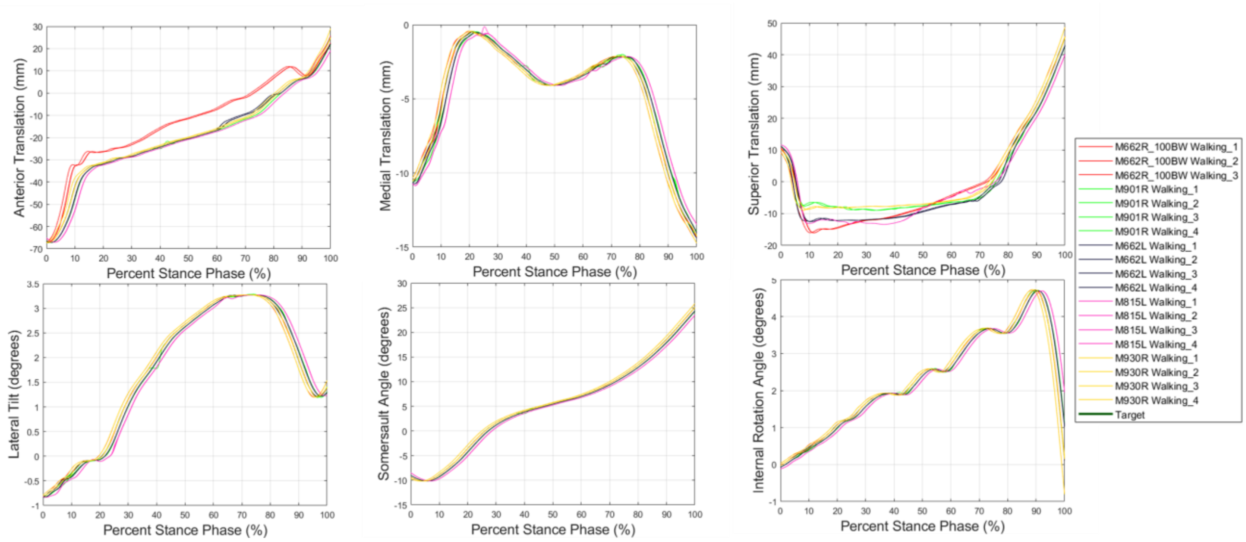

Figure 4-2: Recorded tibia kinematics for each specimen. TOP LEFT to TOP RIGHT: Anterior translation, Medial translation, Superior translation. BOTTOM LEFT to BOTTM RIGHT: Lateral tilt (eversion), Somersault angle (plantarflexion) and internal rotation.

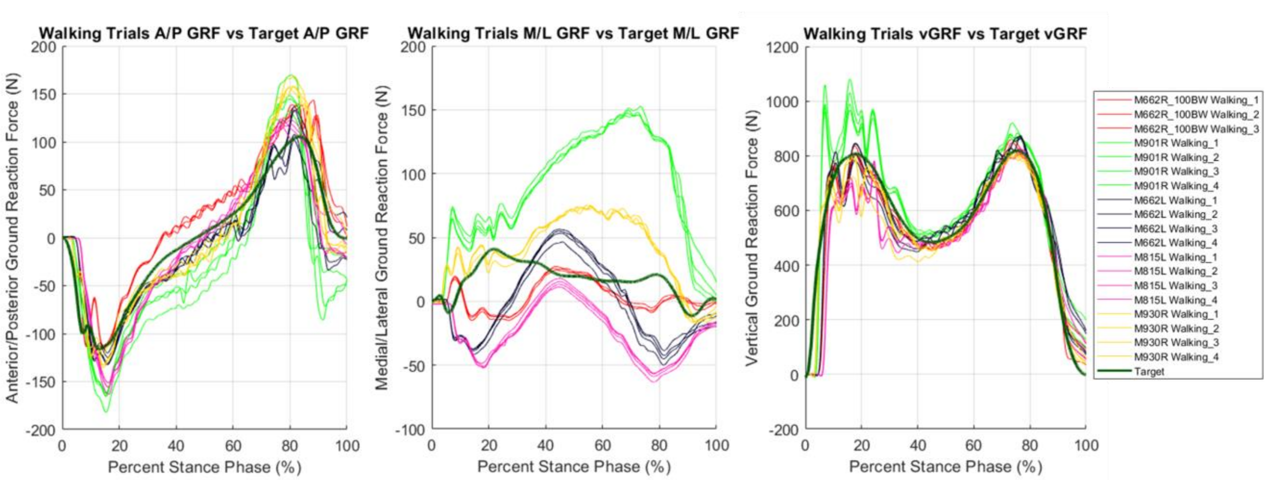

Figure 4-3: Recorded GRFs versus target for each specimen during walking trials. LEFT: Anterior/Posterior GRF. MIDDLE: Medial/Lateral GRF. RIGHT: Vertical GRF.

Appendix A displays each of the optimization trajectories that lead up to the data collection walking trials. The superior force and all of the optimizations runs are plotted along with the accompanying tibialis anterior force, tibia superior position, and Achilles force trajectories that result in the superior force (Figure 4-4). The anterior force and all of the optimization runs are plotted along with the accompanying tibia anterior translation (Figure 4-5). For the forces, a dark line is plotted showing the desired force for that run. Each of the other plotted lines are a different optimization run, plots without the desired line are changed in the optimization to reach the desired force.

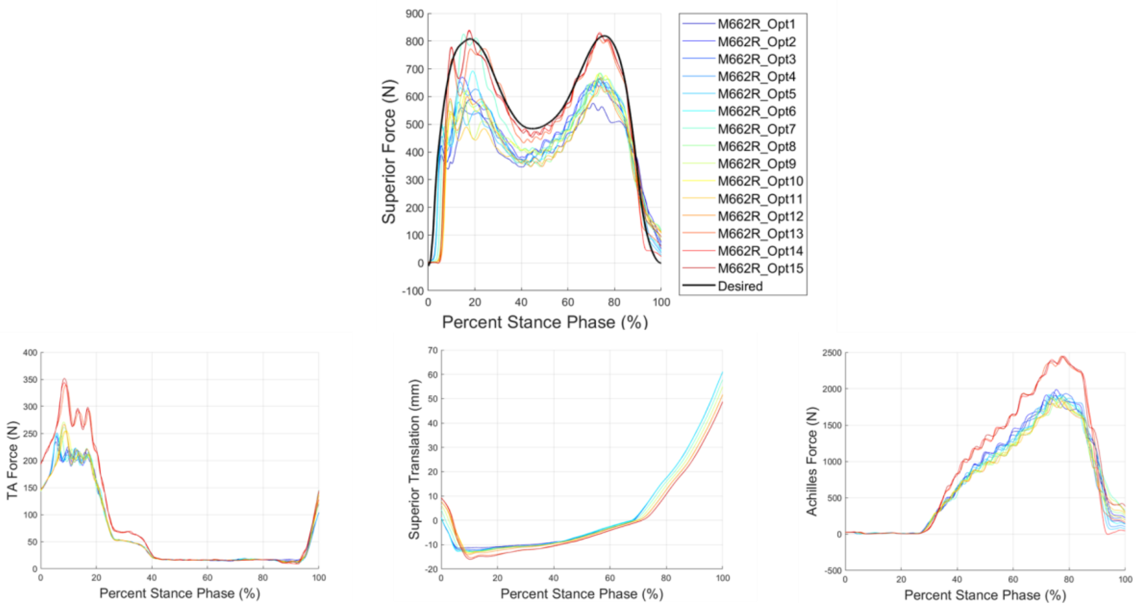

Figure 4-4: TOP: Superior force in optimization runs and desired superior force. BOTTOM LEFT: Tibialis force optimization runs, BOTTOM MIDDLE: Tibia superior translation optimization runs, BOTTOM RIGHT: Achilles force optimization runs.

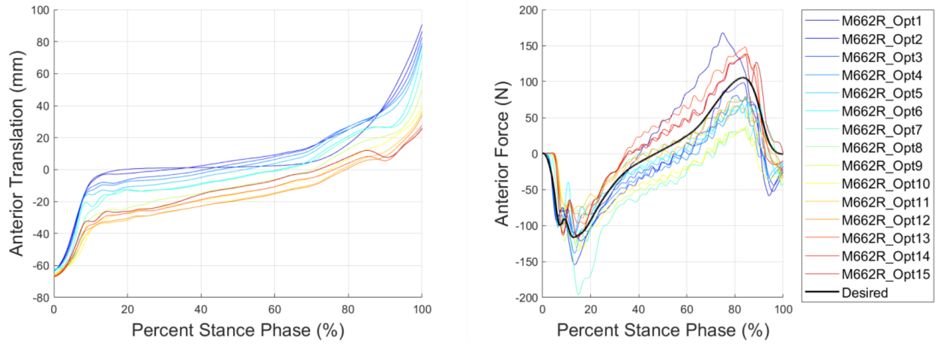

Figure 4-5: LEFT: Tibia anterior translation optimization runs, RIGHT: Anterior force in optimization runs and desired anterior force.

Additionally, bone kinematics data was captured from each repeated walking trial. To determine repeatability, representative averages were constructed from each of the repeated walking trials for each specimen. Each of the repeated walking conditions were then compared to these representative averages using the correlation and analysis tool (CORA, Gehre et al., 2009). CORA compares two signals using the Phase, Size, and Progression of one signal to another and scores each category out of one, where one is a perfect correlation. Phase is a score based on how in-phase the peaks of the desired signal and a representative average of the corridor. Size is a score based on the magnitude at every point between the desired signal and the repetitive average of the corridor. Progression is a score based on a point-to-point cross correlation to compare the shape of the two signals. The Correlation total is a weighted average of 25% of the Phase Score, 25% of the Size Score, and 50% of the Progression Score (Table 4-2).

Table 4-2: Correlation totals for each bone pair in each kinematic direction

	TalinCalc	TalinTib	TalinNav	CubinCal	FifthMetinCub	FibinTib	FirstMetinTal	CalinTib	CubinNav	**Average**
X-Translation	0.945	0.973	0.950	0.960	0.896	0.966	0.936	0.968	0.942	**0.948**
Y-Translation	0.953	0.907	0.941	0.953	0.915	0.942	0.909	0.947	0.942	**0.934**
Z-Translation	0.935	0.950	0.941	0.965	0.917	0.955	0.955	0.961	0.925	**0.945**
Roll	0.984	0.960	0.988	0.985	0.968	0.958	0.988	0.984	0.984	**0.978**
Pitch	0.937	0.955	0.959	0.974	0.978	0.970	0.977	0.978	0.957	**0.965**
Yaw	0.975	0.946	0.976	0.984	0.977	0.980	0.956	0.971	0.969	**0.971**
Average	**0.955**	**0.949**	**0.959**	**0.970**	**0.942**	**0.962**	**0.953**	**0.968**	**0.953**	**0.957**

4.3 Discussion

Quantifying the bony motion of the foot and ankle during gait in a controlled and repeatable manner has the potential to increase understanding of its normal and even pathologic function to assist in clinical decision-making. The purpose of the study was to assess the ability of the MARS, a novel dynamic gait simulator, to replicate foot kinematics during simulated gait. Before the bony motion outputs can be considered, the system needed to be capable of reproducing biofidelic tibia kinematics and GRFs. The MARS system was accurately able to prescribe tibia kinematics within 1 mm of desired translations and 1 degree of desired rotations. Even though the system can replicate the input almost perfectly, it highlights a potential limitation of the system. The input kinematics are based around one person walking over averaged trials, and as shown by Lundgren *et al.* (2008), people have different gait patterns. Vertical GRF was matched within 20% of the desired force throughout stance phase, with the system having the most problem matching the first GRF peak from heel strike into midstance. System performance between the proof of concept and the system evaluation was noted to decrease. This is primarily attributed to the higher force that was seen in the tibialis anterior and its attached motor being too sensitive. During heel strike, the sudden impact would cause a rapid oscillation that the system was not able to quickly deal with. The tendon actuation system was able to control tendon forces; again, the input to the system is called into question as to how accurate it really is. A tradeoff was made for the system while the simulation velocity was approximately ten times slower than in vivo gait; the simulated GRF force was 100% of body weight. This is much slower than other gait simulators, but one of the only that is capable of reliably reproducing full body weight.

It is important to note that medial/lateral shear forces were not taken into account for the optimization routine. However, other than specimen 901R, the specimens are close to the magnitude of the volunteer recorded shear force.

Bone kinematics are also shown to be repeatable. The Correlation totals are all 0.89 or above, meaning that the repeated walking trials are representative of their averages, highlighting how repeatable the system is at repeated tests. Again, CORA scores are from zero to one, where one represents a perfect correlation to the compared system and a zero represents no correlation. The lowest score, of 0.89, was found to be the fifth metatarsal with respect to the cuboid in the X displacement. This could be attributed to proximity of the fifth metatarsal and cuboid marker arrays to one another. The motion capture data for the fifth metatarsal in particular was noisier than any other recorded bone. The displacements were consistently less repeatable than the rotations; this is primarily due to the Size Score. Since the Size Score is a point to point comparison of magnitude, and the relative rotations between bones is small, less than 5mm, small differences in magnitude greatly affect the Size Score. The Size Score is consistently lower for the translations than the rotations, primarily because the joints are able to rotate relative to one another much more than they can translate.

4.4 Conclusions

The goal of this chapter was to present the material needed to address the second goal of this thesis: to use the simulator to capture repeatable foot bone kinematics. An investigation using five specimen and repeated walking trials was used to determine if the bone kinematics were repeatable. Representative averages of the repeated walking conditions were created for each specimen. Each of the walking trials was compared to their respective average using CORA. CORA results in three individual scores and a weighted average. The weighted average, the Correlation Total, was used as the metric to determine repeatability. All of the Correlation Totals were greater than 0.89, with the average of the Totals being 0.957, where a one represents a perfect correlation between two signals. With the Correlation Totals being close to one, the repeated walking trials represent the average, and therefore each other. The next chapter will outline the last two goals of the thesis, to determine how gait-like the output bone kinematics of the system are, and to check if the generalized input used on the different specimen create similar outputs.

5. System Evaluation

Utilizing the data captured by the study done in Chapter 4, an investigation into the last two goals of thesis were conducted. First, the data was compared to the Lundgren bone pin study to determine how gait-like the output bone kinematics of the system are. Second, the generalized input is further examined to see if the different specimen create similar outputs.

5.1 Results

To compare the bony kinematics from the five PMHS specimens, corridors were generated from the Lundgren data for the following bone pairs: fibula to tibia, talus to tibia, calcaneus to tibia, calcaneus to talus, navicular to talus, cuboid to calcaneus, cuboid to navicular, first metatarsal to talus, and fifth metatarsal to cuboid. Each bone pair has rotation data of one bone with respect of the other recorded in the following directions: plantar/dorsiflexion, ev/inversion, and internal/external rotation. Using these corridors and the correlation and analysis tool (CORA) the kinematics from the PMHS specimen were compared to the Lundgren corridors (Gehre & Gades, n.d.). An exemplar data table is shown below (Table 5-1) and all of the tables are presented in Appendix B. Additionally, each bone pair trace for each specimen is plotted over the Lundgren data in Appendix C.

Table 5-1: Example CORA output table

<table>
<tr><td colspan="2">Talus wrt Calcaneus</td><td colspan="6">662L</td></tr>
<tr><td></td><td></td><td colspan="4">Component CORA Scores</td><td colspan="2">Averaged CORA</td></tr>
<tr><td></td><td></td><td>Corridor Score</td><td>Phase Score</td><td>Size Score</td><td>Progression Score</td><td>Correlation Total</td><td>Total Score</td></tr>
<tr><td rowspan="3">Mean + STD Dev</td><td>Flexion</td><td>0.981 ± 0.007</td><td>0.996 ± 0.002</td><td>0.148 ± 0.019</td><td>0.856 ± 0.003</td><td>0.714 ± 0.005</td><td>0.847 ± 0.006</td></tr>
<tr><td>Version</td><td>0.988 ± 0.007</td><td>0.289 ± 0.067</td><td>0.562 ± 0.141</td><td>0.798 ± 0.014</td><td>0.612 ± 0.011</td><td>0.800 ± 0.009</td></tr>
<tr><td>Rotation</td><td>0.755 ± 0.072</td><td>0.695 ± 0.001</td><td>0.194 ± 0.06</td><td>0.909 ± 0.006</td><td>0.677 ± 0.018</td><td>0.716 ±0.045</td></tr>
</table>

Each table includes the mean and standard deviation of the CORA outputs based on the repeated walking condition. One table includes information for only one bone pair, denoted in the top left, and one specimen, denoted in the top right in the form of specimen number then followed by R or L for right or left respectively. Briefly, CORA when used with a corridor, results in four individual scores, and two averaged scores. The four individual scores are Corridor, Phase, Size, and Progression. Corridor is a score based on how well a desired signal fits within a defined corridor, with a 1 representing a curve that fits perfectly with the representative average of the corridor, a sliding scale between 0 and 1 for anything within the upper and lower bound of the corridor, and a 0 for anything outside the corridor. Phase is a score based on how in-phase the peaks of the desired signal and a representative average of the corridor. Size is a score based on the magnitude at every point between the desired signal and the repetitive average of the corridor. Progression is a score based on a point-to-point cross correlation to compare the shape of the two signals. The Correlation total is a weighted average of 25% of the Phase Score, 25% of the Size Score, and 50% of the Progression Score. The Total Score is an average of the Correlation Total and the Corridor Score.

Additionally, the representative averages that were created to check repeatability in Chapter 4 were used to check if the generalized input across different specimen creates similar output bone kinematics. CORA was used between the representative averages across all directions and bone pairs for each specimen. For the five specimen, this resulted in 10 different combinations of comparisons. The Correlation Totals for each direction and bone pair were aggregated to create one overall Correlation Total for the specimen comparison (Table 5-2).

Table 5-2: Specimen Correlation Totals of CORA between two specimens compared

	Correlation Total Average
M662L VS M901R	0.711
M901R VS M930R	0.698
M662L VS M930R	0.695
M662L VS M815L	0.648
M662R VS M901R	0.629
M815L VS M901R	0.622
M662R VS M930R	0.618
M815L VS M930R	0.616
M662L VS M662R	0.602
M662R VS M815L	0.520

5.2 Discussion

In general, the bony kinematics data matches well with the in vivo bone pin study. The ISO TR9790 rating method was used to categorize the Total Scores (International Organization for Standardization, 1997). According to the standard, 0.86-1 is 'Excellent', 0.65-0.86 is 'Good', 0.44-0.65 is 'Fair', 0.26-0.44 is 'Marginal', and 0-0.26 is 'Unacceptable'. It is important to note that these categories were not specifically designed for this application, but represent an already established ranking system for CORA Total Scores that are not assigned arbitrarily. One-hundred and thirty two CORA Total Scores were compared to the Lundgren corridors, 24 scoring

‘Excellent’, 96 scoring ‘Good’, and 12 scoring ‘Fair’. None of the specimens received a Total Score lower than the ‘Fair’ rating (<0.44). Additionally, the average of all of the Corridor Scores was 0.91. Overall, the bony kinematics data matches the Lundgren data; therefore, the system does recreate gait-like kinematics.

Looking at the average Total Score for each joint individually across all the specimen, the calcaneocuboid joint scores the highest (0.815). Interestingly, the two joints including the cuboid are some of the highest average Total Scores with first for the calcaneocuboid and third for the cuboideonavicular. The lowest average Total Score was the first metatarsal with respect to the talus (0.710). Out of all of the relative bone motion comparisons, the first metatarsal with respect to the talus is the only separated bone pair in the study, as none of the cuneiforms were instrumented. The hind- and mid-foot joints scored higher than the forefoot joints. The markers were more clustered in the mid- and fore-foot than the hindfoot. The motion tracking data was the noisiest in the first and fifth metatarsal, primarily due to the proximity to other markers and the proximity to the edge of the capture volume for the motion capture system. It is interesting to note that the midfoot data, even with the clustering of the talus, navicular, and cuboid marker arrays resulted in some of the more biofidelic motions.

Across all of the joints compared, specimen 930R had the highest average Total Score (0.798), followed by 662R (0.784), 662L (0.767), 815L (0.747), and finally 901R (0.744). It is interesting to note that even though all of the limbs have different anthropometries and uniquely optimized inputs, no one specimen scored significantly higher. This may be due partially to the fact that the same inputs (GRFs, tibia kinematics, and muscle forces) were used initially before optimization. The way the software creates coordinate system specific to the joint of an individual specimen, potentially abstracts some of the anatomical differences away. For example, even if one specimen had a much higher heel pad, causing the ankle joint to be higher than a specimen with a smaller heel pad does, the same rotation is applied. This also is a limitation of the study, with the inputs being based on one volunteer and not specific to any of the PMHS.

The Size Score is consistently the lowest component CORA score. Size is a point-to-point magnitude comparison of the representative average of the corridor and the desired signal. The representative average does not necessarily represent someone walking; the corridor is constructed from the traces of five different volunteers walking. Falling within the corridor was determined to be a more important factor as something within the corridor could represent bony kinematics of a volunteer walking instead of matching a representative average. This also highlights the differences in zero between the Lundgren study and the system evaluation. A neutral stance was used in the Lundgren study to set the origin of the bony coordinate system, the assumption that was made, that the specimen will go back through the neutral position and the coordinate systems can be zeroed there was inaccurate. However, this is not an issue, almost all of the cases have a high Corridor, Phase, and Progressions score, meaning the underlying signal is representative of the corridor and its average.

Consistently the Corridor Score is the lowest for the rotation direction in four of the nine bone pairs, specifically calcaneus in tibia, fibula in tibia, talus in calcaneus, and fifth metatarsal in cuboid. The primary directions of motions of the input tibia kinematics are flexion and version, and this small amount of motion is not translated into the desired motion for the tibia and fibula. Interestingly, the fifth metatarsal is included in that list and not the first metatarsal. The relative motion for the fifth metatarsal to the cuboid represents forefoot to midfoot motion, but the first metatarsal relative to the calcaneus represents forefoot to hindfoot motion. The motion of the midfoot to the forefoot in rotation is due primarily to muscle forces, namely the tibialis posterior and the peroneus brevis, which based on the muscle force input are not sufficient to rotate the foot the degree seen in the Lundgren data. Looking at the first metatarsal with respect to the talus, the ev/inversion motion was not sufficiently captured with the version direction having the lowest Score across all specimen, possibly due to insufficient force being pulled on the peroneus longus and brevis.

During testing bony kinematics were reliably captured across all specimen except for the fibula marker on specimen 662R. The marker array was knocked off during initial setup of the specimen. An attempt was made at reattaching the marker array to the mount was made by gluing the array back onto the mount, but the marker data was too noisy to be effectively used.

In general, the specimen comparisons scored lower than when the specimen were compared to Lundgren, with the highest Correlation average being 0.711 between specimen 662L and specimen 901R, and the lowest Correlation average being 0.52, between 662R and 815L. Interestingly, these two specimen represent the ends of the anthropometry measurements out of the entire specimen group, with 662L being the largest specimen and 901R being the smallest. While the donors were of comparable weights and heights, 75 kg and 1730 mm for specimen 662L and 73.9 kg and 1778 mm for 901R. 901R has the smallest heel pad at 7.5 mm, compared to 662L with double the heel pad size at 15.49 mm. 901R has the longest tibia out of all the specimen, at 421.32 mm compared to 662L which has shortest tibia at 389.7 mm.

Conventional PMHS testing practices claim that left and right specimen are similar enough in terms of material composition to produce similar output metrics. In terms of anthropometry measurements, the matched pair are the closest, but have the second lowest Correlation Total average.

Even though the inputs are the same to start for each specimen, the differences that are introduced during optimization cause the output bone kinematics to differ when the specimen are compared. While the Correlation Totals are closer to one than zero, the Totals are lower than the Correlation Totals of the specimen bone kinematics compared to the Lundgren data.

5.3 Conclusions

The goal of this chapter was to present data for the investigation the last two goals of the thesis. How the output bone kinematics of the system compare to the Lundgren bone pin study to determine how gait-like the output bone kinematics of the system are, and if the generalized input used across different specimen create similar output bone kinematics. Output bone kinematics from all of the specimen fall within the corridors of the Lundgren data, shown by the average corridor score of 0.91. Additionally, all of the specimen had a high overall Total Score between 0.789 and 0.744, meaning that the compared signal mostly represents the average of the corridor. Motion in the hind- and mid- foot was than the motion of the forefoot. When the bone kinematics from all of the specimen were compared to each other, the specimen with the most different anthropometries, 662L and 901R, were found to be the most representative of each other. The matched pair, 662R and 662L, were found to have the 2nd worst correlation out of the 10 correlations that were made.

6. Conclusions, Contributions, Limitations, and Future Work

6.1 Conclusion

The goal of the thesis was to:

1. to develop a robotic gait simulator capable of moving the foot relative to the ground in a realistic orientation under varying body weight conditions, with dynamic control of active muscle forces
2. to use the simulator to capture repeatable foot bone kinematics
3. how well the captured foot bone kinematics can predict realistic foot bone kinematics
4. assessing how using the same input across different anthropometries varies the bone kinematic response

The system developed to address these goals was an integration of a 6 degree of freedom serial robot, nine force controlled tendon actuators, multiple real-time controllers, and a PMHS lower limb into a robotics gait simulator. The MARS was capable of gait simulations at 100% body weight, independent force control on nine extrinsic tendons of the lower limb, tracking and adapting based on target GRFs, and replication of 6 degree of freedom tibia kinematics.

Based on the findings of the proof of concept study in Chapter 3, the system was capable of reliably achieving 100% body weight while moving the foot relative to the ground, and dynamically controlling muscle forces. Changes in body weight were found to cause more variation in bony kinematics than changes in stance phase, thus body weight was more heavily taken into account than simulated stance phase. Based on the findings of Chapter 4, data capture techniques, bone mounted motion capture arrays, camera layout, and processing workflow were capable of capturing bony kinematics that allowed for the calculation of relative motions between bones. Additionally, the system was able to create repeatable bone kinematics.

Based on the findings in Chapter 5, the system at 100% body weight and a 10 second simulated gait cycle was able to capture bony kinematics that represent volunteer data from the Lundgren study. These two metrics were measure by the overall CORA total score being relatively high, 90% of the 135 individual observations scored 0.65 or higher, and the low standard of deviation in the averaged walking trials, smaller than 0.1. Motion in the hind- and mid-foot was more accurately captured than the forefoot. Additionally, even though generalized inputs were used the specimen were found to not correlate with each other well, and the match pair specimens (left and right lower extremity from same donor) were found to be some of the worst correlates. Interestingly, the specimen that were the most different in terms of anthropometry were found to correlate the best.

In summary:

- A 6 degree of freedom serial robot, nine force controlled tendon actuators, multiple real-time controllers, and a PMHS lower limb were integrated into a robotics gait simulator.
- Changes in body weight created more variations in bony kinematics than changes in stance phase time.
- The simulator was capable of creating repeatable bone kinematics.
- The simulator was capable of creating biofidelic bone kinematics compared to the Lundgren walking data.
- Recorded motion in the hind- and mid- foot was more biofidelic than the recorded motion in the forefoot.

- Generalized inputs did not cause the bone kinematics from all specimen to correlate.
- Based on data from this study, bone kinematics from a matched pair specimen were found to not match, and two different specimen with distinct anthropometries were better correlates.

The MARS is a powerful tool for clinical research to evaluate existing or novel orthopaedic devices, normal and pathologic gait, surgical treatments, and biological function, but is subject to the following limitations.

6.2 Limitations

6.2.1 Input Kinematics

The tibia kinematics currently used by the simulator are limited because of the small sample size of the original study. The study used to generate input kinematics only included data on a right leg, and only took into account multiple walking trials from the one subject. Both left and right legs are tested on the MARS, assuming that inverting the coordinate system that is created by a right leg results in a left leg. Additionally, since the input data is based on one anthropometry, the assumption that the kinematics apply to other anthropometries may be incorrect.

6.2.2 Input Muscle Forces and Timing

While the Perry EMG data has become a standard among gait simulators, there is a question of how accurate surface EMG is at tracking the firing of individual muscle. This is compounded by the fact that the electrode is located on the skin when the muscle contracts creates a movement of the skin, which causes noise in the electrode. The peroneal tendons are located deep within the tissue, and due to their proximity and similar firing pattern are difficult to discern from one another. Skin temperature, structure of surrounding tissues, and blood flow have also been known to create noise in EMG data.

6.2.3 Tendon Line of Action

One of the more nonrealistic aspects of the gait simulator is the line of action of the tendon to the actuator. In vivo, the tendon connects to the muscle body underneath the skin and retinaculum close to the tibia. Preparation of the specimen for the simulator exposes the tendons at the ankle then attaches the tendon via a suture to a guide ring. Due to the diameter of the guide ring, the tendons are pulled away from the specimen creating a nonbiofidelic line of action.

6.2.4 Smaller Tendon Attachment

Connection to the smaller tendon is done through a surgical suture, which is generally a sufficient for the load required. Attempting to recreate physiologic loading resulted in loads in the tibialis anterior that exceed the tensile strength of the suture. An investigation should be conducted to determine if the amount of loading is realistic, or if the suture is sufficient.

6.2.5 Rigid Body Assumption

A rigid body assumption is made for the bones for the Vicon post processing. Additionally, the assumption is made that the marker array is rigidly attached to the bone, so that any motion of the marker array is translated to any section of the bone. This assumes that the bones cannot deform which might not be true for long bones such as the tibia and fibula, and the soft bones, like the cuboid. An added problem for the soft bones is ensuring the array is rigidly attached to the bone as the slightest over tightening of the screw that mounts the array could weaken the bone. For example, in the System Evaluation testing the fibula marker array broke off on specimen 662R.

An attempt was made to glue the marker array back on the mount, but the resulting fixation was non-rigid and associated motion tracking data was not usable.

6.2.6 Vicon Data Accuracy

The VICON motion capture system has a specific system accuracy that may cause issue with testing of this scale. The accuracy of the system is thought to be around 1 mm. The distance between two markers on any given array is never longer than 22 mm. At any time, the distance between two markers could be 21 or 23 mm, using inverse trigonometry the accuracy of the system with angles is determined to be around 2.6 degrees.

6.2.7 Lundgren Data

The Lundgren data is used as a standard of biofidelity by the other research groups with robotic gait simulators. There is not another as complete data set to compare to for in vivo bony kinematics, as skin marker studies carry a degree of error in capturing the bony motion. The Lundgren corridors that are constructed do not truly translate to a volunteer walking, the corridor is made up of five different smaller corridors from the mean and average of the volunteers repeated walking trials. The representative average, although useful for comparison, may not accurately represent gait. However, a response that is capture within the corridor does potentially represent gait-like kinematics. Additionally, while the study is best dataset for bony kinematics, they may not represent realistic kinematics. The pins were inserted and removed within a matter of hours, sometime was taken for the volunteers to adjust, but pain or other discomfort could have effected how the volunteers walked.

6.3 Contributions

The main contribution of this thesis work was the design, development, and installation of the MARS system for use by the Center for Applied Biomechanics for the future study of gait or orthopaedic endeavors. Other contributions of this work:

- Workflow for processing motion capture data on lower extremity.
- Manual for using the Kuka robot.
- Muscle actuation system and accompanying hardware, which can be used generically in other applications.
- Preparation process for lower extremities for use in the gait simulator, and on the robot.

6.4 Future Work

Now that the groundwork has been laid, further investigation should be made into improving the input parameters for the system, both to alleviate in uncertainty in the inputs and to improve the optimization scheme. Once those are satisfied, the system could be expanded to look at a different set of input kinematics for a different activity. A deeper investigation into quantifying the effect on bone kinematics on the differences in body weight and stance phase time is needed. Utilizing the gait lab at the University of Virginia, a variety of different dynamic conditions, running, jumping, and cutting, and their associated effect on bony motion could be investigated. The system could be applied to orthopaedic testing by looking at the effect of an ankle implant on the bony kinematics during gait. Additionally, work could look at incorporating PMHS anthropometry to alter system inputs, creating unique inputs based on the PMHS. Currently, only GRFs are used the optimize the system , but the incorporation of a plantar pressure mat into the force plate could allow for additional optimization based on the center of pressure and how it moves during gait.

7. References

Aubin, Patrick M., Whittaker, E., & Ledoux, W. R. (2012). A Robotic Cadaveric Gait Simulator With Fuzzy Logic Vertical Ground Reaction Force Control. *IEEE Transactions on Robotics*, *28*(1), 246–255. https://doi.org/10.1109/TRO.2011.2164958

Aubin, P.M., Cowley, M. S., & Ledoux, W. R. (2008). Gait Simulation via a 6-DOF Parallel Robot With Iterative Learning Control. *IEEE Transactions on Biomedical Engineering*, *55*(3), 1237–1240. https://doi.org/10.1109/TBME.2007.908072

Baxter, J. R., Sturnick, D. R., Demetracopoulos, C. A., Ellis, S. J., & Deland, J. T. (2016). Cadaveric gait simulation reproduces foot and ankle kinematics from population-specific inputs: SIMULATOR REPRODUCES POPULATION-SPECIFIC GAIT. *Journal of Orthopaedic Research*, *34*(9), 1663–1668. https://doi.org/10.1002/jor.23169

Fukunaga, T., Roy, R. R., Shellock, F. G., Hodgson, J. A., & Edgerton, V. R. (1996). Specific tension of human plantar flexors and dorsiflexors. *Journal of Applied Physiology*, *80*(1), 158–165. https://doi.org/10.1152/jappl.1996.80.1.158

Gehre, C., & Gades, H. (n.d.). *OBJECTIVE RATING OF SIGNALS USING TEST AND SIMULATION RESPONSES*. 8.

Gehre, C., Gades, H., & Wernicke, P. (2009). Objective rating of signals using test and simulation responses. *21st International Technical Conference on the Enhanced Safety of Vehicles, Stuttgart, Germany*. http://www-nrd.nhtsa.dot.gov/pdf/ESV/esv21/09-0407.pdf

Hurschler, C., Emmerich, J., & Wülker, N. (2003). In Vitro Simulation of Stance Phase Gait Part I: Model Verification. *Foot & Ankle International*, *24*(8), 614–622. https://doi.org/10.1177/107110070302400808

International Organization for Standardization. (1997). *Road vehicles—Anthropomorphic side impact dummy—Lateral impact response requirements to assess the biofidelity of the dummy*.

Komi, P. (1990). Relevance of in vivo force measurements to human biomechanics. *J. Biomechanics*, *23*, 23–34.

Lee, D. G., & Davis, B. L. (2009). Assessment of the Effects of Diabetes on Midfoot Joint Pressures Using a Robotic Gait Simulator. *Foot & Ankle International*, *30*(8), 767–772. https://doi.org/10.3113/FAI.2009.0767

Lundgren, P., Nester, C., Liu, A., Arndt, A., Jones, R., Stacoff, A., Wolf, P., & Lundberg, A. (2008). Invasive in vivo measurement of rear-, mid- and forefoot motion during walking. *Gait & Posture*, *28*(1), 93–100. https://doi.org/10.1016/j.gaitpost.2007.10.009

Nester, C. J., Liu, A. M., Ward, E., Howard, D., Cocheba, J., Derrick, T., & Patterson, P. (2007). In vitro study of foot kinematics using a dynamic walking cadaver model. *Journal of Biomechanics*, *40*(9), 1927–1937. https://doi.org/10.1016/j.jbiomech.2006.09.008

Noble, L. D., Colbrunn, R. W., Lee, D.-G., van den Bogert, A. J., & Davis, B. L. (2010). Design and Validation of a General Purpose Robotic Testing System for Musculoskeletal Applications. *Journal of Biomechanical Engineering*, *132*(2). https://doi.org/10.1115/1.4000851

Perry, J. (1992). *Gait Analysis*. Slack Incorporated.

Sharkey, N. A., & Hamel, A. J. (1998). A dynamic cadaver model of the stance phase of gait: Performance characteristics and kinetic validation. *Clinical Biomechanics*, *13*(6), 420–433. https://doi.org/10.1016/S0268-0033(98)00003-5

Whittaker, E. C., Aubin, P. M., & Ledoux, W. R. (2011). Foot bone kinematics as measured in a cadaveric robotic gait simulator. *Gait & Posture*, *33*(4), 645–650. https://doi.org/10.1016/j.gaitpost.2011.02.011

Wickiewicz, T., Roy, R., Powell, P., & Edgerton, R. (1983). Muscle Architecture of the Human Lower Limb. *Clinical Orthopaedics and Related Research*.

Wright, C. J., Arnold, B. L., Coffey, T. G., & Pidcoe, P. E. (2011). Repeatability of the modified Oxford foot model during gait in healthy adults. *Gait & Posture*, *33*(1), 108–112. https://doi.org/10.1016/j.gaitpost.2010.10.084

Wu, G., Siegler, S., Allard, P., Kirtley, C., Leardini, A., Rosenbaum, D., Whittle, M., D'Lima, D. D., Cristofolini, L., Witte, H., Schmid, O., & Stokes, I. (2002). ISB recommendation on definitions of joint coordinate system of various joints for the reporting of human joint motion—part I: Ankle, hip, and spine. *Journal of Biomechanics*, *35*(4), 543–548. https://doi.org/10.1016/S0021-9290(01)00222-6

8. Appendix A: Optimization Trajectories

8.1 662R

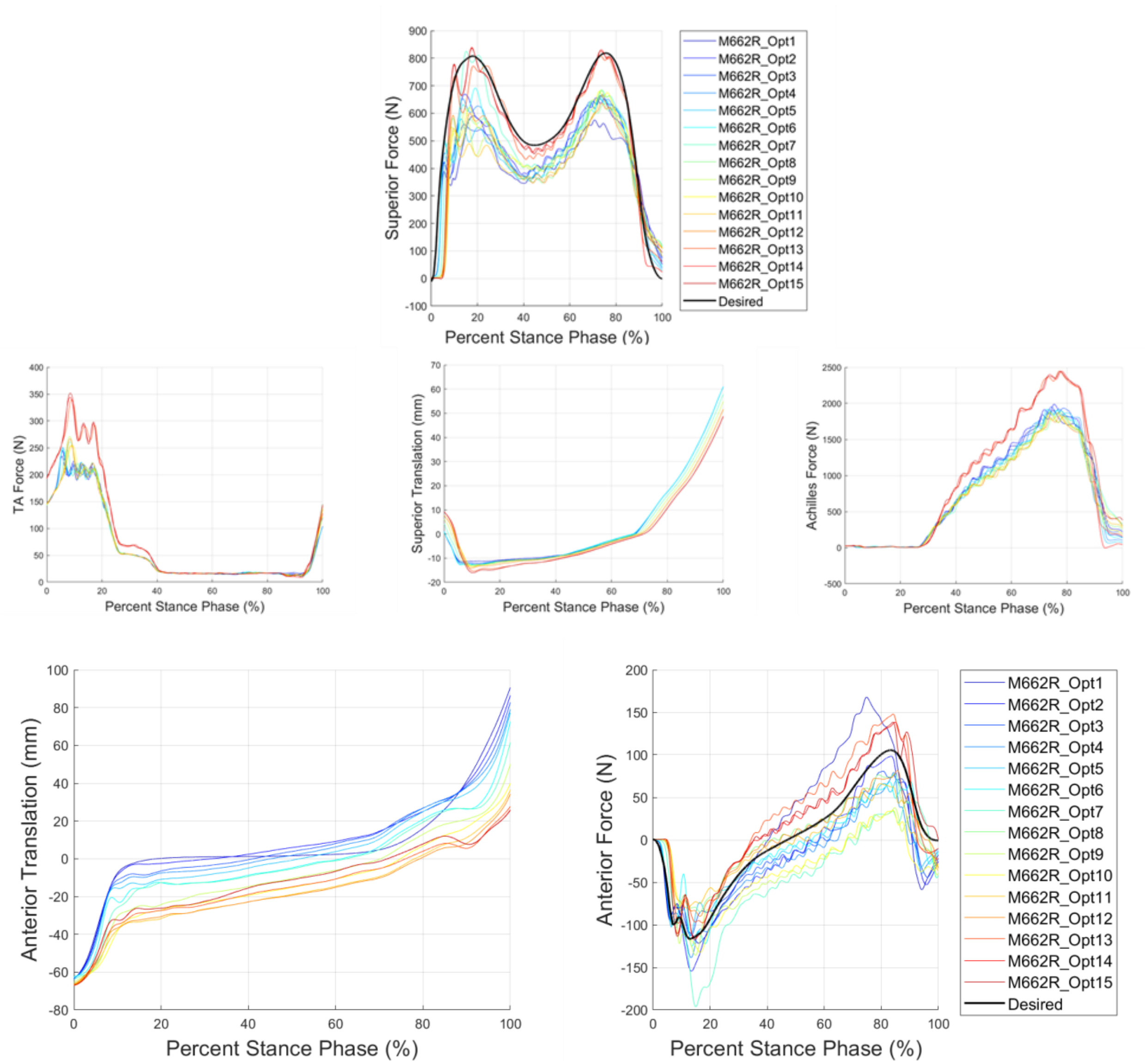

8.2 901R

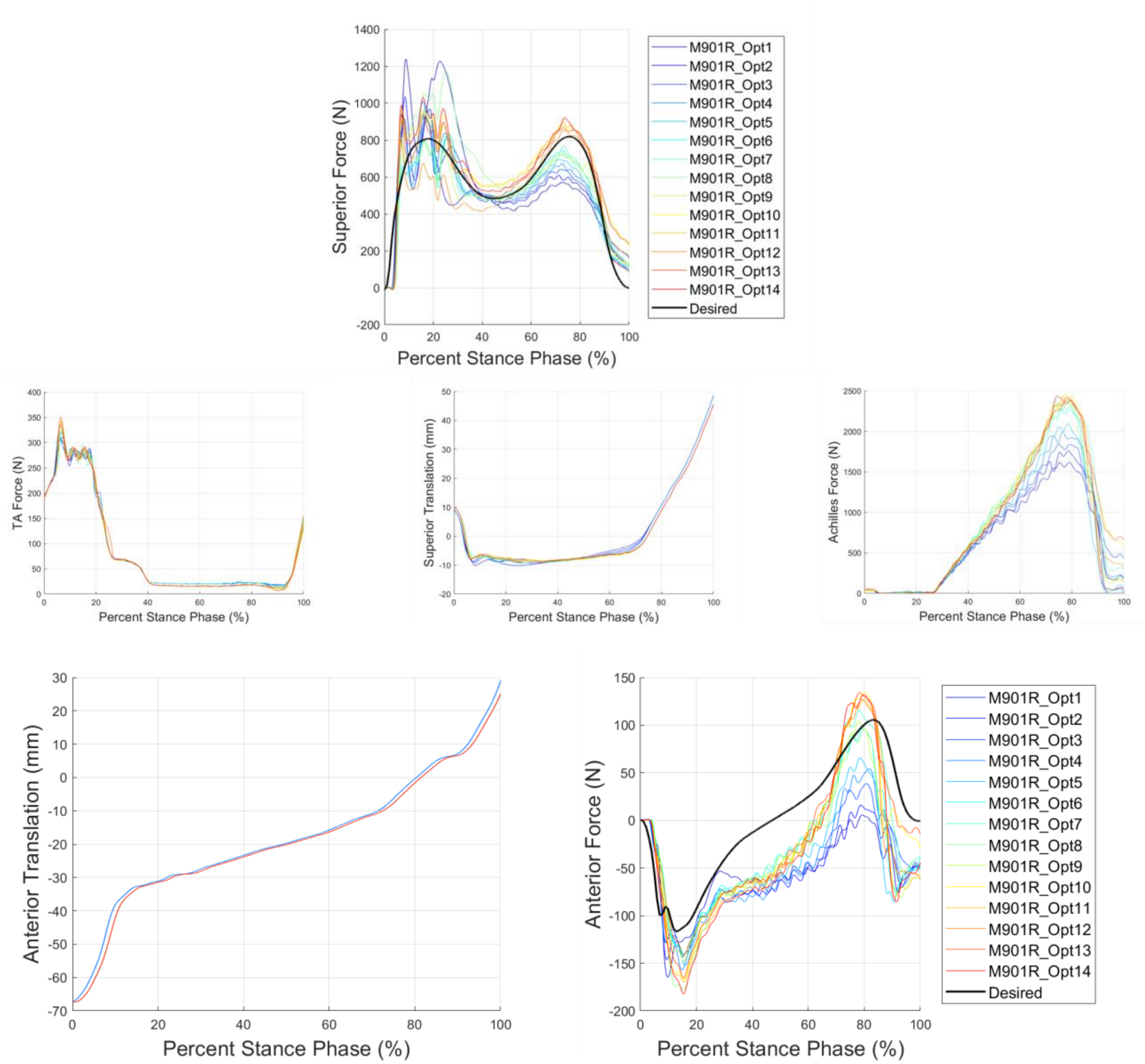
Superior Force (N)
Percent Stance Phase (%)
M901R_Opt1
M901R_Opt2
M901R_Opt3
M901R_Opt4
M901R_Opt5
M901R_Opt6
M901R_Opt7
M901R_Opt8
M901R_Opt9
M901R_Opt10
M901R_Opt11
M901R_Opt12
M901R_Opt13
M901R_Opt14
Desired
TA Force (N)
Percent Stance Phase (%)
Superior Translation (mm)
Percent Stance Phase (%)
Achilles Force (N)
Percent Stance Phase (%)
Anterior Translation (mm)
Percent Stance Phase (%)
Anterior Force (N)
Percent Stance Phase (%)
M901R_Opt1
M901R_Opt2
M901R_Opt3
M901R_Opt4
M901R_Opt5
M901R_Opt6
M901R_Opt7
M901R_Opt8
M901R_Opt9
M901R_Opt10
M901R_Opt11
M901R_Opt12
M901R_Opt13
M901R_Opt14
Desired

8.3 662L

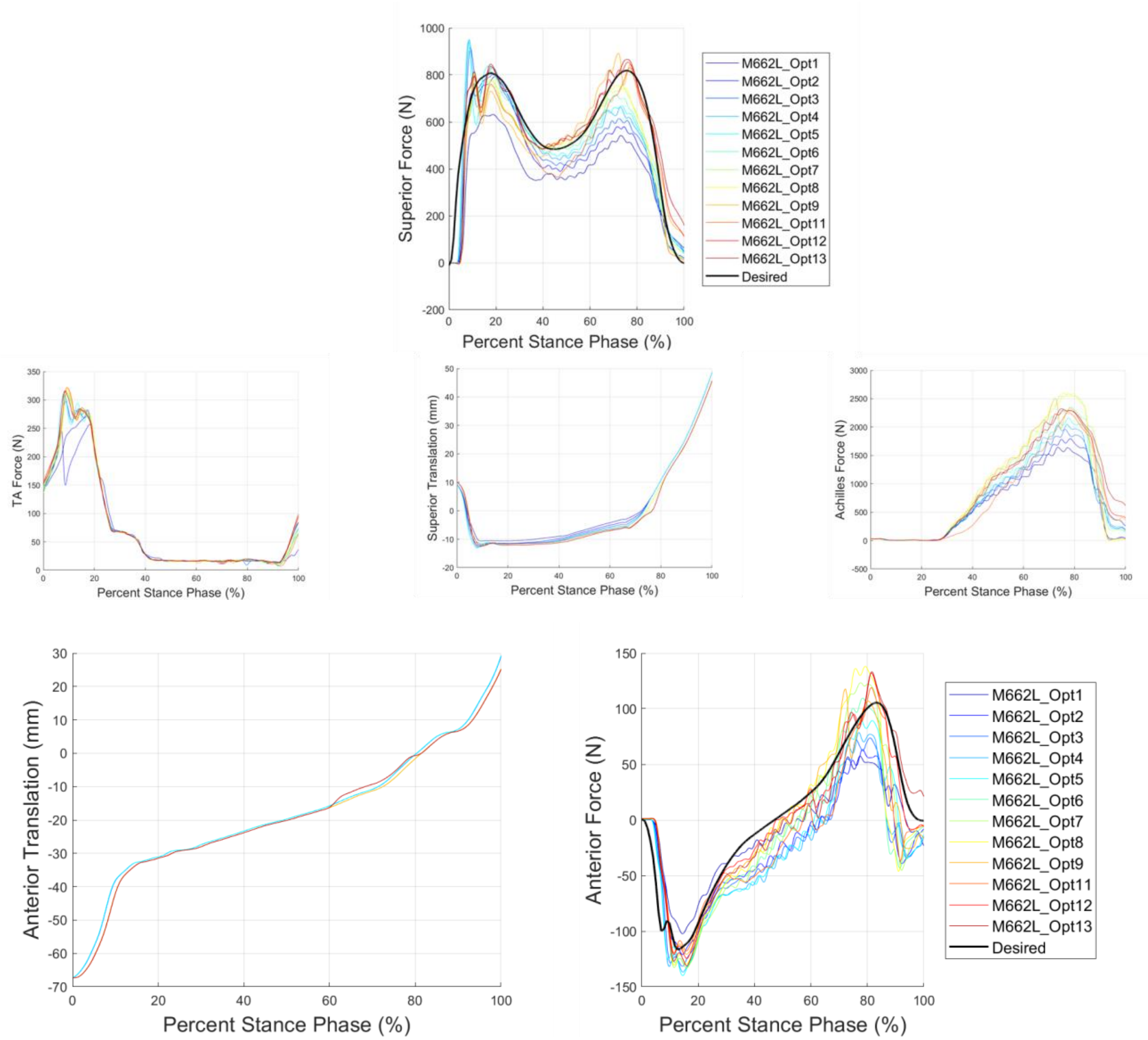

Superior Force (N)
Percent Stance Phase (%)
M662L_Opt1
M662L_Opt2
M662L_Opt3
M662L_Opt4
M662L_Opt5
M662L_Opt6
M662L_Opt7
M662L_Opt8
M662L_Opt9
M662L_Opt11
M662L_Opt12
M662L_Opt13
Desired
TA Force (N)
Percent Stance Phase (%)
Superior Translation (mm)
Percent Stance Phase (%)
Achilles Force (N)
Percent Stance Phase (%)
Anterior Translation (mm)
Percent Stance Phase (%)
Anterior Force (N)
Percent Stance Phase (%)
M662L_Opt1
M662L_Opt2
M662L_Opt3
M662L_Opt4
M662L_Opt5
M662L_Opt6
M662L_Opt7
M662L_Opt8
M662L_Opt9
M662L_Opt11
M662L_Opt12
M662L_Opt13
Desired

8.4 815L

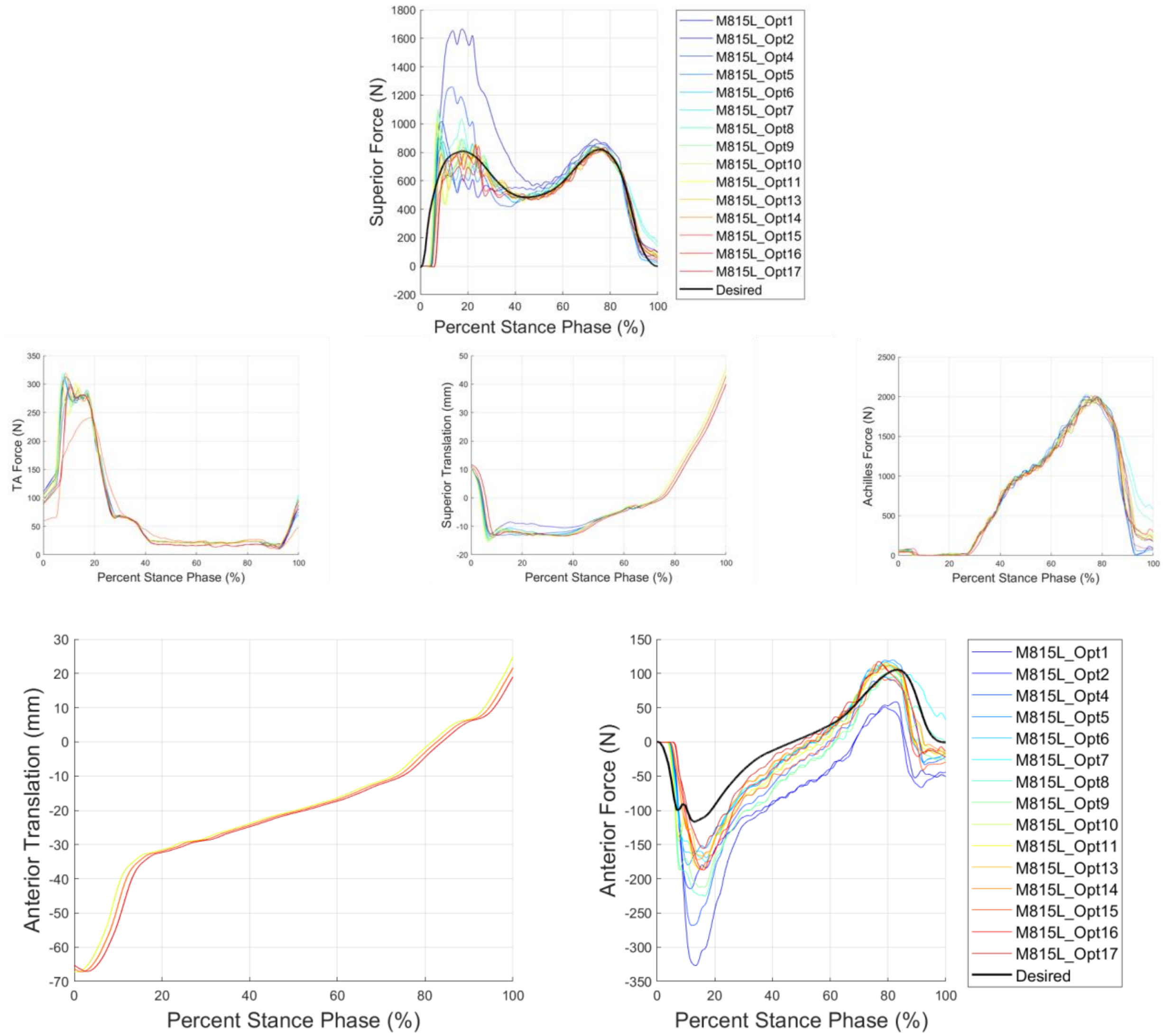

Superior Force (N)
Percent Stance Phase (%)
M815L_Opt1
M815L_Opt2
M815L_Opt4
M815L_Opt5
M815L_Opt6
M815L_Opt7
M815L_Opt8
M815L_Opt9
M815L_Opt10
M815L_Opt11
M815L_Opt13
M815L_Opt14
M815L_Opt15
M815L_Opt16
M815L_Opt17
Desired
TA Force (N)
Percent Stance Phase (%)
Superior Translation (mm)
Percent Stance Phase (%)
Achilles Force (N)
Percent Stance Phase (%)
Anterior Translation (mm)
Percent Stance Phase (%)
Anterior Force (N)
Percent Stance Phase (%)
M815L_Opt1
M815L_Opt2
M815L_Opt4
M815L_Opt5
M815L_Opt6
M815L_Opt7
M815L_Opt8
M815L_Opt9
M815L_Opt10
M815L_Opt11
M815L_Opt13
M815L_Opt14
M815L_Opt15
M815L_Opt16
M815L_Opt17
Desired

8.5 930R

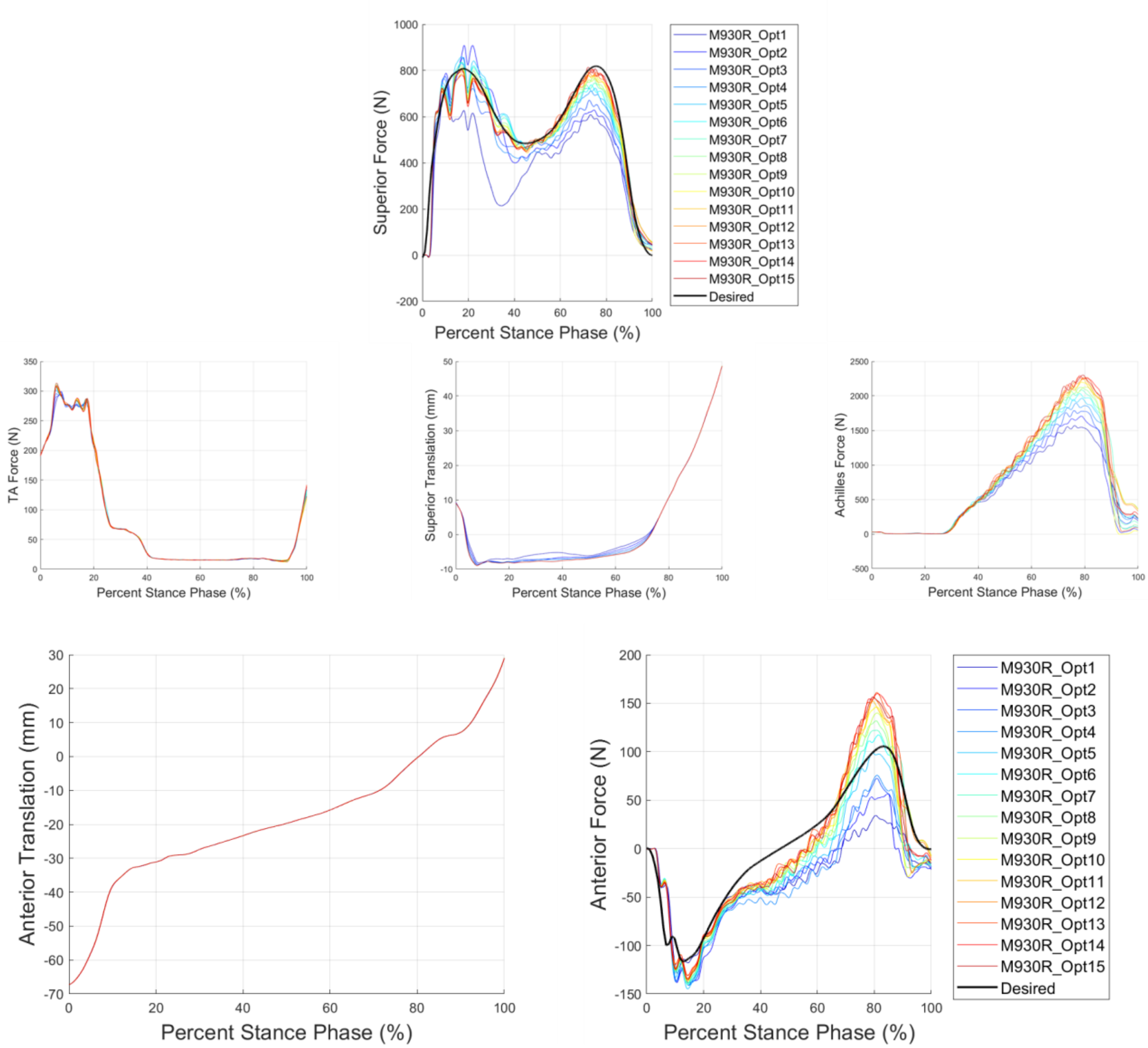
Superior Force (N)
Percent Stance Phase (%)
M930R_Opt1
M930R_Opt2
M930R_Opt3
M930R_Opt4
M930R_Opt5
M930R_Opt6
M930R_Opt7
M930R_Opt8
M930R_Opt9
M930R_Opt10
M930R_Opt11
M930R_Opt12
M930R_Opt13
M930R_Opt14
M930R_Opt15
Desired
TA Force (N)
Percent Stance Phase (%)
Superior Translation (mm)
Percent Stance Phase (%)
Achilles Force (N)
Percent Stance Phase (%)
Anterior Translation (mm)
Percent Stance Phase (%)
Anterior Force (N)
Percent Stance Phase (%)
M930R_Opt1
M930R_Opt2
M930R_Opt3
M930R_Opt4
M930R_Opt5
M930R_Opt6
M930R_Opt7
M930R_Opt8
M930R_Opt9
M930R_Opt10
M930R_Opt11
M930R_Opt12
M930R_Opt13
M930R_Opt14
M930R_Opt15
Desired

9. Appendix B: CORA Tables

9.1 662L

Talus wrt Calcaneus		662L					
		Component CORA Scores				Averaged CORA	
		Corridor Score	Phase Score	Size Score	Progression Score	Correlation Total	Total Score
Mean + STD Dev	Flexion	0.981±0.007	0.997±0.002	0.149±0.02	0.856±0.003	0.715±0.005	0.848±0.006
	Version	0.989±0.008	0.289±0.067	0.562±0.141	0.799±0.015	0.612±0.011	0.801±0.009
	Rotation	0.755±0.073	0.695±0.001	0.195±0.061	0.909±0.006	0.677±0.018	0.716±0.046
Talus wrt Tibia		662L					
		Component CORA Scores				Averaged CORA	
		Corridor Score	Phase Score	Size Score	Progression Score	Correlation Total	Total Score
Mean + STD Dev	Flexion	0.935±0.021	0.611±0.006	0.131±0.028	0.7±0.076	0.536±0.045	0.735±0.014
	Version	0.941±0.028	0.5±0.1	0.184±0.022	0.798±0.026	0.57±0.043	0.755±0.008
	Rotation	0.999±0.002	0.564±0.095	0.701±0.117	0.871±0.02	0.752±0.019	0.875±0.01
Talus wrt Navicular		662L					
		Component CORA Scores				Averaged CORA	
		Corridor Score	Phase Score	Size Score	Progression Score	Correlation Total	Total Score
Mean + STD Dev	Flexion	0.911±0.021	1±0	0.369±0.03	0.734±0.008	0.709±0.011	0.81±0.016
	Version	0.94±0.035	0.322±0.005	0.444±0.313	0.756±0.014	0.569±0.07	0.755±0.053
	Rotation	0.963±0.008	0.708±0.011	0.105±0.016	0.8±0.038	0.603±0.02	0.783±0.013
Cuboid wrt Navicular		662L					
		Component CORA Scores				Averaged CORA	
		Corridor Score	Phase Score	Size Score	Progression Score	Correlation Total	Total Score
Mean + STD Dev	Flexion	0.958±0.011	0.4±0.024	0.327±0.083	0.734±0.009	0.549±0.022	0.753±0.017
	Version	0.975±0.028	0.914±0.029	0.616±0.024	0.89±0.025	0.827±0.025	0.901±0.027
	Rotation	0.912±0.008	0.818±0	0.316±0.034	0.74±0.004	0.654±0.011	0.783±0.009
Fifth Metatarsal wrt Cuboid		662L					
		Component CORA Scores				Averaged CORA	
		Corridor Score	Phase Score	Size Score	Progression Score	Correlation Total	Total Score
Mean + STD Dev	Flexion	0.999±0.001	0.319±0.002	0.187±0.072	0.72±0.036	0.487±0.036	0.743±0.018
	Version	1±0	1±0	0.537±0.06	0.82±0.034	0.794±0.032	0.897±0.016
	Rotation	0.749±0.011	0.723±0.002	0.328±0.009	0.71±0.006	0.618±0.001	0.684±0.005

Fibula wrt Tibia		662L					
		Component CORA Scores				Averaged CORA	
		Corridor Score	Phase Score	Size Score	Progression Score	Correlation Total	Total Score
Mean + STD Dev	Flexion	1±0	0.58±0.128	0.373±0.165	0.617±0.043	0.547±0.095	0.773±0.047
	Version	1±0	0.768±0.003	0.574±0.062	0.726±0.018	0.699±0.025	0.849±0.012
	Rotation	0.765±0.017	0.577±0.006	0.187±0.011	0.936±0	0.659±0.004	0.712±0.01

First Metatarsal wrt Talus		662L					
		Component CORA Scores				Averaged CORA	
		Corridor Score	Phase Score	Size Score	Progression Score	Correlation Total	Total Score
Mean + STD Dev	Flexion	0.783±0.008	0.548±0.002	0.147±0.008	0.684±0.001	0.516±0.001	0.649±0.005
	Version	0.538±0.07	0.92±0.007	0.861±0.175	0.647±0.019	0.769±0.036	0.653±0.017
	Rotation	0.881±0.002	0.633±0.063	0.179±0.031	0.671±0.023	0.539±0.009	0.71±0.005

Calcaneus wrt Tibia		662L					
		Component CORA Scores				Averaged CORA	
		Corridor Score	Phase Score	Size Score	Progression Score	Correlation Total	Total Score
Mean + STD Dev	Flexion	0.868±0.005	0.452±0.007	0.534±0.158	0.769±0.004	0.631±0.039	0.749±0.022
	Version	0.869±0.034	0.222±0.003	0.32±0.168	0.661±0.014	0.466±0.036	0.668±0.035
	Rotation	0.683±0.017	0.779±0.006	0.75±0.017	0.62±0.004	0.692±0.001	0.687±0.008

Cuboid wrt Navicular		662L					
		Component CORA Scores				Averaged CORA	
		Corridor Score	Phase Score	Size Score	Progression Score	Correlation Total	Total Score
Mean + STD Dev	Flexion	1±0	0.45±0.008	0.295±0.027	0.694±0.011	0.533±0.014	0.766±0.007
	Version	1±0	0.96±0.019	0.875±0.016	0.808±0.024	0.863±0.018	0.931±0.009
	Rotation	1±0	0.621±0.184	0.039±0.004	0.594±0.006	0.462±0.044	0.731±0.022

9.2 662R

Talus wrt Calcaneus		662R					
		Component CORA Scores				Averaged CORA	
		Corridor Score	Phase Score	Size Score	Progression Score	Correlation Total	Total Score
Mean + STD Dev	Flexion	1±0	0.993±0	0.185±0.008	0.903±0.002	0.746±0.001	0.873±0.001
	Version	1±0	0.586±0.009	0.179±0.023	0.821±0.01	0.602±0.01	0.801±0.005
	Rotation	0.772±0.02	0.832±0.076	0.418±0.236	0.538±0.006	0.582±0.041	0.677±0.03

Talus wrt Tibia		662R					
		Component CORA Scores				Averaged CORA	
		Corridor Score	Phase Score	Size Score	Progression Score	Correlation Total	Total Score
Mean + STD Dev	Flexion	0.98±0.017	0.953±0.06	0.339±0.03	0.85±0.01	0.748±0.022	0.864±0.019
	Version	0.942±0.001	0.96±0.005	0.313±0.015	0.744±0.015	0.69±0.006	0.816±0.003
	Rotation	0.704±0.008	0.789±0.005	0.198±0.009	0.567±0.002	0.53±0.003	0.617±0.005

Talus wrt Navicular		662R					
		Component CORA Scores				Averaged CORA	
		Corridor Score	Phase Score	Size Score	Progression Score	Correlation Total	Total Score
Mean + STD Dev	Flexion	0.925±0.003	1±0	0.476±0.009	0.804±0.006	0.771±0.005	0.848±0.004
	Version	0.973±0.002	0.677±0.003	0.258±0.047	0.691±0.01	0.58±0.015	0.776±0.009
	Rotation	0.915±0.006	0.587±0.369	0.072±0.026	0.535±0.029	0.432±0.109	0.674±0.058

Cuboid wrt Navicular		662R					
		Component CORA Scores				Averaged CORA	
		Corridor Score	Phase Score	Size Score	Progression Score	Correlation Total	Total Score
Mean + STD Dev	Flexion	1±0	0.722±0.003	0.58±0.005	0.77±0.004	0.71±0.001	0.855±0.001
	Version	0.986±0.009	0.932±0.016	0.475±0.02	0.939±0.003	0.821±0.008	0.904±0.009
	Rotation	0.916±0.009	0.675±0.004	0.737±0.028	0.708±0.019	0.707±0.016	0.811±0.011

Fifth Metatarsal wrt Cuboid		662R					
		Component CORA Scores				Averaged CORA	
		Corridor Score	Phase Score	Size Score	Progression Score	Correlation Total	Total Score
Mean + STD Dev	Flexion	0.989±0.012	0.401±0.02	0.38±0.213	0.654±0.004	0.522±0.058	0.756±0.033
	Version	1±0	1±0	0.457±0.045	0.816±0.017	0.772±0.012	0.886±0.006
	Rotation	0.745±0.007	0.702±0.022	0.253±0.03	0.784±0.01	0.631±0.008	0.688±0.007

Fibula wrt Tibia		662R					
		Component CORA Scores				Averaged CORA	
		Corridor Score	Phase Score	Size Score	Progression Score	Correlation Total	Total Score
Mean + STD Dev	Flexion	NAN	NAN	NAN	NAN	NAN	NAN
	Version	NAN	NAN	NAN	NAN	NAN	NAN
	Rotation	NAN	NAN	NAN	NAN	NAN	NAN

First Metatarsal wrt Talus		662R					
		Component CORA Scores				Averaged CORA	
		Corridor Score	Phase Score	Size Score	Progression Score	Correlation Total	Total Score
Mean + STD Dev	Flexion	0.838±0.004	0.543±0.001	0.103±0.003	0.718±0.001	0.521±0.001	0.68±0.002
	Version	0.803±0.02	0.962±0.009	0.183±0.007	0.679±0.017	0.626±0.012	0.714±0.016
	Rotation	0.956±0.021	0.601±0.006	0.572±0.112	0.845±0.005	0.716±0.029	0.836±0.005

Calcaneus wrt Tibia		662R					
		Component CORA Scores				Averaged CORA	
		Corridor Score	Phase Score	Size Score	Progression Score	Correlation Total	Total Score
Mean + STD Dev	Flexion	0.884±0.008	0.409±0.002	0.817±0.178	0.743±0.01	0.678±0.05	0.781±0.021
	Version	0.979±0.002	0.244±0.134	0.451±0.027	0.63±0.011	0.489±0.046	0.734±0.023
	Rotation	0.915±0.009	0.76±0.111	0.477±0.145	0.729±0.008	0.674±0.007	0.794±0.005

Cuboid wrt Navicular		662R					
		Component CORA Scores				Averaged CORA	
		Corridor Score	Phase Score	Size Score	Progression Score	Correlation Total	Total Score
Mean + STD Dev	Flexion	0.999±0.001	0.797±0.009	0.251±0.031	0.693±0.023	0.609±0.021	0.804±0.01
	Version	1±0	0.956±0.007	0.553±0.019	0.807±0.01	0.781±0.01	0.89±0.005
	Rotation	0.997±0.002	0.47±0.111	0.07±0.018	0.708±0.062	0.489±0.062	0.743±0.03

9.3 815L

Talus wrt Calcaneus		815L					
		Component CORA Scores				Averaged CORA	
		Corridor Score	Phase Score	Size Score	Progression Score	Correlation Total	Total Score
Mean + STD Dev	Flexion	0.925±0.007	0.476±0.228	0.096±0.028	0.684±0.015	0.485±0.069	0.705±0.032
	Version	0.996±0.002	0.951±0.001	0.708±0.155	0.873±0.017	0.851±0.047	0.924±0.024
	Rotation	0.744±0.019	0.538±0.005	0.028±0.004	0.799±0.002	0.541±0.003	0.643±0.008
Talus wrt Tibia		815L					
		Component CORA Scores				Averaged CORA	
		Corridor Score	Phase Score	Size Score	Progression Score	Correlation Total	Total Score
Mean + STD Dev	Flexion	0.52±0.007	0.636±0.003	0.237±0.016	0.769±0.004	0.603±0.006	0.561±0.006
	Version	0.897±0.007	0.991±0.013	0.057±0.012	0.863±0.018	0.693±0.013	0.795±0.01
	Rotation	0.814±0.005	0.335±0.001	0.026±0.003	0.861±0.007	0.521±0.004	0.667±0
Talus wrt Navicular		815L					
		Component CORA Scores				Averaged CORA	
		Corridor Score	Phase Score	Size Score	Progression Score	Correlation Total	Total Score
Mean + STD Dev	Flexion	0.906±0.008	0.131±0	0.278±0.027	0.728±0.004	0.466±0.008	0.686±0.008
	Version	0.993±0.002	0.948±0.008	0.854±0.102	0.88±0.015	0.891±0.031	0.942±0.016
	Rotation	0.859±0.005	0.69±0.008	0.836±0.093	0.769±0.003	0.766±0.026	0.812±0.011
Cuboid wrt Navicular		815L					
		Component CORA Scores				Averaged CORA	
		Corridor Score	Phase Score	Size Score	Progression Score	Correlation Total	Total Score
Mean + STD Dev	Flexion	1±0	0.809±0.008	0.556±0.009	0.792±0.006	0.737±0.006	0.869±0.003
	Version	0.964±0.025	0.666±0.304	0.623±0.235	0.724±0.144	0.684±0.104	0.824±0.061
	Rotation	0.725±0.096	0.509±0.258	0.305±0.145	0.68±0.071	0.543±0.059	0.634±0.076
Fifth Metatarsal wrt Cuboid		815L					
		Component CORA Scores				Averaged CORA	
		Corridor Score	Phase Score	Size Score	Progression Score	Correlation Total	Total Score
Mean + STD Dev	Flexion	1±0	0.779±0.016	0.472±0.047	0.694±0.064	0.66±0.044	0.83±0.022
	Version	0.97±0.008	0.508±0.334	0.471±0.127	0.663±0.099	0.576±0.161	0.773±0.084
	Rotation	0.658±0.04	0.665±0.067	0.167±0.077	0.755±0.012	0.586±0.016	0.622±0.027

Fibula wrt Tibia		815L					
		Component CORA Scores				Averaged CORA	
		Corridor Score	Phase Score	Size Score	Progression Score	Correlation Total	Total Score
Mean + STD Dev	Flexion	1±0	0.86±0.009	0.533±0.294	0.823±0.078	0.76±0.111	0.88±0.055
	Version	1±0	0.578±0.16	0.455±0.298	0.658±0.057	0.588±0.037	0.794±0.019
	Rotation	0.96±0.01	0.6±0.003	0.092±0.011	0.541±0.008	0.443±0.008	0.701±0.001

First Metatarsal wrt Talus		815L					
		Component CORA Scores				Averaged CORA	
		Corridor Score	Phase Score	Size Score	Progression Score	Correlation Total	Total Score
Mean + STD Dev	Flexion	0.693±0.007	0.554±0.002	0.052±0.008	0.702±0.008	0.503±0.001	0.598±0.004
	Version	0.612±0.023	0.135±0.007	0.146±0.014	0.568±0.006	0.355±0.002	0.483±0.013
	Rotation	0.923±0.021	0.994±0.005	0.701±0.076	0.657±0.017	0.752±0.024	0.838±0.022

Calcaneus wrt Tibia		815L					
		Component CORA Scores				Averaged CORA	
		Corridor Score	Phase Score	Size Score	Progression Score	Correlation Total	Total Score
Mean + STD Dev	Flexion	0.881±0.005	0.499±0.136	0.716±0.139	0.721±0.004	0.664±0.028	0.773±0.015
	Version	0.93±0.016	0.223±0.061	0.69±0.218	0.616±0.009	0.536±0.07	0.733±0.027
	Rotation	0.952±0.014	0.855±0.018	0.202±0.015	0.734±0.031	0.631±0.023	0.792±0.018

Cuboid wrt Navicular		815L					
		Component CORA Scores				Averaged CORA	
		Corridor Score	Phase Score	Size Score	Progression Score	Correlation Total	Total Score
Mean + STD Dev	Flexion	0.999±0.001	0.439±0.005	0.084±0.009	0.665±0.024	0.464±0.014	0.731±0.008
	Version	0.998±0.003	0.619±0.107	0.41±0.326	0.655±0.039	0.584±0.101	0.791±0.051
	Rotation	0.937±0.015	0.519±0.015	0.541±0.13	0.721±0.133	0.625±0.091	0.781±0.041

9.4 901R

Talus wrt Calcaneus		901R					
		Component CORA Scores				Averaged CORA	
		Corridor Score	Phase Score	Size Score	Progression Score	Correlation Total	Total Score
Mean + STD Dev	Flexion	0.921±0.015	0.995±0.001	0.081±0.005	0.864±0.015	0.701±0.009	0.811±0.012
	Version	1±0	1±0	0.193±0.031	0.948±0.01	0.772±0.013	0.886±0.006
	Rotation	0.581±0.017	0.817±0.032	0.165±0.024	0.552±0.01	0.522±0.008	0.551±0.012
Talus wrt Tibia		901R					
		Component CORA Scores				Averaged CORA	
		Corridor Score	Phase Score	Size Score	Progression Score	Correlation Total	Total Score
Mean + STD Dev	Flexion	0.88±0.011	0.833±0.007	0.852±0.064	0.914±0.003	0.878±0.015	0.879±0.002
	Version	0.996±0.002	0.745±0.361	0.527±0.124	0.836±0.007	0.736±0.061	0.866±0.031
	Rotation	0.58±0.007	0.734±0.001	0.111±0.001	0.542±0.003	0.482±0.001	0.531±0.003
Talus wrt Navicular		901R					
		Component CORA Scores				Averaged CORA	
		Corridor Score	Phase Score	Size Score	Progression Score	Correlation Total	Total Score
Mean + STD Dev	Flexion	0.758±0.01	1±0	0.18±0.009	0.797±0.003	0.693±0.002	0.726±0.006
	Version	0.983±0.003	0.34±0.001	0.352±0.028	0.67±0.005	0.508±0.007	0.746±0.003
	Rotation	0.885±0.003	0.825±0.004	0.109±0.004	0.577±0.012	0.522±0.008	0.703±0.005
Cuboid wrt Navicular		901R					
		Component CORA Scores				Averaged CORA	
		Corridor Score	Phase Score	Size Score	Progression Score	Correlation Total	Total Score
Mean + STD Dev	Flexion	0.922±0.005	0.226±0.003	0.117±0.008	0.723±0.001	0.447±0.002	0.685±0.004
	Version	0.932±0.005	0.888±0.015	0.432±0.032	0.879±0.001	0.769±0.011	0.851±0.008
	Rotation	0.966±0.006	0.493±0.002	0.568±0.007	0.714±0.005	0.622±0.005	0.794±0.005
Fifth Metatarsal wrt Cuboid		901R					
		Component CORA Scores				Averaged CORA	
		Corridor Score	Phase Score	Size Score	Progression Score	Correlation Total	Total Score
Mean + STD Dev	Flexion	0.993±0.001	0.434±0	0.346±0.026	0.675±0.004	0.532±0.005	0.763±0.002
	Version	0.888±0.018	0.682±0.391	0.261±0.07	0.593±0.019	0.532±0.086	0.71±0.046
	Rotation	0.622±0.027	0.381±0.001	0.107±0.004	0.632±0	0.438±0	0.53±0.014

Fibula wrt Tibia		901R					
		Component CORA Scores				Averaged CORA	
		Corridor Score	Phase Score	Size Score	Progression Score	Correlation Total	Total Score
Mean + STD Dev	Flexion	0.949±0.003	0.415±0.001	0.513±0.013	0.6±0.004	0.532±0.001	0.74±0.001
	Version	0.998±0.001	0.791±0.003	0.323±0.02	0.721±0.006	0.639±0.002	0.819±0.001
	Rotation	0.993±0.003	0.522±0.006	0.789±0.133	0.848±0.007	0.752±0.035	0.872±0.017

First Metatarsal wrt Talus		901R					
		Component CORA Scores				Averaged CORA	
		Corridor Score	Phase Score	Size Score	Progression Score	Correlation Total	Total Score
Mean + STD Dev	Flexion	0.754±0.005	0.605±0.007	0.012±0.002	0.841±0.007	0.575±0.005	0.665±0.001
	Version	0.703±0.066	0.789±0.007	0.414±0.137	0.88±0.043	0.741±0.012	0.722±0.029
	Rotation	0.696±0.094	0.736±0.079	0.512±0.053	0.705±0.013	0.665±0.039	0.68±0.066

Calcaneus wrt Tibia		901R					
		Component CORA Scores				Averaged CORA	
		Corridor Score	Phase Score	Size Score	Progression Score	Correlation Total	Total Score
Mean + STD Dev	Flexion	0.827±0.003	0.653±0.01	0.3±0.011	0.844±0.001	0.66±0.002	0.744±0.002
	Version	0.911±0.016	0.196±0.009	0.583±0.229	0.624±0.022	0.506±0.044	0.709±0.03
	Rotation	0.966±0.021	0.881±0.034	0.281±0.026	0.764±0.05	0.672±0.035	0.819±0.028

Cuboid wrt Navicular		901R					
		Component CORA Scores				Averaged CORA	
		Corridor Score	Phase Score	Size Score	Progression Score	Correlation Total	Total Score
Mean + STD Dev	Flexion	0.952±0.01	0.174±0.012	0.25±0.035	0.68±0.001	0.446±0.011	0.699±0.011
	Version	1±0	0.723±0.391	0.71±0.177	0.751±0.013	0.734±0.141	0.867±0.071
	Rotation	1±0	0.124±0	0.641±0.001	0.541±0.002	0.461±0.001	0.731±0

9.5 930R

Talus wrt Calcaneus		930R					
		Component CORA Scores				Averaged CORA	
		Corridor Score	Phase Score	Size Score	Progression Score	Correlation Total	Total Score
Mean + STD Dev	Flexion	0.999±0.002	0.975±0.001	0.24±0.014	0.771±0.005	0.69±0.002	0.844±0.002
	Version	1±0	0.959±0.009	0.072±0.02	0.879±0.019	0.697±0.015	0.848±0.008
	Rotation	0.996±0.001	0.597±0.046	0.161±0.024	0.713±0.013	0.546±0.005	0.771±0.003

Talus wrt Tibia		930R					
		Component CORA Scores				Averaged CORA	
		Corridor Score	Phase Score	Size Score	Progression Score	Correlation Total	Total Score
Mean + STD Dev	Flexion	0.911±0.011	0.602±0.001	0.126±0.001	0.75±0.01	0.557±0.005	0.734±0.008
	Version	0.999±0	0.973±0.006	0.525±0.136	0.846±0.01	0.797±0.028	0.898±0.014
	Rotation	0.974±0.028	0.797±0.004	0.927±0.042	0.659±0.022	0.76±0.021	0.867±0.023

Talus wrt Navicular		930R					
		Component CORA Scores				Averaged CORA	
		Corridor Score	Phase Score	Size Score	Progression Score	Correlation Total	Total Score
Mean + STD Dev	Flexion	0.92±0.014	0.934±0.005	0.437±0.027	0.6±0.007	0.643±0.004	0.781±0.009
	Version	0.92±0.026	0.615±0.002	0.307±0.006	0.557±0.012	0.509±0.005	0.715±0.015
	Rotation	0.983±0.001	0.652±0.011	0.015±0.001	0.712±0.008	0.522±0.006	0.753±0.003

Cuboid wrt Navicular		930R					
		Component CORA Scores				Averaged CORA	
		Corridor Score	Phase Score	Size Score	Progression Score	Correlation Total	Total Score
Mean + STD Dev	Flexion	0.979±0.008	0.365±0.002	0.284±0.06	0.815±0	0.57±0.014	0.774±0.011
	Version	0.983±0.004	0.924±0.003	0.73±0.055	0.932±0.004	0.879±0.011	0.931±0.004
	Rotation	0.957±0.002	0.654±0.001	0.85±0.016	0.746±0.001	0.749±0.004	0.853±0.003

Fifth Metatarsal wrt Cuboid		930R					
		Component CORA Scores				Averaged CORA	
		Corridor Score	Phase Score	Size Score	Progression Score	Correlation Total	Total Score
Mean + STD Dev	Flexion	1±0	0.771±0.006	0.182±0.03	0.83±0.032	0.653±0.021	0.827±0.01
	Version	1±0	0.957±0.03	0.616±0.036	0.794±0.003	0.79±0.015	0.895±0.007
	Rotation	0.884±0.011	0.754±0.034	0.458±0.037	0.751±0.008	0.678±0.015	0.781±0.002

Fibula wrt Tibia		930R					
		Component CORA Scores				Averaged CORA	
		Corridor Score	Phase Score	Size Score	Progression Score	Correlation Total	Total Score
Mean + STD Dev	Flexion	0.997±0.001	0.541±0.375	0.604±0.426	0.506±0.006	0.539±0.202	0.768±0.101
	Version	1±0	0.842±0	0.439±0.025	0.624±0.003	0.632±0.005	0.816±0.002
	Rotation	0.818±0.002	0.641±0.007	0.136±0.005	0.53±0.002	0.459±0.002	0.639±0.002
First Metatarsal wrt Talus		930R					
		Component CORA Scores				Averaged CORA	
		Corridor Score	Phase Score	Size Score	Progression Score	Correlation Total	Total Score
Mean + STD Dev	Flexion	0.938±0.008	0.606±0.004	0.245±0.031	0.793±0.008	0.609±0.003	0.774±0.005
	Version	0.757±0.023	0.882±0.013	0.243±0.026	0.708±0.011	0.635±0.002	0.696±0.012
	Rotation	0.924±0.001	0.608±0.002	0.117±0.002	0.758±0.011	0.56±0.006	0.742±0.003
Calcaneus wrt Tibia		930R					
		Component CORA Scores				Averaged CORA	
		Corridor Score	Phase Score	Size Score	Progression Score	Correlation Total	Total Score
Mean + STD Dev	Flexion	0.892±0.013	0.595±0.002	0.79±0.149	0.83±0.01	0.761±0.042	0.826±0.014
	Version	0.939±0.009	0.251±0.013	0.613±0.18	0.628±0.015	0.53±0.041	0.735±0.025
	Rotation	0.864±0.022	0.836±0.005	0.455±0.077	0.712±0.019	0.679±0.011	0.772±0.006
Cuboid wrt Navicular		930R					
		Component CORA Scores				Averaged CORA	
		Corridor Score	Phase Score	Size Score	Progression Score	Correlation Total	Total Score
Mean + STD Dev	Flexion	0.993±0.004	0.788±0.002	0.611±0.031	0.845±0.009	0.772±0.011	0.883±0.007
	Version	1±0	0.981±0.006	0.825±0.111	0.785±0.018	0.844±0.024	0.922±0.012
	Rotation	1±0	0.313±0.339	0.287±0.193	0.601±0.003	0.451±0.037	0.725±0.018

10. Appendix C: PMHS Bony Motion versus Lundgren Corridor

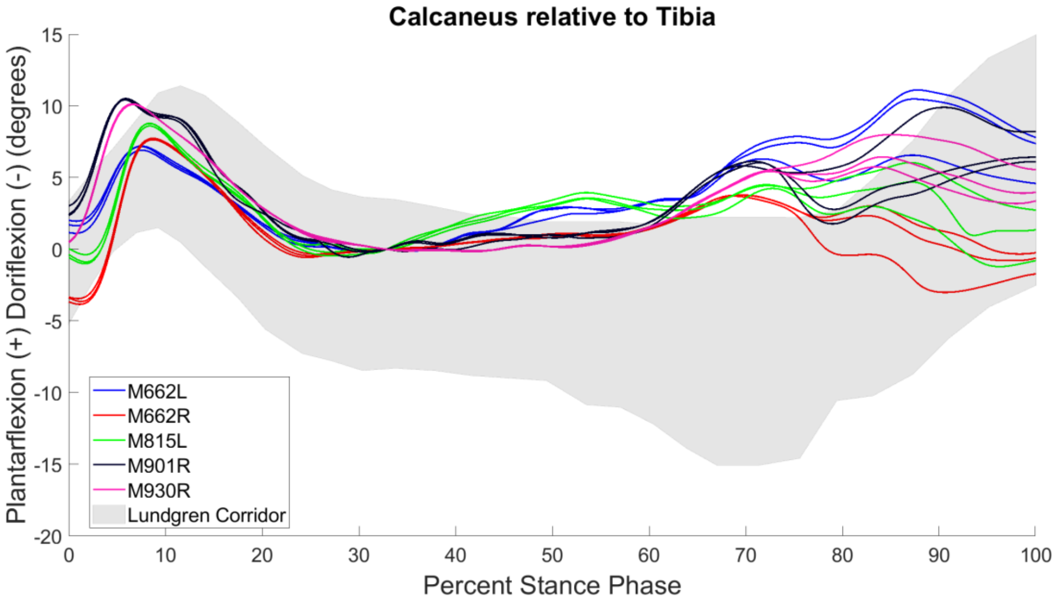

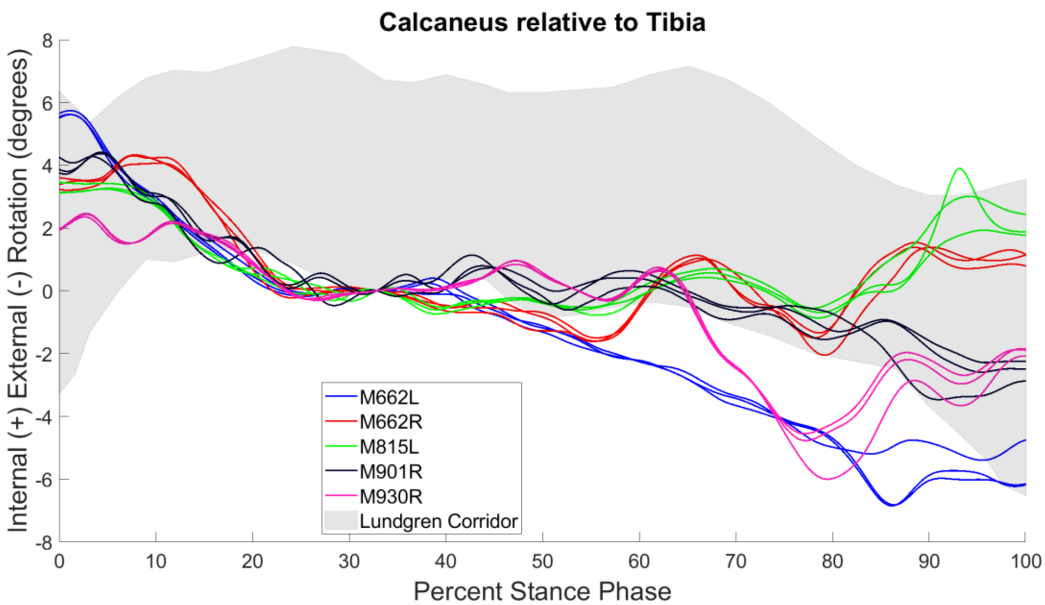

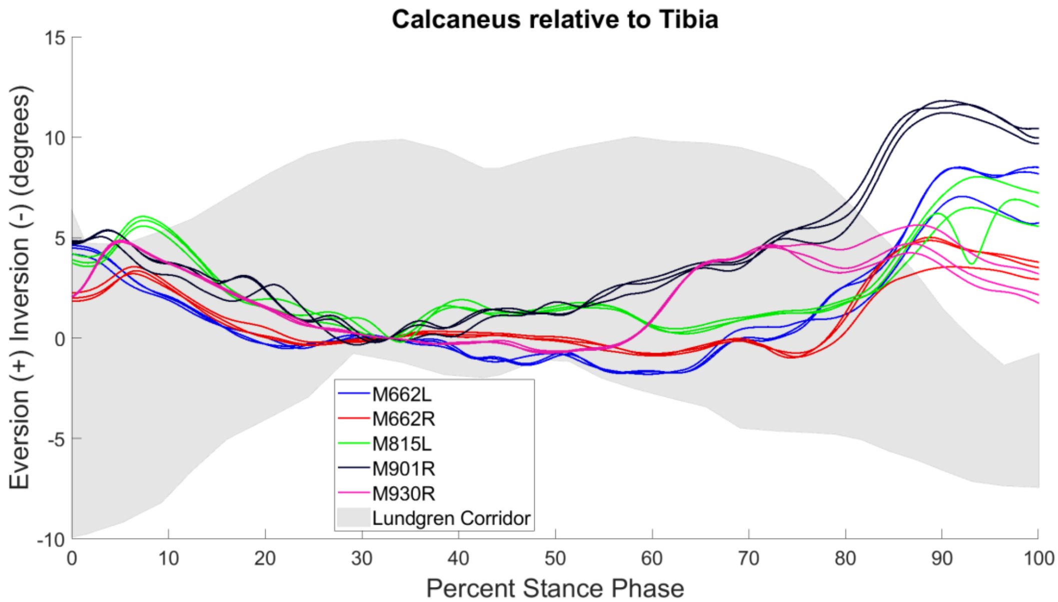
Calcaneus relative to Tibia
Eversion (+) Inversion (-) (degrees)
Percent Stance Phase
M662L
M662R
M815L
M901R
M930R
Lundgren Corridor

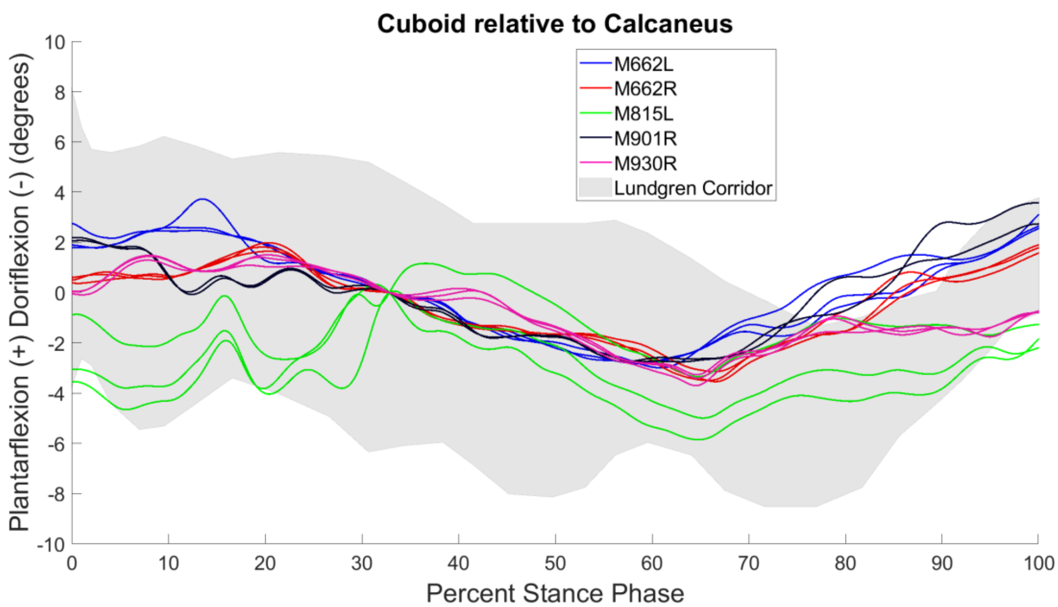
Cuboid relative to Calcaneus
Plantarflexion (+) Doriflexion (-) (degrees)
Percent Stance Phase
M662L
M662R
M815L
M901R
M930R
Lundgren Corridor

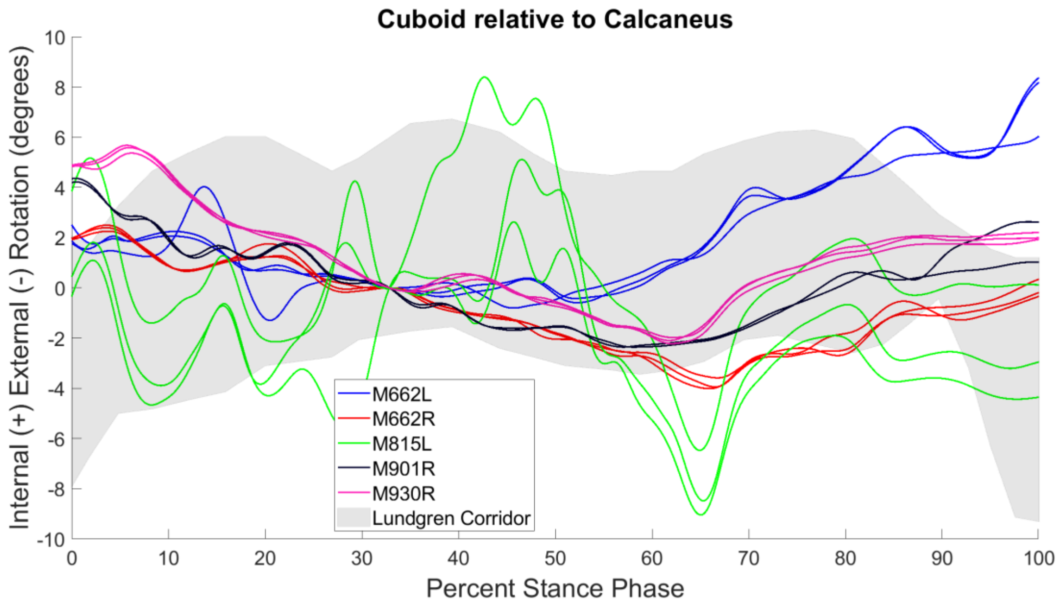
Cuboid relative to Calcaneus
Internal (+) External (-) Rotation (degrees)
Percent Stance Phase
M662L
M662R
M815L
M901R
M930R
Lundgren Corridor

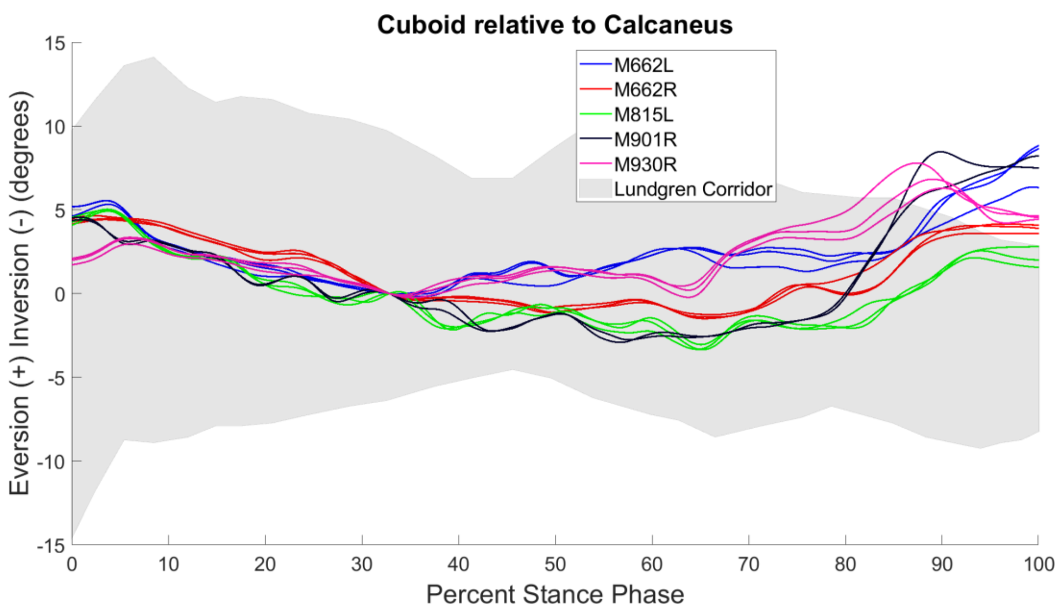
Cuboid relative to Calcaneus
Eversion (+) Inversion (-) (degrees)
Percent Stance Phase
M662L
M662R
M815L
M901R
M930R
Lundgren Corridor

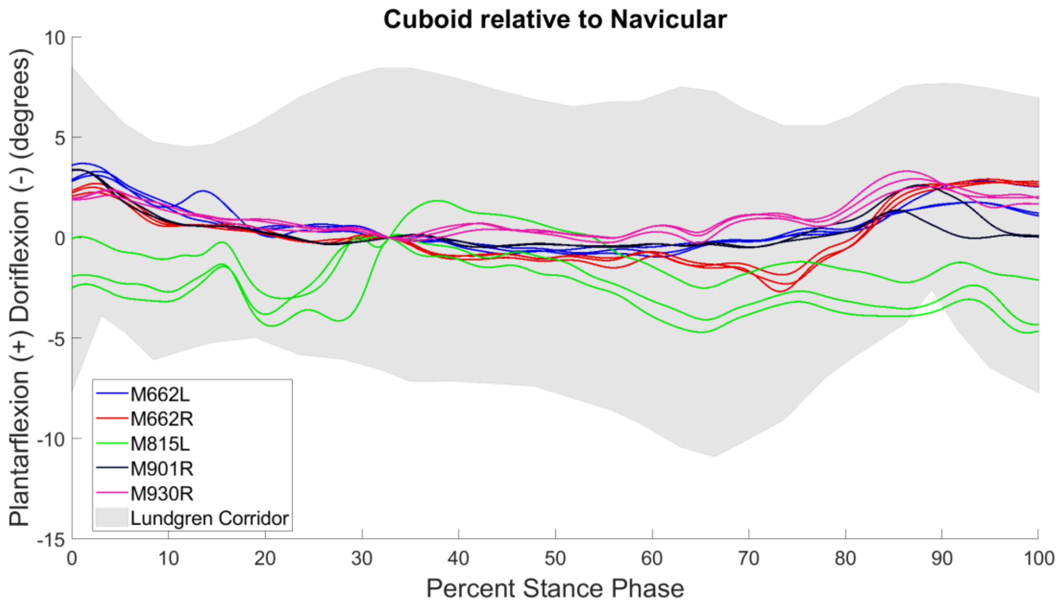
Cuboid relative to Navicular
Plantarflexion (+) Doriflexion (-) (degrees)
Percent Stance Phase
M662L
M662R
M815L
M901R
M930R
Lundgren Corridor

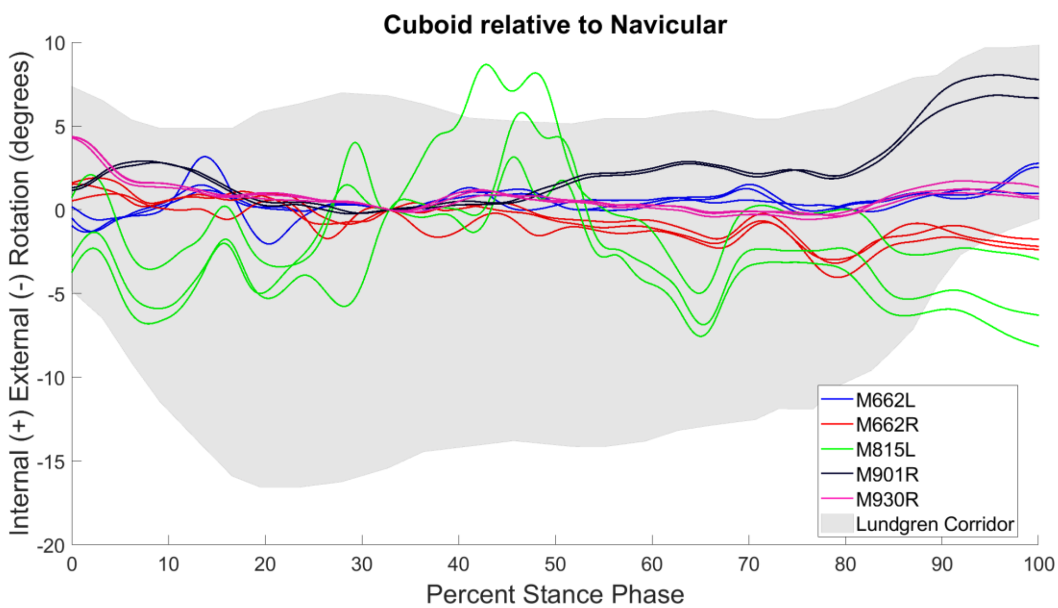
Cuboid relative to Navicular
Internal (+) External (-) Rotation (degrees)
Percent Stance Phase
M662L
M662R
M815L
M901R
M930R
Lundgren Corridor

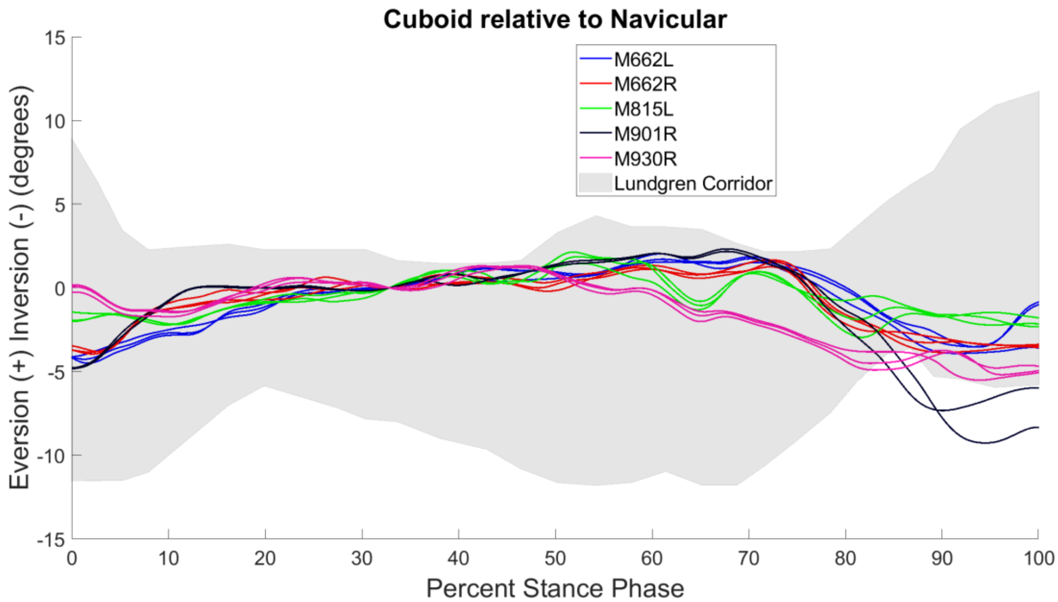
Cuboid relative to Navicular
M662L
M662R
M815L
M901R
M930R
Lundgren Corridor
Eversion (+) Inversion (-) (degrees)
Percent Stance Phase
15
10
5
0
-5
-10
-15
0
10
20
30
40
50
60
70
80
90
100

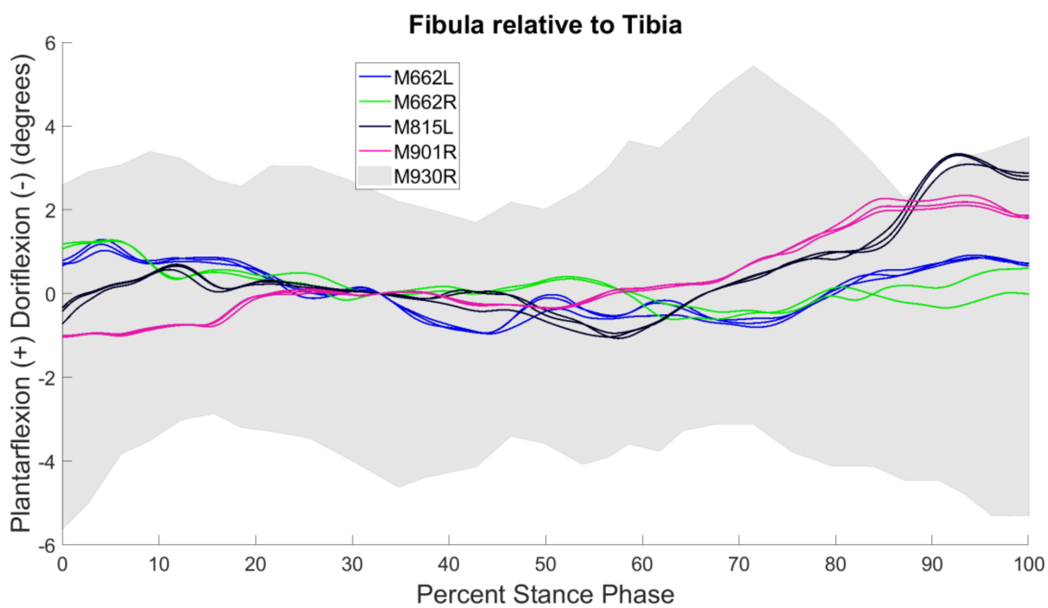
Fibula relative to Tibia
M662L
M662R
M815L
M901R
M930R
Plantarflexion (+) Doriflexion (-) (degrees)
Percent Stance Phase
6
4
2
0
-2
-4
-6
0
10
20
30
40
50
60
70
80
90
100

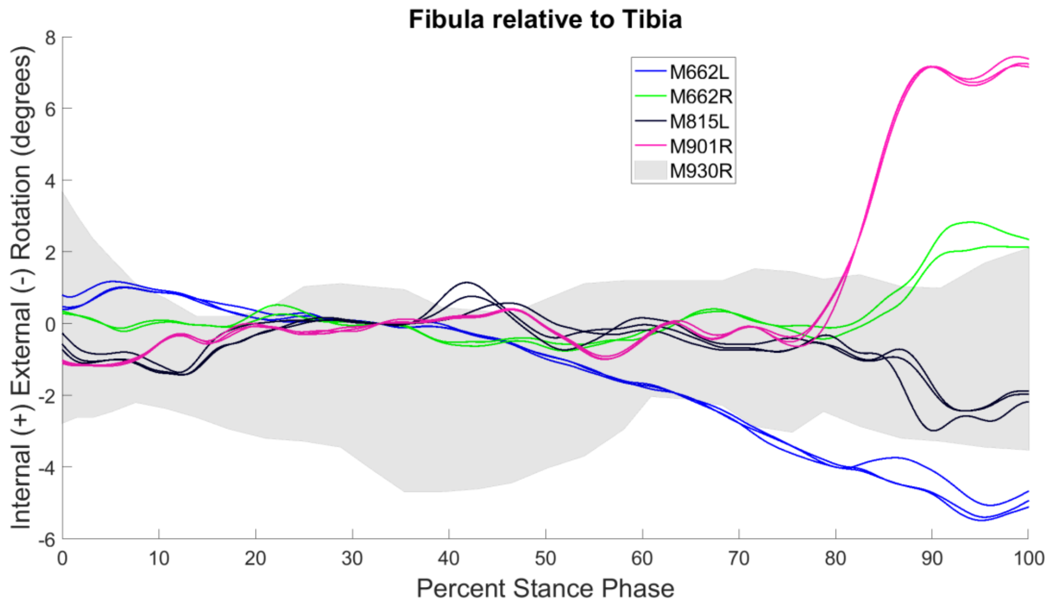
Fibula relative to Tibia
M662L
M662R
M815L
M901R
M930R
Internal (+) External (-) Rotation (degrees)
Percent Stance Phase

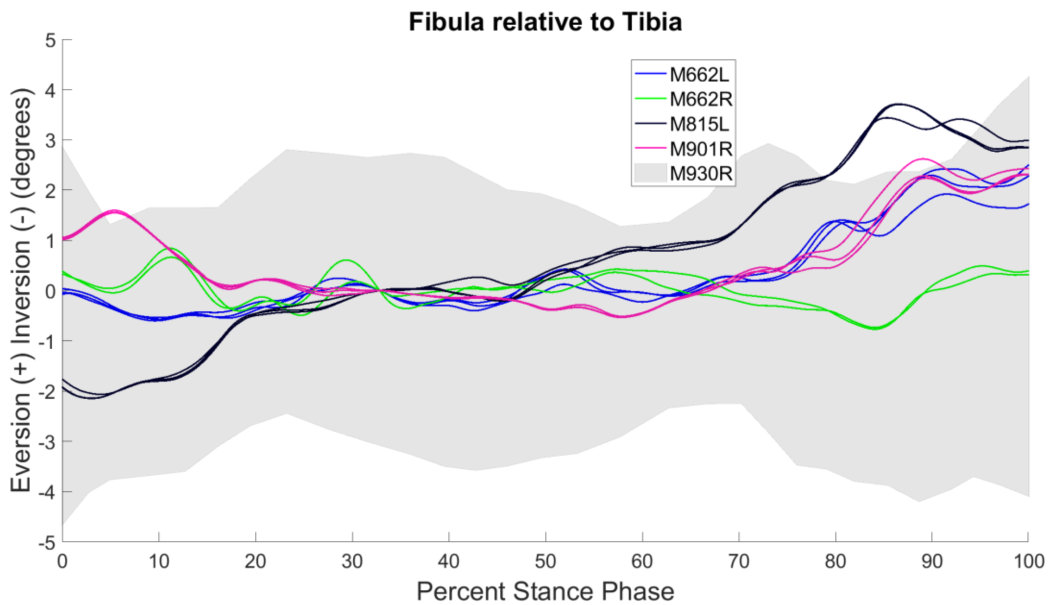
Fibula relative to Tibia
M662L
M662R
M815L
M901R
M930R
Eversion (+) Inversion (-) (degrees)
Percent Stance Phase

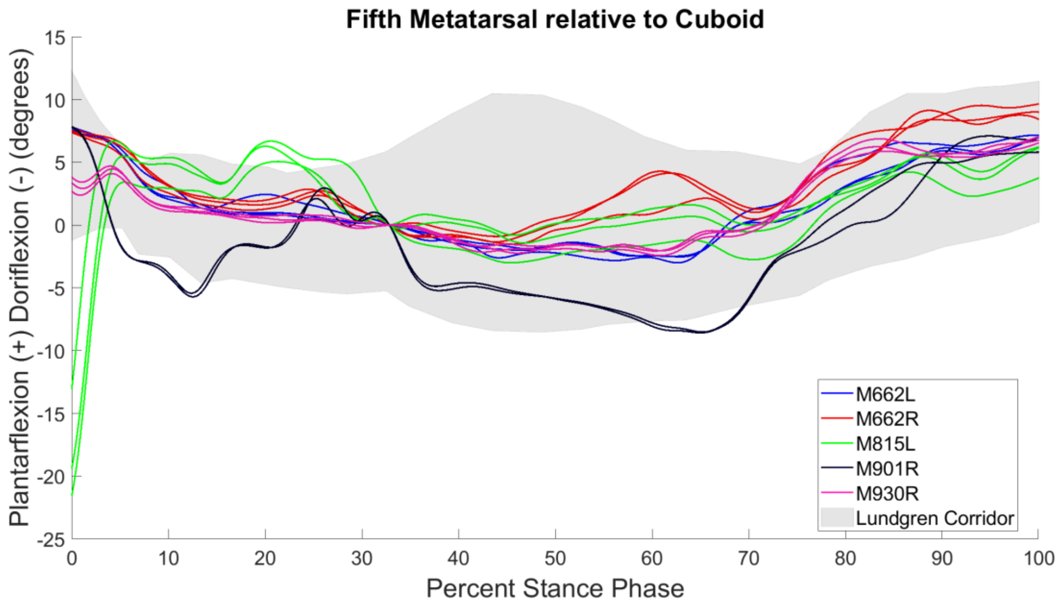
Fifth Metatarsal relative to Cuboid
Plantarflexion (+) Doriflexion (-) (degrees)
Percent Stance Phase
M662L
M662R
M815L
M901R
M930R
Lundgren Corridor
15
10
5
0
-5
-10
-15
-20
-25
0
10
20
30
40
50
60
70
80
90
100

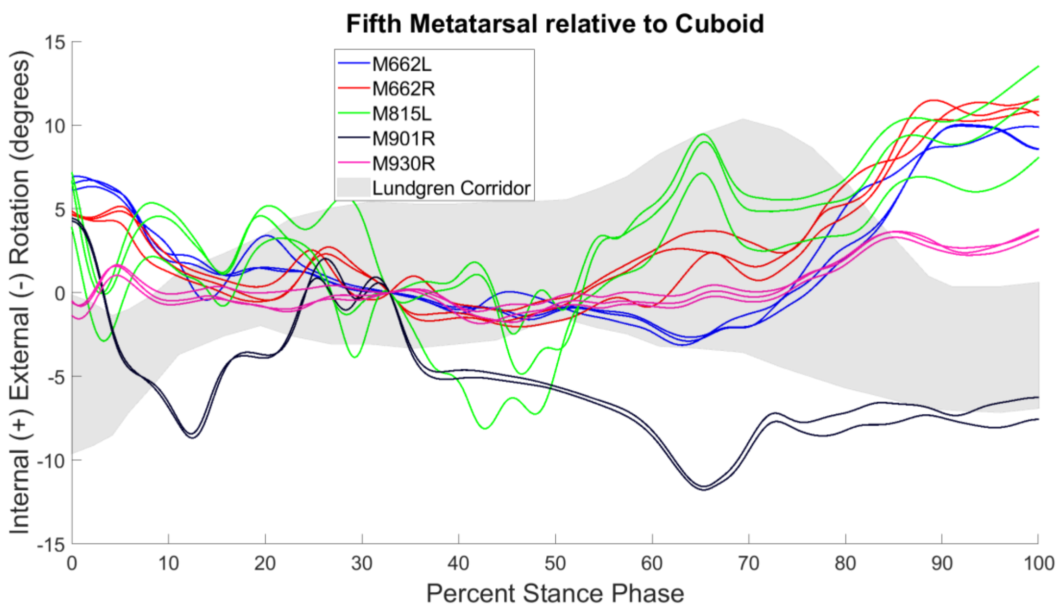
Fifth Metatarsal relative to Cuboid
Internal (+) External (-) Rotation (degrees)
Percent Stance Phase
M662L
M662R
M815L
M901R
M930R
Lundgren Corridor
15
10
5
0
-5
-10
-15
0
10
20
30
40
50
60
70
80
90
100

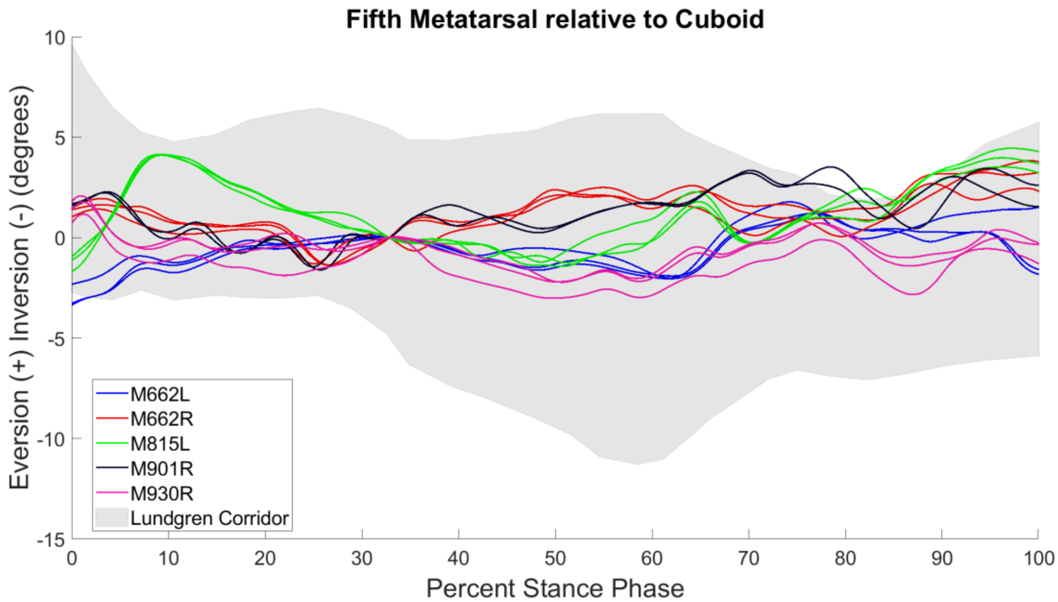

Fifth Metatarsal relative to Cuboid
Eversion (+) Inversion (-) (degrees)
Percent Stance Phase
M662L
M662R
M815L
M901R
M930R
Lundgren Corridor

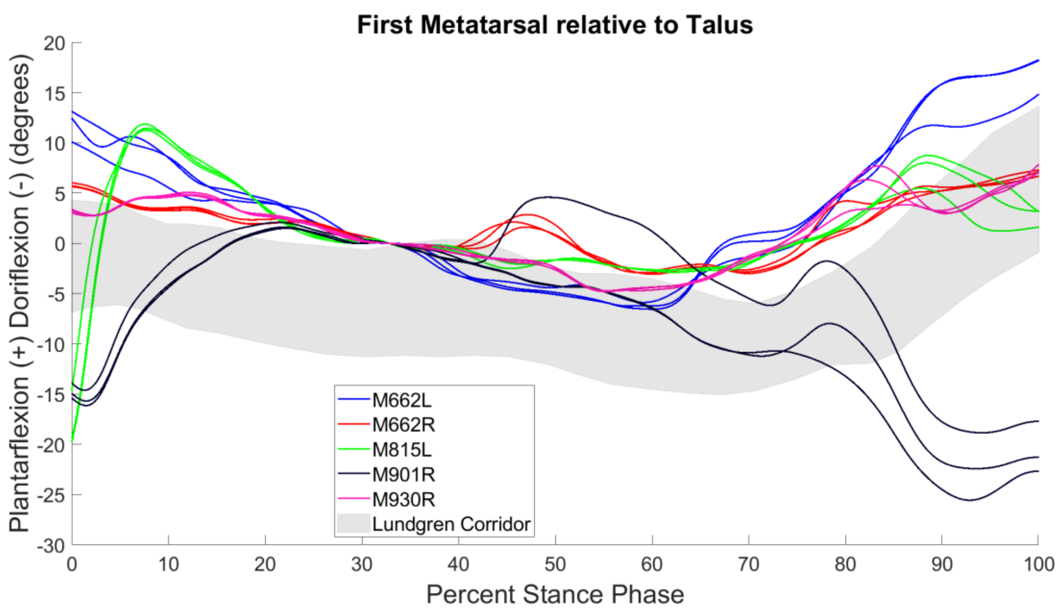

First Metatarsal relative to Talus
Plantarflexion (+) Doriflexion (-) (degrees)
Percent Stance Phase
M662L
M662R
M815L
M901R
M930R
Lundgren Corridor

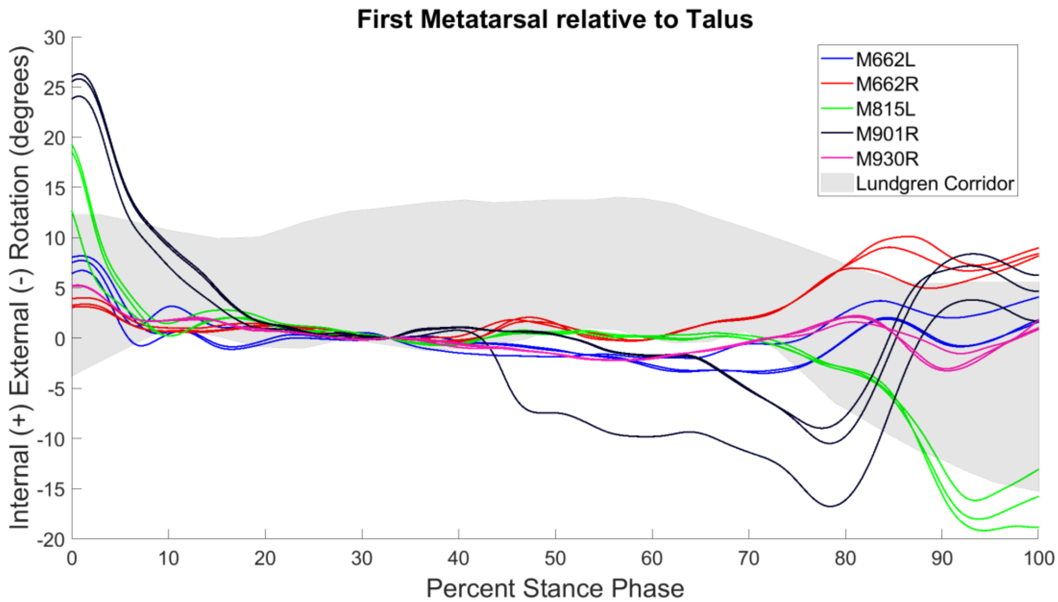
First Metatarsal relative to Talus
Internal (+) External (-) Rotation (degrees)
Percent Stance Phase
M662L
M662R
M815L
M901R
M930R
Lundgren Corridor
30
25
20
15
10
5
0
-5
-10
-15
-20
0
10
20
30
40
50
60
70
80
90
100

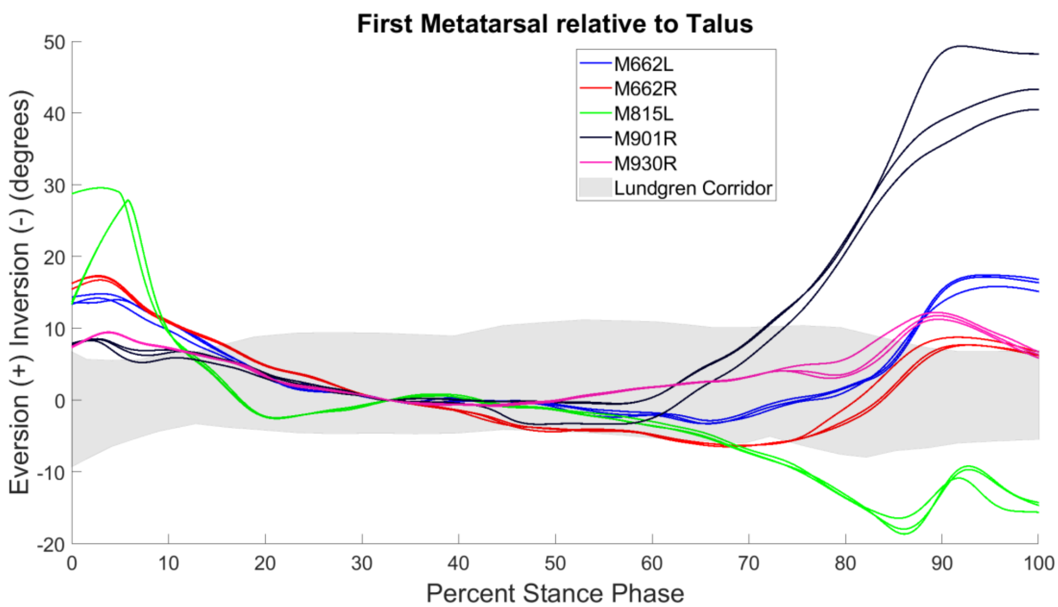
First Metatarsal relative to Talus
Eversion (+) Inversion (-) (degrees)
Percent Stance Phase
M662L
M662R
M815L
M901R
M930R
Lundgren Corridor
50
40
30
20
10
0
-10
-20
0
10
20
30
40
50
60
70
80
90
100

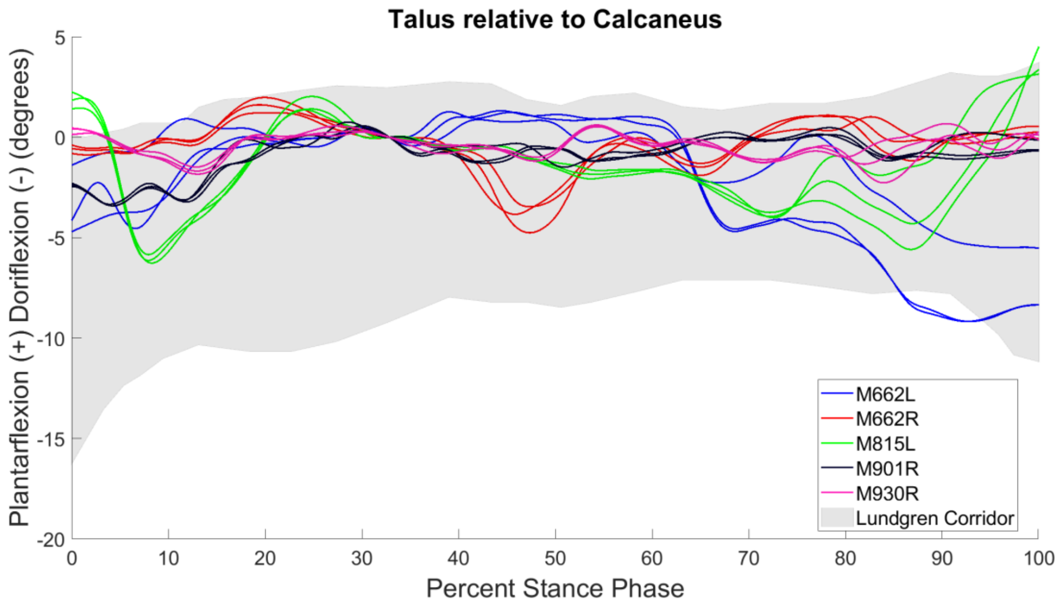
Talus relative to Calcaneus
Plantarflexion (+) Doriflexion (-) (degrees)
Percent Stance Phase
M662L
M662R
M815L
M901R
M930R
Lundgren Corridor

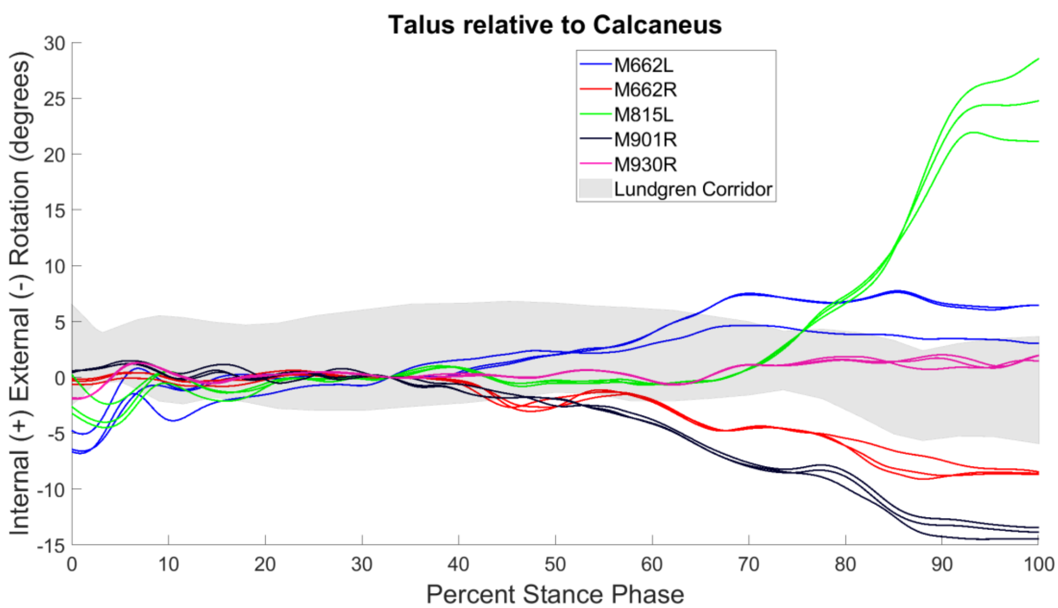
Talus relative to Calcaneus
Internal (+) External (-) Rotation (degrees)
Percent Stance Phase
M662L
M662R
M815L
M901R
M930R
Lundgren Corridor

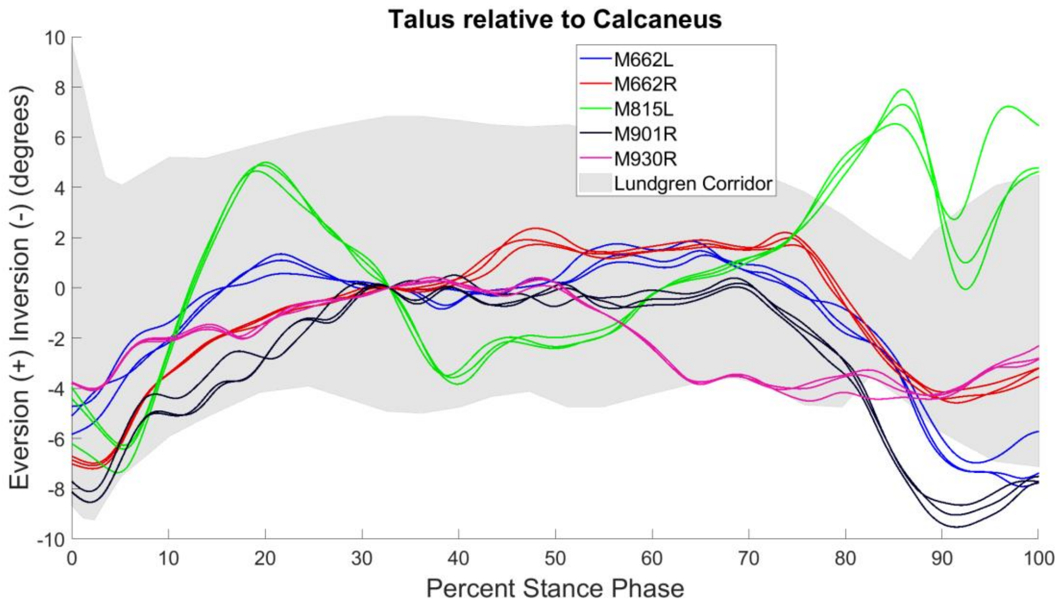
Talus relative to Calcaneus
Eversion (+) Inversion (-) (degrees)
Percent Stance Phase
M662L
M662R
M815L
M901R
M930R
Lundgren Corridor

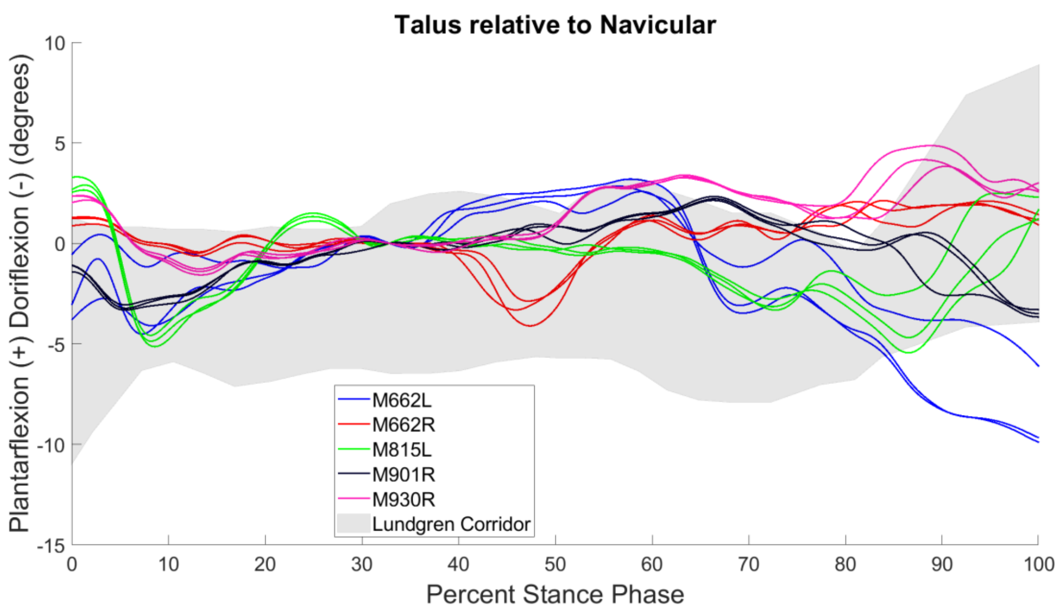
Talus relative to Navicular
Plantarflexion (+) Doriflexion (-) (degrees)
Percent Stance Phase
M662L
M662R
M815L
M901R
M930R
Lundgren Corridor

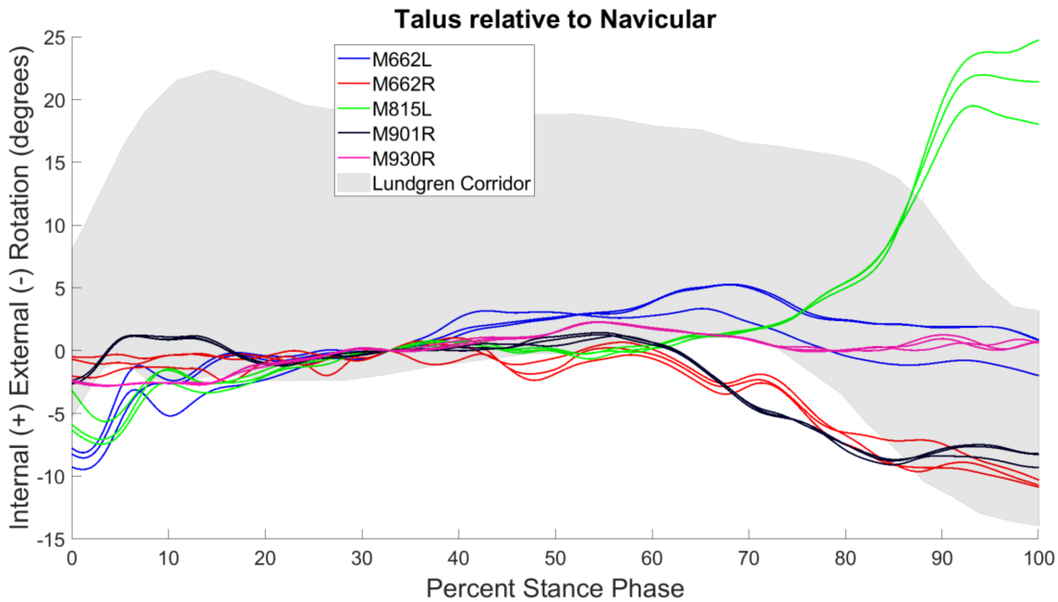
Talus relative to Navicular
M662L
M662R
M815L
M901R
M930R
Lundgren Corridor
Internal (+) External (-) Rotation (degrees)
Percent Stance Phase

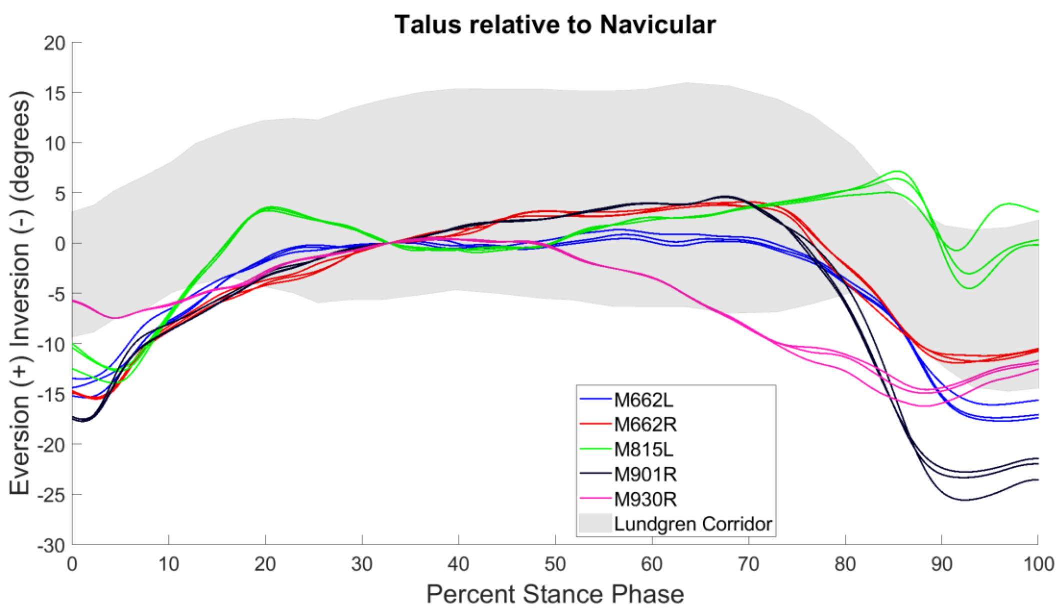
Talus relative to Navicular
M662L
M662R
M815L
M901R
M930R
Lundgren Corridor
Eversion (+) Inversion (-) (degrees)
Percent Stance Phase

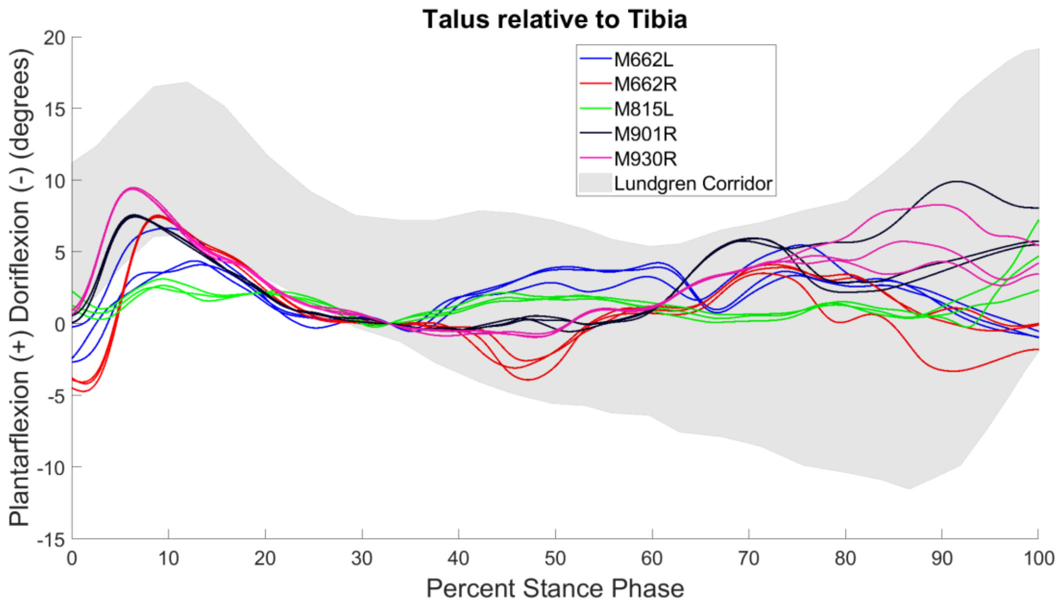
Talus relative to Tibia
Plantarflexion (+) Doriflexion (-) (degrees)
Percent Stance Phase
M662L
M662R
M815L
M901R
M930R
Lundgren Corridor
20
15
10
5
0
-5
-10
-15
0
10
20
30
40
50
60
70
80
90
100

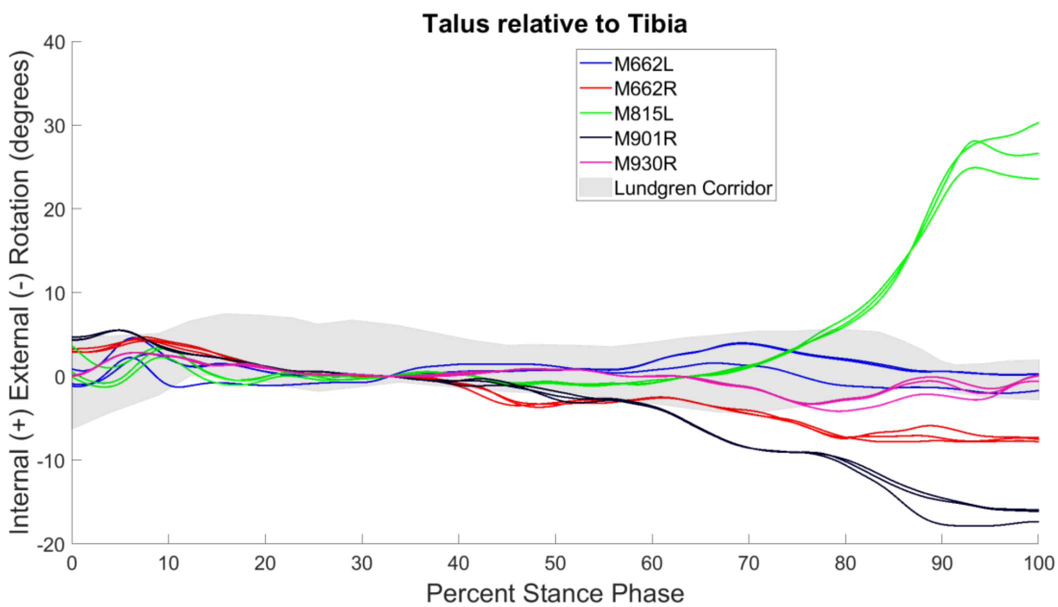
Talus relative to Tibia
Internal (+) External (-) Rotation (degrees)
Percent Stance Phase
M662L
M662R
M815L
M901R
M930R
Lundgren Corridor
40
30
20
10
0
-10
-20
0
10
20
30
40
50
60
70
80
90
100

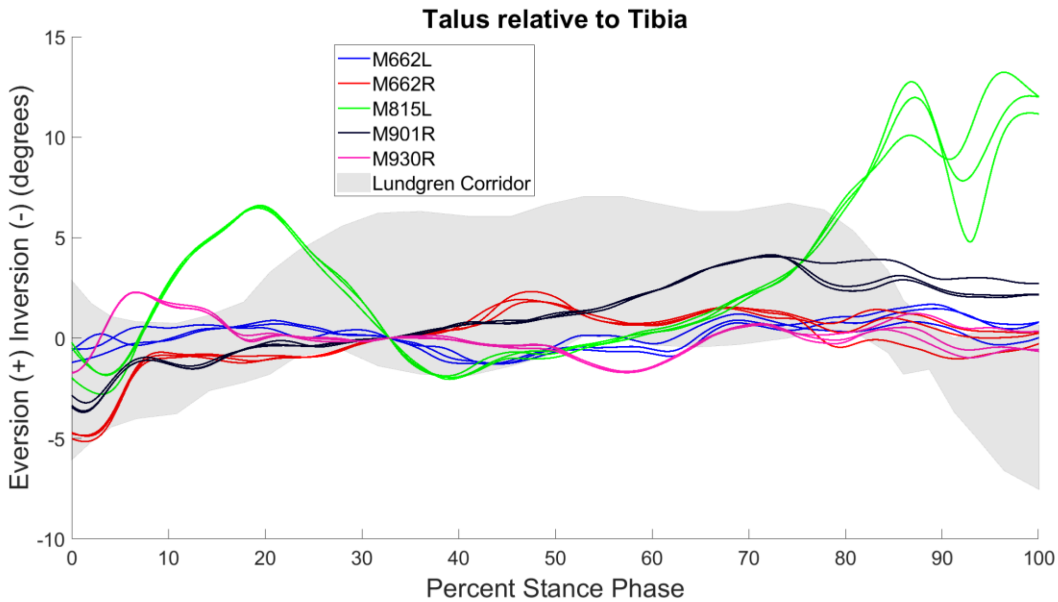

Talus relative to Tibia
M662L
M662R
M815L
M901R
M930R
Lundgren Corridor
Eversion (-) Inversion (+) (degrees)
15
10
5
0
-5
-10
0
10
20
30
40
50
60
70
80
90
100
Percent Stance Phase